Bioorthogonal labeling tools to study pathogenic intracellular bacteria

Bakkum, T.

Chapter 3

Quantification of Bioorthogonal Stability in Immune Phagocytes Using Flow Cytometry Reveals Rapid Degradation of Strained Alkynes

Published as:
Thomas Bakkum, Tyrza van Leeuwen, Alexi J. C. Sarris, Daphne M. van Elsland, Dimitrios Poulcharidis, Herman S. Overkleeft and Sander I. van Kasteren. *ACS Chemical Biology*, **2018**; 13(5): 1173-1179

Abstract

One of the areas in which bioorthogonal chemistry has become of pivotal importance is in the study of host− pathogen interactions. The incorporation of bioorthogonal groups into the cell wall or proteome of intracellular pathogens has allowed study within the endolysosomal system. However, for the approach to be successful, the incorporated bioorthogonal groups must be stable to chemical conditions found within these organelles, which are some of the harshest found in metazoans: the groups are exposed to oxidizing species, acidic conditions, and reactive thiols. This chapter presents an assay that allows the assessment of the stability of bioorthogonal groups within host cell phagosomes. Using a flow cytometry-based assay, the relative label stability inside dendritic cell phagosomes of strained and unstrained alkynes were quantified. Strained alkynes that displayed stability in other systems, were found to be degraded by as much as 79% after maturation of the phagosome.

3.1 Introduction

Bioorthogonal chemistry is the execution of a selective chemical reaction within the complex composition of a biological system.[1] Bioorthogonal chemistry is often used for ligation purposes, whereby a small abiotic chemical functionality is first introduced into a biomolecule (or class of biomolecules) through metabolic engineering.[2] This chemical group is subsequently modified with a large detectable/retrievable group to realize its detection. Bioorthogonal ligation approaches have been used extensively; for example to study the *in vitro*[3,4] and *in vivo*[5] dynamics of glycans, lipids[6], nucleic acids[7,8], prokaryotic[9] and eukaryotic proteomes[10], and peptidoglycan.[11] Bioorthogonal peptidoglycan structures for instance were used to label intracellular pathogens inside a phagocytic host cell to visualize this interaction.[12] The fact that bioorthogonal groups can be incorporated within amino acid sidechains, has even allowed for the visualization of pathogens as they are being degraded by the lysosomal hydrolases in macrophages and dendritic cells (DCs).[13–16] However, to provide unbiased results, the stability of bioorthogonal functionalities to intracellular conditions is essential to prevent label loss during the biological time course. The Antigen-Presenting Cells (APCs) used in the above studies expose their phagosomal content to some of harshest chemistries found in the body (**Figure 1A**).[17,18] When an APC phagocytoses a bacterium, the activity of the NADPH oxidase-2 complex (NOX2) will first result in the intraphagosomal generation of superoxide radicals ($O_2^{-}\cdot$) to concentrations up to 25-100 µM[19] (in absence of myeloperoxidase; MPO). These will rapidly be converted to hydrogen peroxide (< 30 µM)[19], but also NO-radicals (<15 µM)[20], and hydroxyl radicals (·OH).[21] MPO can further react hydrogen peroxide with chloride anions to yield hypochlorous acid (HOCl).[22,23] This oxidative burst in APCs is followed by acidification of the phagosome down to pH-values as low as 4.8 through the action of the vATPase proton pump.[24] During this process, the phagosome fuses with lysosomes containing a wide range of highly proteolytic and reducing enzymes, including the Gamma Interferon-inducible Lysosomal Thioreductase (GILT)[25], a wide range of cathepsins[26] and various other types of hydrolases.[27] This sequence of events renders traditional genetic labeling approaches of partial use as they will be degraded by the lysosomal proteases over time and thus rendered invisible. Even small molecule fluorophores can easily become damaged due to their general sensitivity to oxidation, reduction and pH.[28,29]

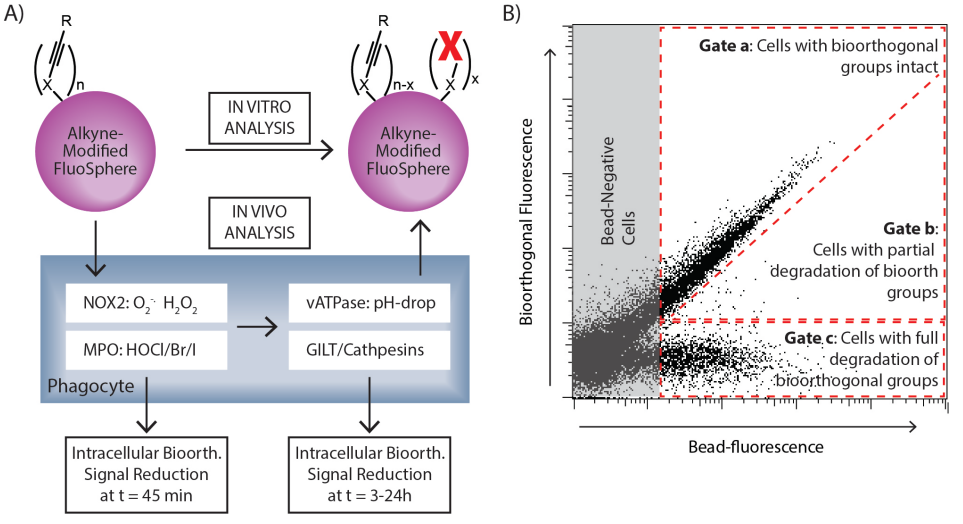

Figure 1. Outline of the stability assays and flow cytometric analysis. (**A**) Alkyne-modified fluorescent latex beads were incubated either in vitro or fed to APCs and the reduction in the number of reactive alkynes was assessed either on the naked beads, or of the cells containing the beads. **X** depicts alkynes rendered unreactive. (**B**) Degradation in cells was quantified as the percentage of cells in which all bioorthogonal groups were degraded to avoid ambiguity. Bead fluorescence was used as an internal standard to negate differences in bead uptake between cells.

Copper-catalyzed and strain-promoted Huisgen-type cycloaddition reactions (ccHc and spHc, also known as CuAAC and SPAAC, respectively) are amongst the most widely applied reactions for the study of intraphagosomal events.[11,12,30,31] However, the stability of the reaction partners in this environment has not previously been characterized. It has, for example, been reported that alkynes are sensitive to thiols and/or radical conditions[32–35], such as these found in phagosomes.[36] Yet, despite this potential stability risk, most stability studies of bioorthogonal groups have been performed in either buffered growth media or cell lysates[35], or the cytosol of intact target cells.[37,38] None of these conditions recapitulate the chemical harshness of the maturing phagosome. To fill this knowledge gap, the method described here was developed to quantify bioorthogonal group stability inside phagosomes. Fluorescent beads (FluoSpheres™) were modified with terminal alkynes or azides (for ccHc) or strained alkynes (for spHc), and used to quantify their stability against the chemistries encountered during phagosomal maturation, using flow cytometry. Strained alkynes were found to be rapidly degraded under these intraphagosomal conditions. Terminal alkynes on the other hand remained stable to the conditions found during the entire phagosomal maturation pathway. The stability of azides proved more difficult to study due to the high background observed for the alkyne-

fluorophore but seemed to display a similar stability profile as the terminal alkynes. Subsequent *in vitro* analysis revealed that a reaction between the spHc-reagents and HOCl was a likely culprit for the inactivation of the bioorthogonal groups, although additional reactive species could not be excluded.

3.2 Results and Discussion

3.2.1 Development of a bioorthogonal stability assay in phagocytes

There are three main classes of phagocytes in the immune system, macrophages, dendritic cells (DCs), and neutrophils, of which DCs and macrophages are most important for antigen processing and presentation.[39,40] They are also the main reservoir for intracellular pathogenic bacteria and thus under intense scrutiny to study the host-pathogen interactions. DCs and macrophages – as well as their subsets – display wide heterogeneity regarding their phagocytic capacity and intracellular chemistries.[41,42] In order to develop an assay that would allow the assessment of the stability of bioorthogonal groups after phagocytosis independent of the differences in uptake, an approach was designed where the phagocytes would take up microspheres, that were not only surface modified with the bioorthogonal groups, but that also contained intra-bead fluorophores, not exposed to the phagosomal environment (**Figure 1A**) and thus showing minimal bleaching.[43] These beads would allow the quantification of bioorthogonal handles per bead over time inside a phagocyte, by measuring the change in ratio of fluorescent signal resulting from a bioorthogonal ligation to that of the internal fluorophore. This approach would negate not only differences in uptake between cells, but also signal changes resulting from any potential expulsion of beads through exocytosis[41] (**Figure 1B**). The approach is also facile, as the whole analysis could also be performed in fixed cells, preventing the need for re-isolating the spheres after the biological time course.

Amine-functionalized 0.2 µm polystyrene FluoSpheres (excitation/emission = 580/605 nm, **5**) were modified with various bioorthogonal ligands for the azide-alkyne [3+2] cycloaddition (**Figure 2**) using hydroxysuccinimidyl (**1-4**)-mediated amide/carbamate condensation reactions.[44] The acetylenyl and azido-groups were chosen for their widespread application in the copper-catalyzed[45] or strain-promoted Huisgen cycloaddition[46], or the Bertozzi-Staudinger ligation.[3] The strained dibenzocyclooctynyl (DBCO, also known as DIBAC; **3**) and bicyclo[6.1.0.]nonyne (BCN; **4**) were chosen for their copper-independency, relatively fast reaction rates (0.31 $M^{-1}s^{-1}$ and 0.14 $M^{-1}s^{-1}$ respectively)[47] and widespread use in literature.[48–52] Optimal reaction conditions were found to be

shaking the unmodified beads for two days at 20°C in a 1:5 mixture of DMSO in PBS, containing a large excess of the succinimidyl esters **1-4** to yield acetylenyl- (**6**), azido- (**7**), dibenzocyclooctynyl (**8**), or bicyclo[6.1.0]nonyne (**9**)-modified FluoSpheres.

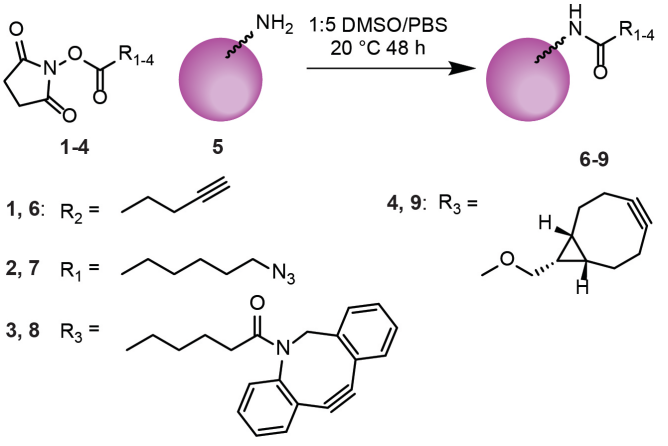

Figure 2. Synthesis of bioorthogonal fluorescent polystyrene beads. Amine-functionalized FluoSpheres **5** (200 nm) were modified with hydroxysuccinimidyl esters **1-4** to yield bioorthogonal FluoSpheres **6-9**.

The fluorescence of the beads allowed their assessment by bead-only flow cytometry: using either a copper-catalyzed or copper-free [3+2] cycloaddition reaction (in case of **6** and **7**) with AF488-azide (or alkyne for **7**)[8,53], followed by flow cytometric analysis of the FluoSpheres (**Figure 3**, t = 0) to visualize the introduced alkynes or fluorescamine to visualize the remaining unreacted amines (**Figure S1**).[54] Complete disappearance of the fluorescamine signal was observed for all particles indicating complete consumption of the free amine functionalities in all reactions.

3.2.2 Stability of bioorthogonal FluoSpheres in vitro

It was first determined whether this assay could recapitulate previously reported stability properties of the various above bioorthogonal groups (**Figure 3**, **Figure S2-S7**).[37] All groups were previously reported to be stable in PBS and cell lysates, but strained alkynes were reported to react with thiols[32,55], and thiyl radicals.[32] Terminal alkynes were also shown to be reactive towards thiyl radicals[32], as well as to hydroxyl radicals.[56,57]

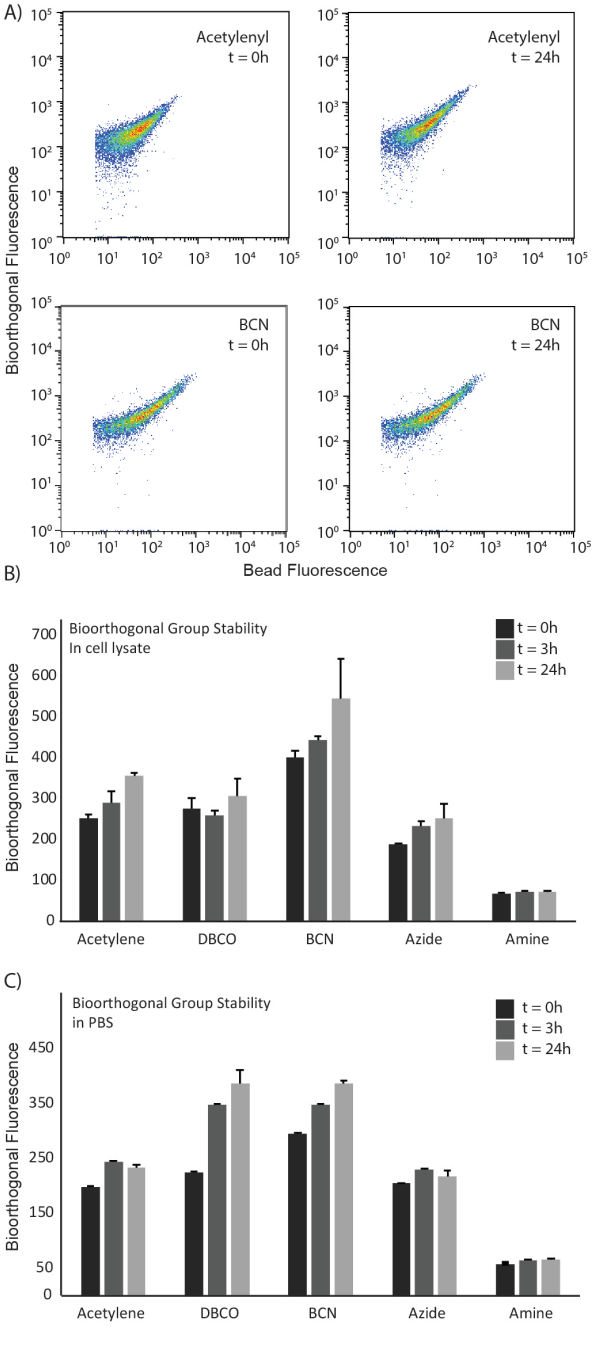

Figure 3. Assessment of stability of bioorthogonal groups in cell lysate or PBS. (**A**) plots at t = 0 and t = 24 of an incubation of acetylenyl-FluoSpheres **5** and BCN-FluoSpheres **9** in cell lysate. Y-axis shows the fluorescence stemming from bioorthogonal ligations, x-axis the intrinsic fluorescence of the spheres; (**B**) quantification of the median bioorthogonal fluorescence over time of the modified FluoSpheres **5-9** in cell lysate and (**C**) in PBS. (See also Figure S2-S4). N = 3 for all.

The bioorthogonal FluoSpheres were first incubated (in triplicate) in cell lysate (**Figure S3**) or PBS (**Figure S4**) for up to 24 h and subsequently reacted with AF488-azide or alkyne using the appropriate bioorthogonal ligation conditions (**Figure 3**, **Figure S2**). The beads were then injected directly into the flow cytometer for quantification of both bead-based and bioorthogonal-based fluorescent signal. The internal fluorescent dye could readily be used to discriminate beads from cellular debris of a similar size. Changes in the median fluorescence intensity (MFI) of the bioorthogonally introduced fluorophore allowed quantification of the remaining signal.

None of the bioorthogonal groups showed significant reduction in lysate (**Figure 3B**, **Figure S2/S3**) and PBS (**Figure 3C**, **Figure S2/S4**). An increase in signal over time was even observed, possibly due to de-aggregation of the beads in these media, increasing the available surface area and thus bioorthogonal groups. A similar effect was observed for the amine control beads, although to a much lesser extent, possibly by virtue of the more hydrophilic nature of these beads. When assessing whether the thiol and thiyl-reactivity could be recapitulated, it was indeed found that all groups completely degraded, in presence of a high concentration (250 mM) of glutathione (GSH) and the free radical photoinitiator 2-Hydroxy-4'-(2-hydroxyethoxy)-2-methylpropiophenone (25 mM) after 5 or 10 minutes irradiation with UV-light (145 μW/cm^2) to generate radicals *in-situ* (**Figure S2/S5**). Even without radicals, all bioorthogonal signal disappeared after incubation with 250 mM GSH for 30 minutes (**Figure S2/S6**). Radicals alone resulted in selective (partial) degradation of BCN, DBCO and azide (**Figure S2/S7**), confirming the suitability of this approach at least *in vitro.*

3.2.3 Stability of bioorthogonal FluoSpheres in cells

Next, the stability of bioorthogonal FluoSpheres **6-9** was tested in the endolysosomal environment of phagocytes (*in cellula*). DCs (DC2.4 cell line[58]) and macrophages (RAW264.7 cell line[59,60]) were used, as they are at the opposite ends of the property spectrum of phagocytes.[61] DC2.4 cells phagocytose in a controlled manner and use their oxidative burst to attenuate protease activity leading to improved antigen presentation, either by oxidizing cysteine proteases and decreasing the reductive capacity of the phagosome[62], or by limiting the acidification of the phagosome.[63,64] RAW264.7 cells are macrophage-like and have a very high phagocytic capacity.[65] They are also capable of producing Reactive Oxygen Species (ROS) in high amounts[66], as well as secondary ROS-metabolites through the action of MPO.[67]

The assay was designed in the following manner. The APCs were first allowed to take up the bioorthogonal FluoSpheres for 45 minutes (t = 0), after which uptake and the initial oxidative burst should be complete, as suggested in literature.[68] The cells were then washed and chased for 3 or 24 hours to determine to what extent the combination of acidification, thioreductase expression[25] and proteolysis[69,70] in the matured phagosome contributes to bioorthogonal handle degradation. Cells were then fixed and permeabilized (allowing free entry of bioorthogonal reagents and neutralization of the phagosomal compartment), ligated with a complementary bioorthogonal fluorophore, before quantification of the two fluorescent signals by flow cytometry (**Figure 4**, **Figure S8/S9**). Fluorescence in the red channel (FluoSpheres) was plotted against the green channel (AF488 coupled to the bioorthogonal groups). Quantification gates were set to exclude cells and debris that had not taken up beads (bead-negative cells). Bioorthogonal degradation was quantified by looking at the percentage of cells in which the bioorthogonal fluorescence had been reduced to the level of unmodified FluoSpheres **5** (**Figure 4A**).

The acetylenyl-groups on FluoSpheres **6** showed a remarkable stability in both DCs and macrophages (**Figure 4A/B** and **Figure S8/S9**) with <6% degradation observed at any time point in either cell types. BCN-groups showed the poorest stability, especially to the intracellular conditions found in macrophages: 79% (±2%) of cells had fully degraded all bioorthogonal groups after 24h). DBCO-groups showed a moderate stability (36% ±1% degradation after 24h). Azide-modified spheres showed very poor uptake in macrophages preventing the quantification of their degradation in these cells. In DCs, the degradation of azides was minimal (**Figure 4A**, **Figure S8/S9**). Attempts to further enhance degradation by stimulating the oxidative burst by adding LPS or a combination of phorbol-12-myristoyl-13-acetate (PMA)[71] and yeast-derived zymosan particles[72,73] to both cell lines did not yield a further increase in degradation (**Figure S10/S11**). Moreover, these stimuli either resulted in reduced degradation or extensive cell death over the time course of the experiment, again preventing quantification of the degradation.

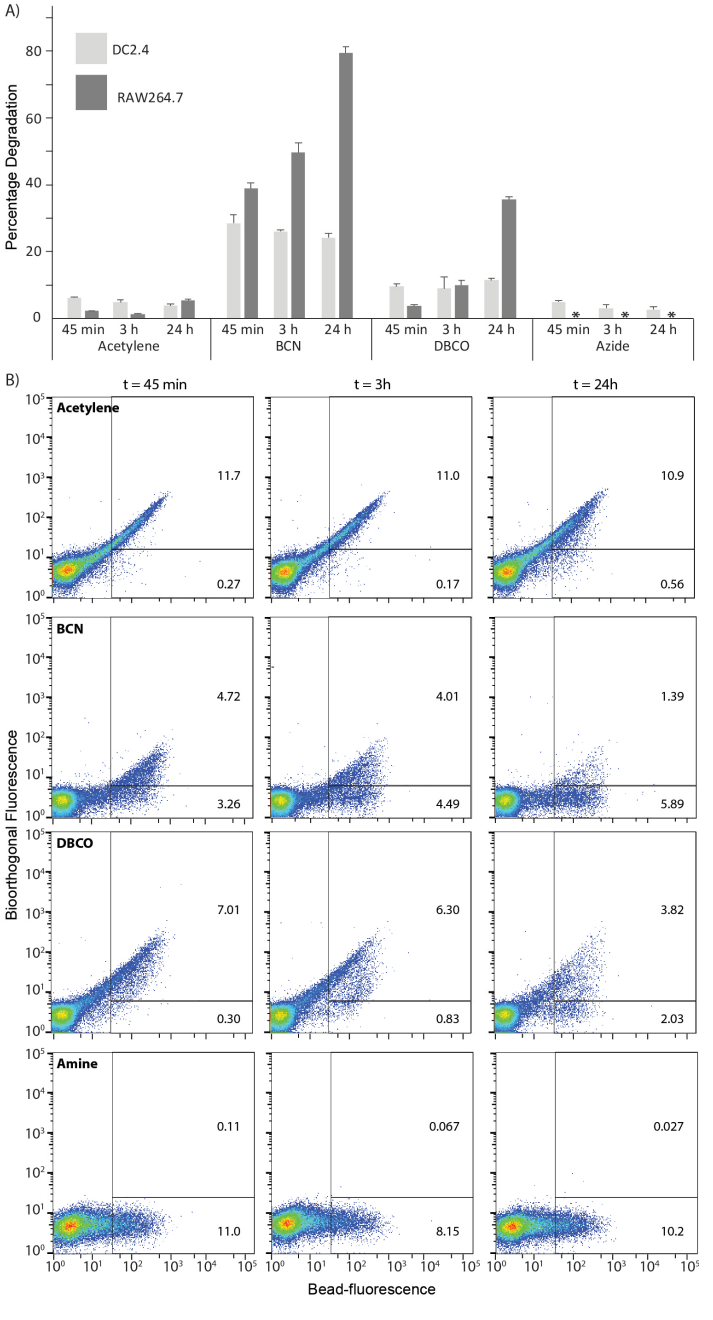

Figure 4. Quantification of bioorthogonal group stability. (**A**) Percentage of degraded bioorthogonal groups after incubation in DCs (DC2.4) or macrophages (RAW264.7), as quantified by illustrated gating strategy. Cells that had not taken up beads (bead-negative cells) were excluded from the gated area, cells in which the bioorthogonal signal had fully degraded to background (gate b) were counted, as were the cells still positive for bioorthogonal signal (gate a); (**B**) Quantification of percentage macrophages (RAW264.7) containing degraded beads (a/[a+b]) (see also Figure S9). Indicated values are fractions of total cell count.

Since only the strained alkynes showed degradation but not the terminal acetylene or azide groups, it was hypothesized that this might be caused by radicals during the oxidative burst, as extensive degradation was already observed at the earliest time point. It was hypothesized that the potential culprits could be either superoxide, the superoxide metabolite H_2O_2, which can reach levels of 100 µM if MPO is inhibited[74], or one of the species produced by MPO, such as hypochlorous acid (HOCl). This species is produced by MPO in presence of imported chloride and can reach high µM concentrations in the phagosome.[18,75] However, HOCl-production is well established in neutrophils but less is known about its intracellular concentrations in DCs and macrophages, due to the interplay between MPO and chloride channels in these cells.[75–78] Other potential reaction partners could be hydroxyl-radicals produced through Fenton chemistry, or thiol oxidation products produced during the oxidative burst.[19]

To determine the responsible species, the *in vitro* system was used once more to assess whether the reactive species in the endosome could degrade bioorthogonal handles at the concentrations found in the phagosome (**Table 1**). **6-9** were incubated with hydrogen peroxide concentrations of 50, 100 or 200 µM at pH 7.4 or 5.0, either in the dark (**Figure S12**) or whilst exposed to UV radiation (145 µW/cm^2 for 5 minutes, **Figure S13**). All particles proved stable under these conditions suggesting that primary products of oxidative burst are not responsible for the in cell-degradation. Incubation with the MPO product HOCl at 50, 100 or 200 µM at pH 7.4 showed a surprisingly similar stability pattern as observed in both macrophages and DCs: **8** and **9** were degraded under these conditions, whereas **5** and **6** remained stable (**Figure S14**). The degradation of BCN and DBCO occurred at neutral pH but not at acidic pH, which is in agreement with the relatively high pH during the oxidative burst[64,79] and the lack of further degradation observed after t = 0 *in cellula*, when acidification occurs. The stability of the bioorthogonal FluoSpheres to GSH (100 µM or 1 mM) in combination with *in situ*-generated radicals was also assessed to investigate the potential role of thiols and thiyl-radicals. Surprisingly, the strained alkynes proved stable to these conditions, whereas the acetylene and azide were degraded under acidic incubation with GSH and radicals (**Figure S15**). This makes the thiyl-radical species an unlikely candidate for the observed degradation *in cellula*.

Alternatively, thiols can be oxidized by ROS-metabolites such as H_2O_2 or HOCl to form short-lived sulfenic acids (SOH)[80,81], which could very well be responsible for the degradation of the strained alkynes, as these have been described as sulfenic acid traps.[82] However, it is not straightforward to reproduce these transient

compounds *in vitro* due to rapid overoxidation. Although HOCl appears to play a part in the observed degradation, the true mechanism may very well be a combination of the above factors, or a set of conditions as yet undescribed.

Table 1. Overview of bioorthogonal group stability to degradative conditions *in vitro* and *in cellula*. The relevant conditions are listed and the stability of the corresponding bioorthogonal groups is indicated with green (negligible degradation), red (significant degradation) or grey (unclear due to specified reason). RPI = radical photoinitiator. Asterisk (*) indicates the formation of radicals during the indicated conditions.

Test conditions	Acetylene	BCN	DBCO	Azide
PBS				
Cell lysate				
1% APS + 0.5% TEMED*				
25 mM RPI				
25 mM RPI + UV*				
200 µM H_2O_2 (pH 7.4)				
200 µM H_2O_2 (pH 7.4) + UV*				
50 µM HOCl (pH 7.4)				
200 µM HOCl (pH 7.4)				
200 µM H_2O_2 (pH 5) + UV*				
200 µM H_2O_2 (pH 5)				
50 µM HOCl (pH 5)				
200 µM HOCl (pH 5)				
1 mM GSH (pH 7.4)				
1 mM GSH (pH 7.4) + H_2O_2				
1 mM GSH (pH 7.4) + RPI + UV*				
1 mM GSH (pH 5)				
1 mM GSH (pH 5) + H_2O_2				
1 mM GSH (pH 5) + RPI + UV*				
2.5 mM GSH (1:3 MeOH/H_2O)				
250 mM GSH (1:3 MeOH/H_2O)				
250 mM GSH (1:3 MeOH/H_2O) + RPI + UV*				
In dendritic cells				Background
In dendritic cells + LPS				Background
In dendritic cells + zymosan/PMA				Background
In macrophages				Background
In macrophages + LPS			Not tested	Not tested
In macrophages + zymosan/PMA	Cell death	Cell death	Cell death	Cell death
In macrophages + NOX2 inhibitor	Not tested		Not tested	Not tested

3.3 Conclusion

Using a straightforward bead-based assay to test the stability of bioorthogonal handles within the endolysosomal compartments of dendritic cells, a striking difference was observed in the disappearance of reactivity between strained alkynes and terminal alkynes in phagocytes. These are obviously not the only class of bioorthogonal reactions available to date. Many other bioorthogonal ligation reactions have been developed[83], such as the Inverse Electron-Demand Diels-Alder (IEDDA) cycloaddition[84,85], the [4+1] photoclick[86], diazo-based ligation reactions[87], and many more. Most of these reactions have been incompletely profiled with regards to their *in cellula* stability and it is thus foreseen that this simple assay could also provide insight into the biochemical stability of these groups and those yet to be discovered.

3.4 Experimental

Mammalian cell culture and lysate preparation

RAW264.7 cells (Merck) were cultured in DMEM (Sigma-Aldrich) supplemented with 10% heat-inactivated fetal calf serum (FCS), 1% GlutaMAX and 1% penicillin/streptomycin. DC2.4 cells (Merck) were cultured in IMDM (Sigma-Aldrich) supplemented with 10% heat-inactivated fetal calf serum (FCS), 1% GlutaMAX, 1% penicillin/streptomycin, 10 mM HEPES, 1 mM pyruvate and 1x MEM non-essential amino-acids (Life Technologies). 2-Mercaptoethanol (final concentration: 50 µM, Life Technologies) was freshly added to the medium every time after splitting the cells. Cells were grown at 37 °C under a humidified atmosphere containing 5% CO_2. Cell lysates were obtained by harvesting DC2.4 cells at confluence, washing with ice-cold PBS and subsequently resuspending in 10 µL lysis buffer (150 mM NaCl, 1% IGEPAL in 50 mM HEPES pH 7.4) per $1x10^6$ cells. The resulting suspension was subjected to a triple freeze-thaw cycle in liquid nitrogen and subsequently diluted 1:100 in ice-cold PBS and stored in aliquots at -20 °C for until further use.

Bioorthogonal group-functionalization and characterization of polystyrene fluorescent beads

FluoSpheres® Amine-Modified Microspheres, 0.2 µm, red fluorescent (580/605), 2% solids (Thermo Scientific; F8763) were functionalized with a series of bioorthogonal groups (**Figure 2**) through a *N*-hydroxysuccinimide (NHS) ester coupling to the free amines on the bead surface. 100 µL of bead stock suspension was diluted 1:2 in milliQ H_2O and washed twice by centrifugation (30 min, 30000 rcf, 10 °C). After washing, the beads were resuspended in 160 µL PBS after which 0.5 µmol NHS-reagents in 40 µL DMSO was added to the beads to end up with a final concentration of 20% DMSO. The reaction mixture was shaken for 2 days, 20 °C & 1000 rpm after which the conjugated beads were washed 4x with 200 µL 20% DMSO in MilliQ, 1 x with 200 µL MilliQ, resuspended in 1 mL milliQ and stored at 4 °C until further use. Control (unmodified amine) beads were treated similarly, omitting only the NHS-modified bioorthogonal groups. The resulting FluoSpheres **5-9** were first characterized by ligating to Alexa Fluor 488 (AF488) by ccHc (1 mM copper sulfate, 10 mM sodium ascorbate, 1 mM THPTA ligand, 10 mM aminoguanidine and 2 µM AF488-alkyne or azide in 100 mM HEPES pH 7.4) or spHc (2 µM AF488-azide in 100 mM HEPES pH 7.4) for 1 hour at RT in the dark, to determine the relative labeling density. Alternatively, FluoSpheres **5-9** were reacted with fluorescamine (1 mM in PBS) for 30 min at RT in the dark, to determine the relative amount of free amines remaining after ligation of the bioorthogonal groups. The resulting fluorophore-modified beads were further diluted 1:20 in FACS

buffer (1% FCS, 1% BSA, 0.1% NaN_3 and 2 mM EDTA in PBS pH 7.4) and immediately measured by flow cytometry.

In vitro bioorthogonal group stability assay

Buffer or cell lysate

1 µL bioorthogonal group-functionalized or control bead suspension was diluted 1:100 in PBS buffer or cell lysate and shaken at 37 °C, 600 rpm for the indicated time points (0, 3, 24 h). After the indicated time points, the beads were ligated to AF488 by ccHc or spHc for 1 hour at RT in the dark. The resulting fluorophore-modified beads were further diluted 1:20 in FACS buffer and immediately measured by flow cytometry.

Oxidative conditions (Lo Conte conditions[32])

1 µL bioorthogonal group-functionalized or control bead suspension was diluted 1:100 in 250 mM glutathione (GSH) and 10% (25 mM) free radical photoinitiator (RPI) 2-Hydroxy-4'-(2-hydroxyethoxy)-2-methylpropiophenone (Sigma-Aldrich; 410896) in 1:3 MeOH/H_2O in open glass tubes. Samples were exposed to UV-irradiation (280-320 nm, 145 µW/cm^2) for 5 or 10 minutes. After a total incubation of 30 minutes, the beads were ligated to AF488 by ccHc or spHc for 1 hour at RT in the dark. The resulting fluorophore-modified beads were further diluted 1:20 in FACS buffer and immediately measured by flow cytometry. Additional experiments were performed with either 2.5 or 250 mM GSH or 25 mM free radical photoinitiator under the same reaction conditions to observe their individual effects.

Physiological oxidative conditions

1 µL bioorthogonal group-functionalized or control bead suspension was diluted 1:100 in 0.1 M phosphate buffer (pH=7.4) or 0.1 M citrate buffer (pH=5) with 1 mM or 100 µM GSH and 10% free radical photoinitiator. Open glass tubes were used for incubation. Samples were exposed to UV- irradiation (280-320 nm, 145 µW/cm^2) for 5 minutes. After total incubation of 30 minutes, the beads were ligated to AF488 by ccHc or spHc and immediately measured by flow cytometry as described before. Additional experiments were performed with 50, 100 and 200 µM H_2O_2 or NaClO in 0.1 M phosphate buffer (pH=7.4) or in 0.1 M citrate buffer (pH=5). Incubation in H_2O_2 was performed with and without 5 minutes of UV irradiation, while incubation in NaClO was performed only without UV-irradiation.

In cellula bioorthogonal group stability assay in dendritic cells and macrophages

DC2.4 or RAW264.7 cells were seeded onto 6-well plates containing $1x10^6$ cells/well and rested for at least 3 hours. Cells were pulsed with 10 µL beads for 45 min, washed with PBS and fresh medium was added for further incubation of indicated time points (0, 3, 24 h). After incubation, all cells were harvested, washed twice with PBS and fixed in suspension in 4% PFA in PBS for 20 min at RT. Next, cells were washed twice with PBS, gently permeabilized with 0.1% IGEPAL in PBS for 20 min at RT and blocked with 3% BSA in PBS twice for 15 minutes. The cells containing bioorthogonal beads were then reacted with a fluorophore by ccHc or spHc for 1 hour at RT in the dark. The resulting cells, containing fluorophore-modified beads were finally washed twice with FACS buffer and resuspended in FACS buffer for flow cytometry measurements.

In cellula pre-clicked beads stability assay in dendritic cells

Pre-clicked FluoSpheres were prepared by reacting 100 µL acetylenyl-functionalized FluoSpheres with AF488-azide by ccHc for 1 hour at RT in the dark. The reaction was quenched by adding 5 mM EDTA and 5% DMSO and washed with 100 µL MilliQ by centrifugation (30 min, 30000 rcf, 10°C). Pre-clicked beads were resuspended in 100 µL MilliQ and stored at 4 °C until further use. Cell experiments were performed as described above. After fixation, cells were washed twice with PBS and resuspended in FACS buffer for flow cytometry measurements.

Flow cytometry

All flow cytometry measurements were performed on a Guava® easyCyte 12 HT Sampling Flow Cytometer and data analysis was performed with FlowJo V10. Beads in suspension were gated manually using internal bead fluorescence (to exclude signal resulting from debris). The resulting data was visualized in pseudocolor dot plots, plotting the internal bead fluorescence (Cytometer Channel RED-V) against the external fluorophore fluorescence (Cytometer Channel GRN-B) to show the correlation between external and internal fluorescence, as a measure for the number of stable bioorthogonal groups per bead.

Quantification of degradation

The relative percentage of stable bioorthogonal groups in DC2.4 cells was quantified by first excluding cells containing insufficient beads for accurate differentiation and subsequently dividing the remaining cells into two groups; those containing fully degraded bioorthogonal groups and those containing unaffected or partially degraded bioorthogonal groups. The ratio of cells with fully

degraded bioorthogonal groups to the total cell count (**Figure 4A**; b/[a+b]), provided a robust estimate of the percentage of degraded bioorthogonal groups, avoiding subjective interpretation of the data and minimizing false positives.

3.5 Supplemental Figures

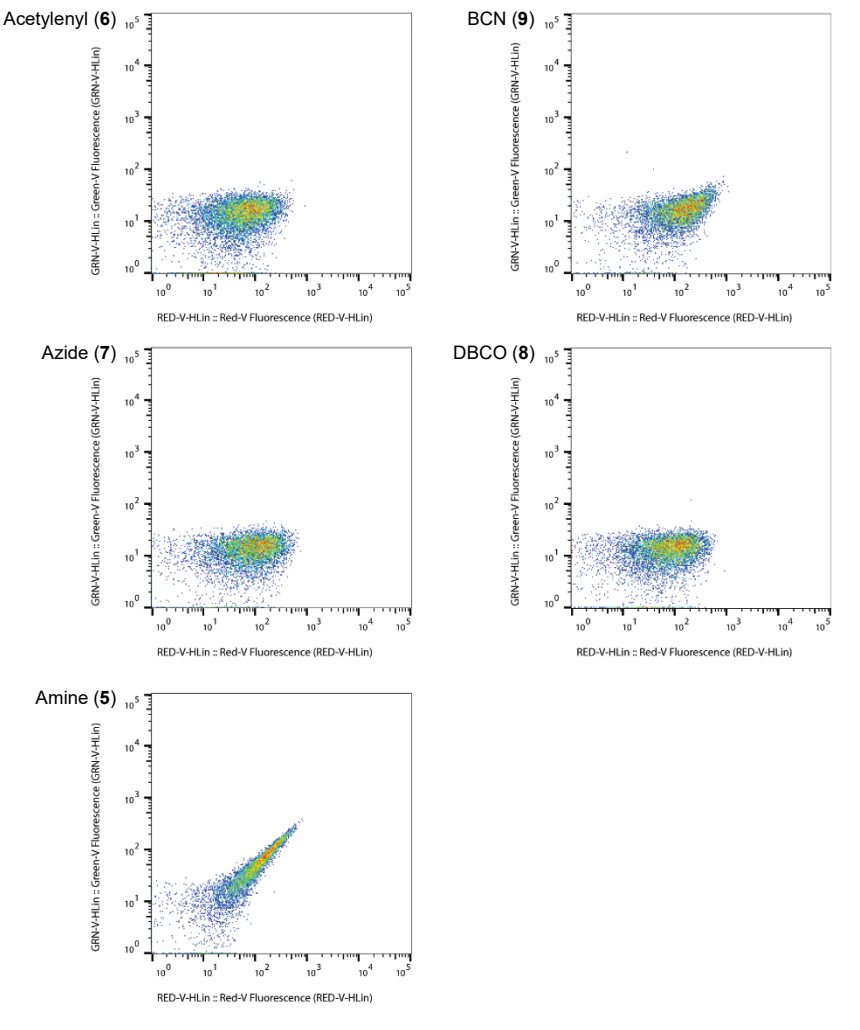

Figure S1. Visualization of remaining unreacted amines on FluoSpheres **5**-**9** with fluorescamine. FluoSpheres, GRN-V: fluorescamine, arbitrary fluorescence units. Intermediate patterns were found for suboptimal modification conditions (data not shown).

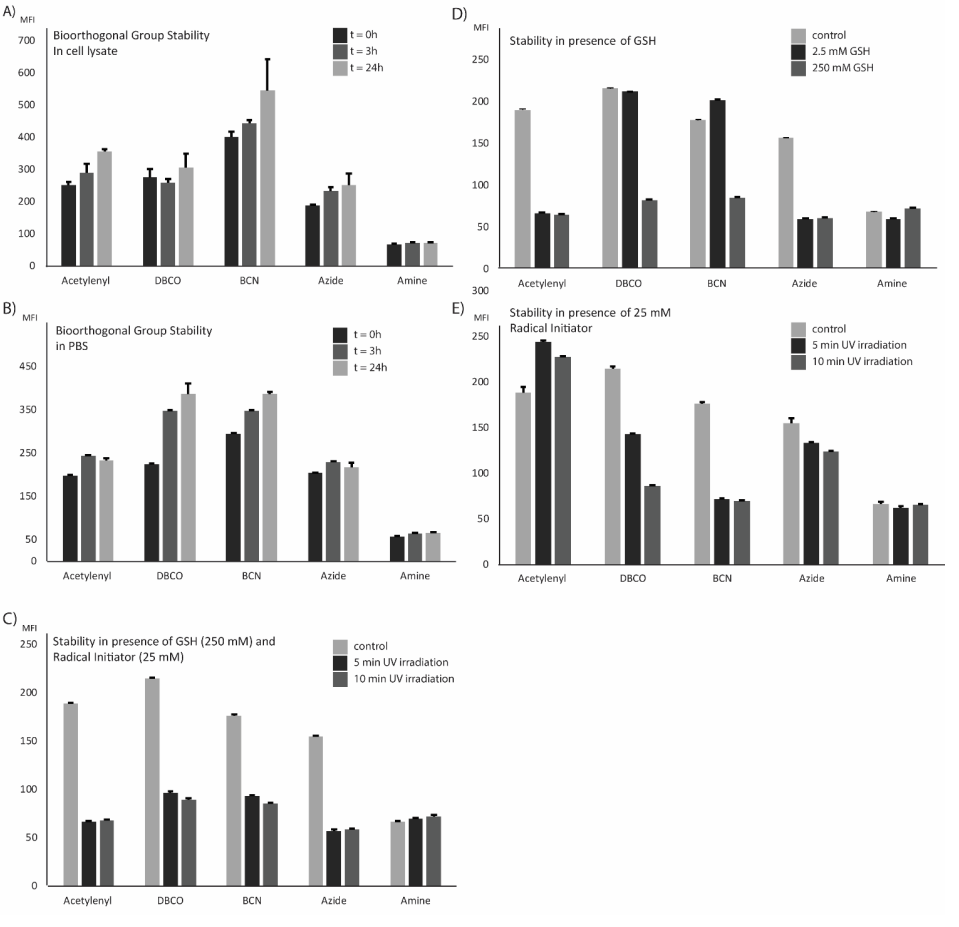

Figure S2. Bioorthogonal group stability of FluoSpheres **5-9** in vitro, quantified using the median fluorescence intensity (MFI) of the GRN-B channel (AF488) on the y-axis. (**A**) Stability in cell lysate: no degradation of any groups is observed. (**B**) Stability in PBS; showing no degradation of any groups. (**C**) Stability in the presence of GSH and in situ-generated radicals, after UV irradiation and 30 minutes of total incubation; showing near complete degradation for all groups tested. (**D**) Stability in the presence of GSH alone after 30 minutes of incubation; showing complete degradation for acetylene **6** and azide **7** already at 2.5 mM, while DBCO **8** and BCN **9** are degraded only at 250 mM. (**E**) Stability in the presence of in situ-generated radicals alone, after UV irradiation with a chase totaling 30 minutes of incubation; on-sphere BCN **9** is degraded after 5 minutes irradiation, DBCO 8 becomes increasingly degraded with increased UV-irradiation. Acetylene **6** and azide **7** are degraded by 2.5 mM GSH plus radicals, but are resistant to radicals alone. N=3 for all experiments. Raw data underlying this quantification are presented in Figure S3-S7.

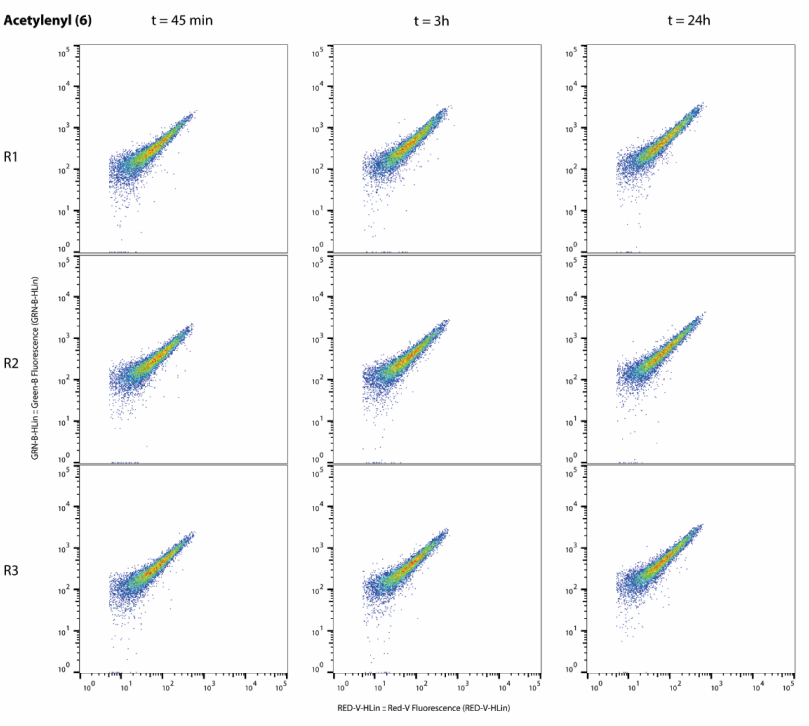
Acetylenyl (6)
t = 45 min
t = 3h
t = 24h
R1
R2
R3
GRN-B-HLin :: Green-B Fluorescence (GRN-B-HLin)
RED-V-HLin :: Red-V Fluorescence (RED-V-HLin)

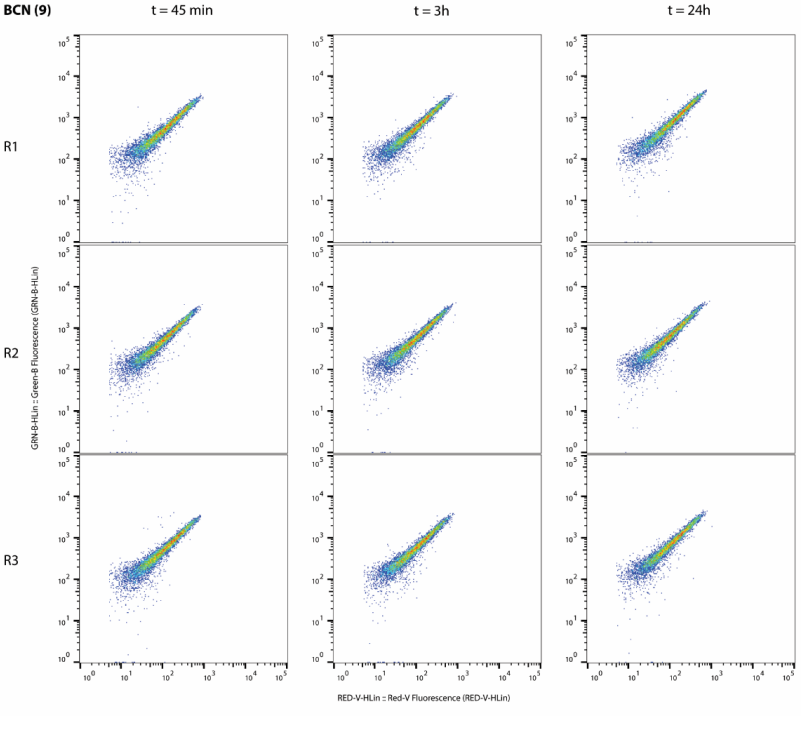
BCN (9)
t = 45 min
t = 3h
t = 24h
R1
R2
R3
GRN-B-HLin :: Green-B Fluorescence (GRN-B-HLin)
RED-V-HLin :: Red-V Fluorescence (RED-V-HLin)

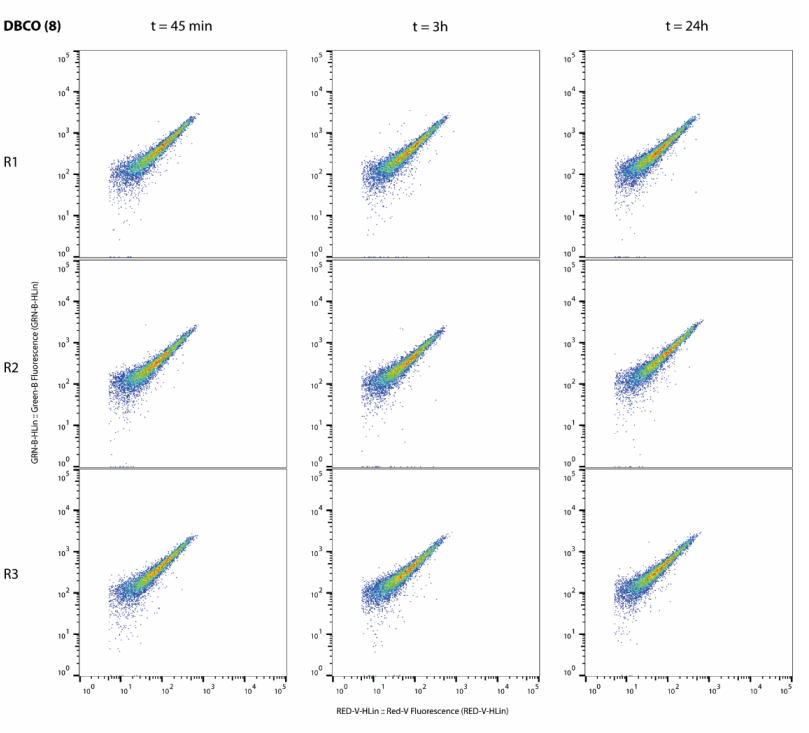
DBCO (8)
t = 45 min
t = 3h
t = 24h
R1
R2
R3
GRN-B-HLin :: Green-B Fluorescence (GRN-B-HLin)
RED-V-HLin :: Red-V Fluorescence (RED-V-HLin)

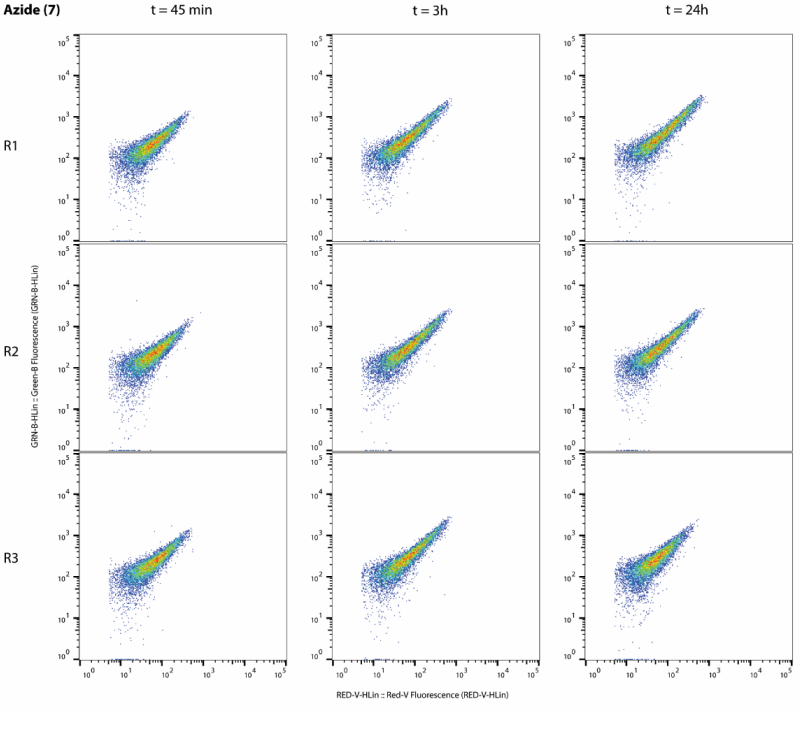
Azide (7)
t = 45 min
t = 3h
t = 24h
R1
R2
R3
GRN-B-HLin :: Green-B Fluorescence (GRN-B-HLin)
RED-V-HLin :: Red-V Fluorescence (RED-V-HLin)

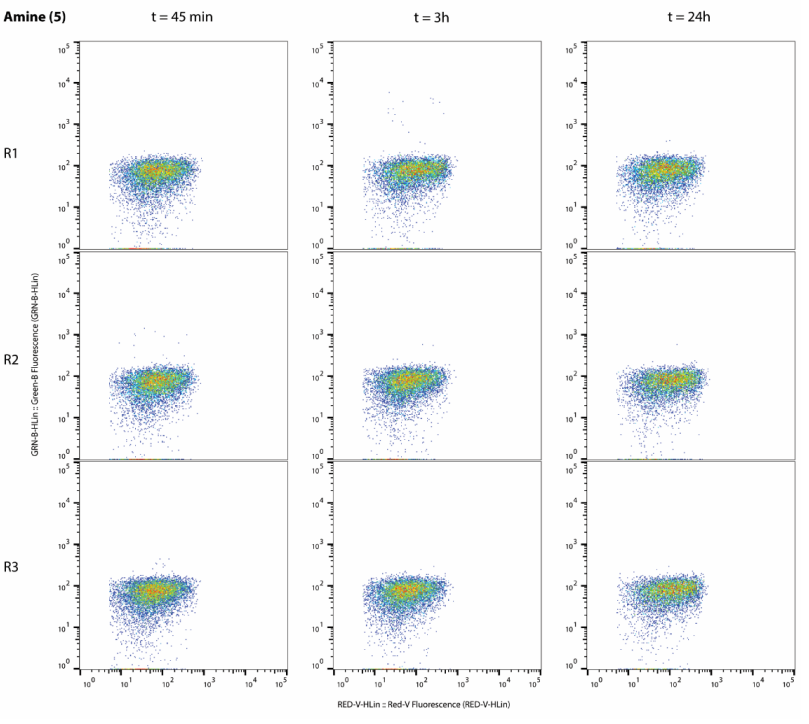

Figure S3. Stability assessment of bioorthogonal groups in DC2.4 cell lysate. None of the bioorthogonal groups tested show any degradation over the entire time course of 24h. Amine **5** was included as a control. N=3 for all experiments (R1-3).

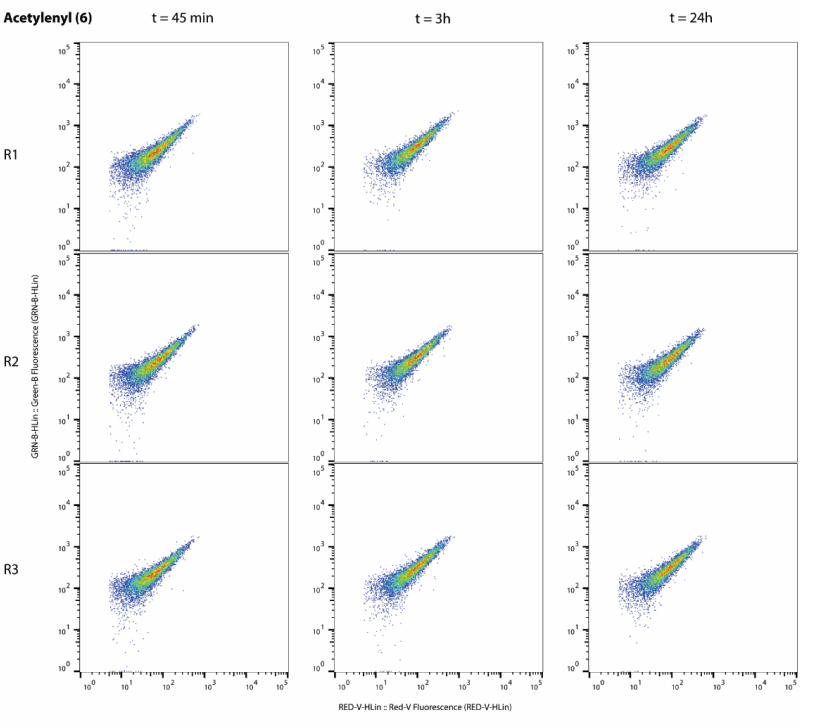
Acetylenyl (6)
t = 45 min
t = 3h
t = 24h
R1
R2
R3
GRN-B-HLin :: Green-B Fluorescence (GRN-B-HLin)
RED-V-HLin :: Red-V Fluorescence (RED-V-HLin)

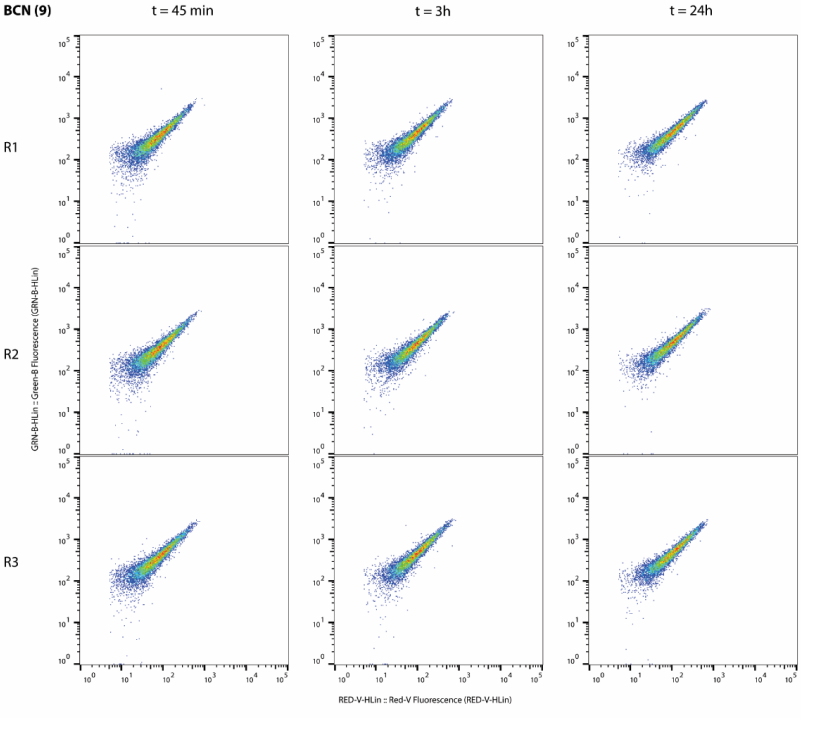
BCN (9)
t = 45 min
t = 3h
t = 24h
R1
R2
R3
GRN-B-HLin :: Green-B Fluorescence (GRN-B-HLin)
RED-V-HLin :: Red-V Fluorescence (RED-V-HLin)

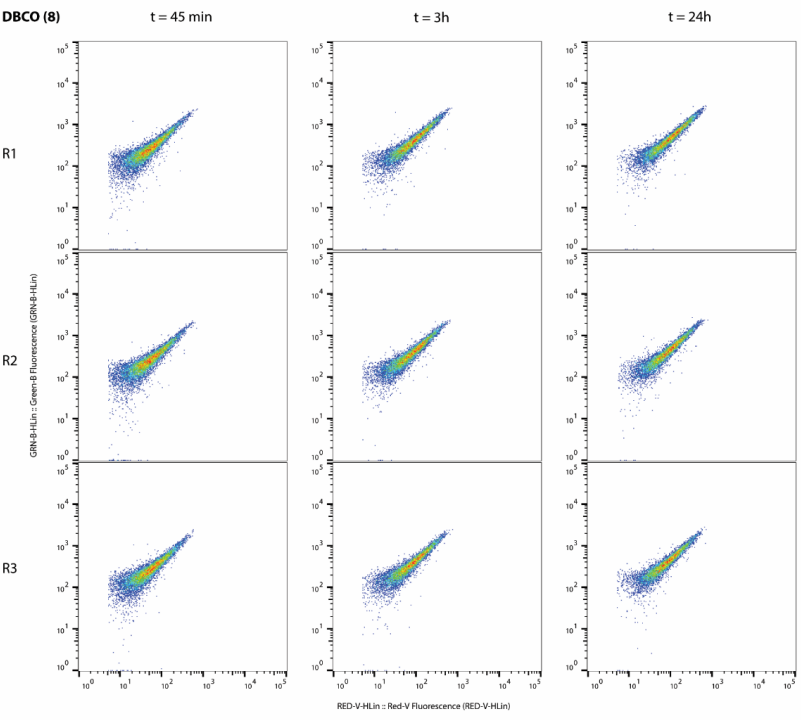
DBCO (8)
t = 45 min
t = 3h
t = 24h
R1
R2
R3
GRN-B-HLin :: Green-B Fluorescence (GRN-B-HLin)
RED-V-HLin :: Red-V Fluorescence (RED-V-HLin)

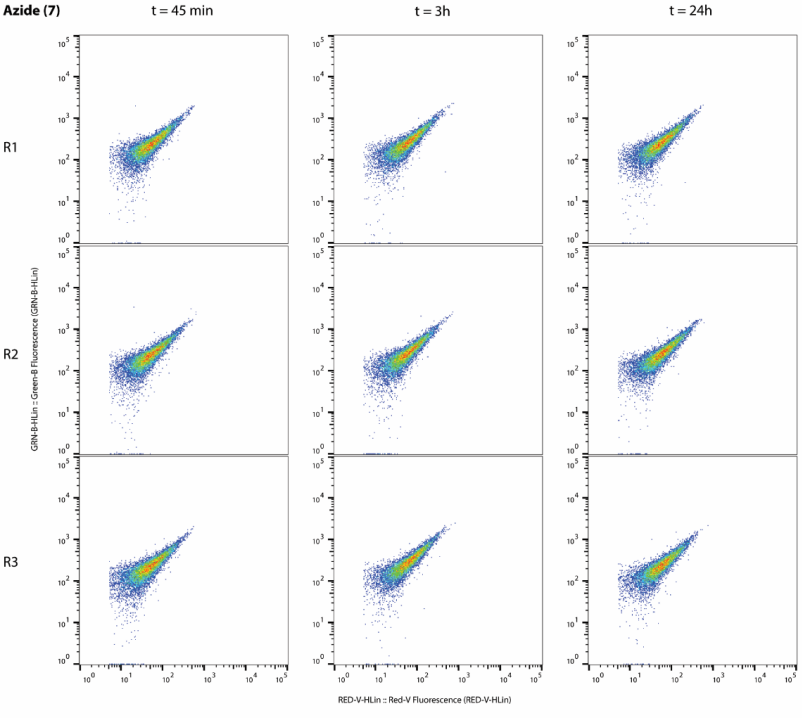
Azide (7)
t = 45 min
t = 3h
t = 24h
R1
R2
R3
GRN-B-HLin :: Green-B Fluorescence (GRN-B-HLin)
RED-V-HLin :: Red-V Fluorescence (RED-V-HLin)

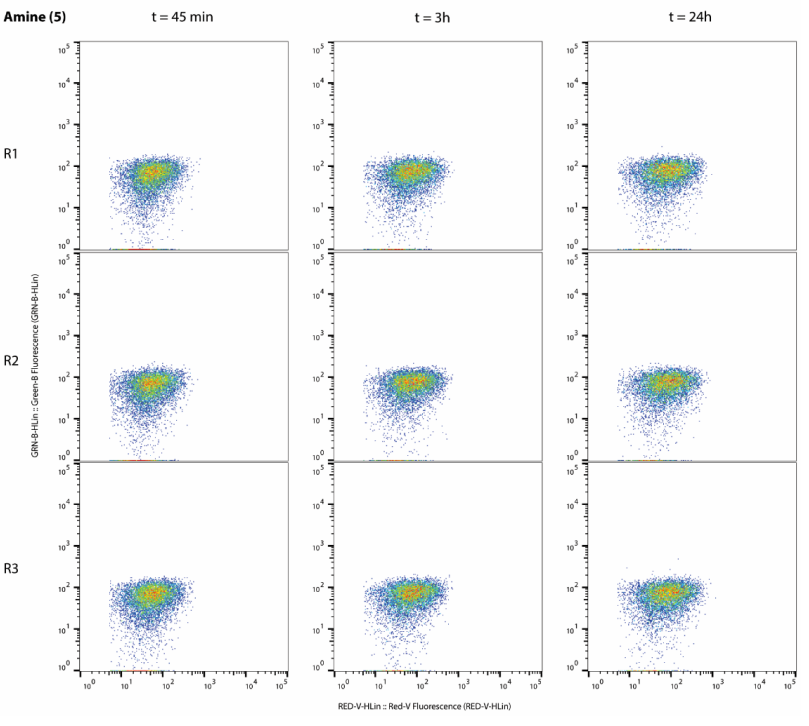

Figure S4. Stability assessment of bioorthogonal groups in PBS. None of the bioorthogonal groups tested show any degradation over the entire time course of 24h. N=3 for all experiments (R1-3) shown.

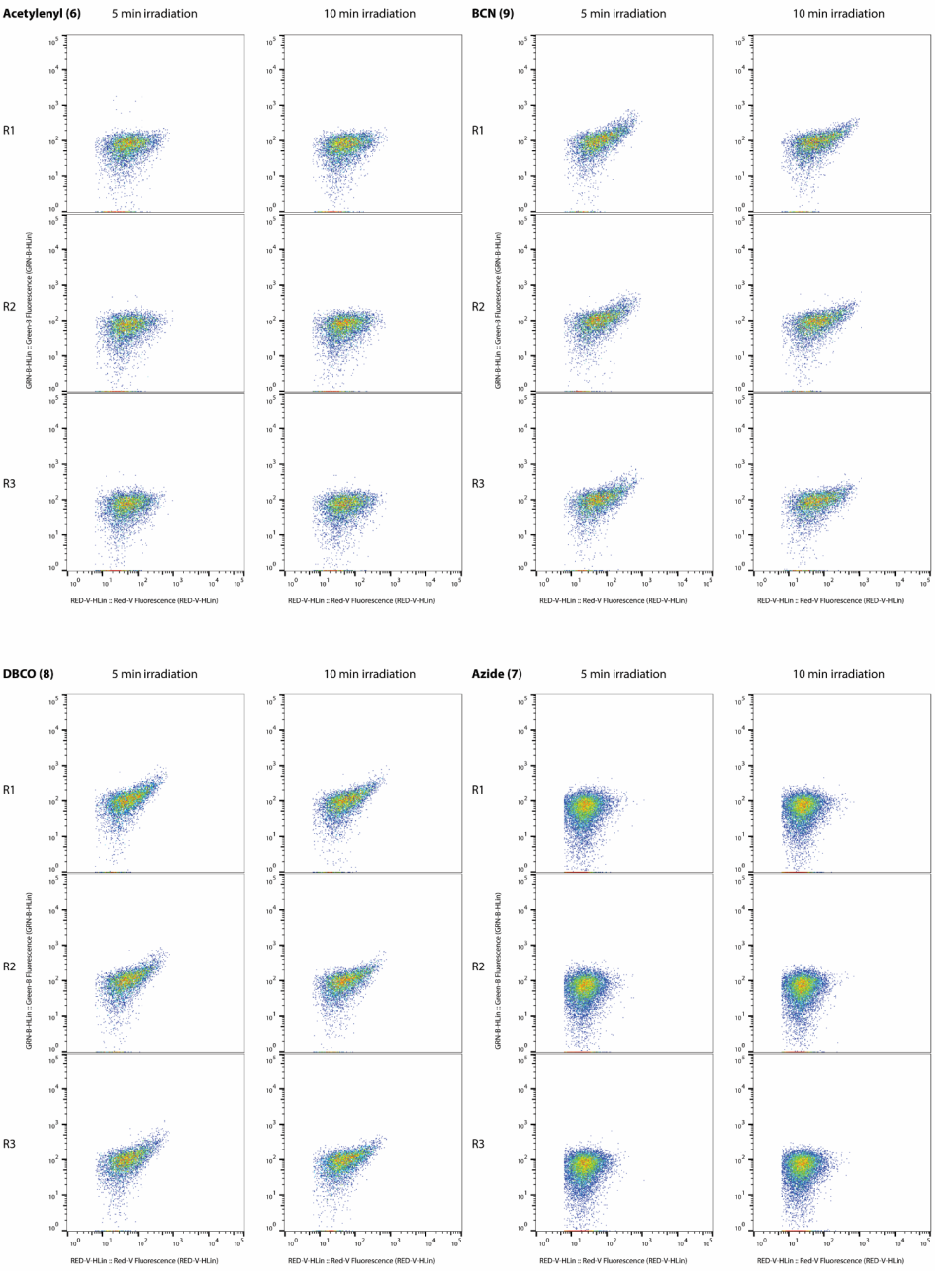
Acetylenyl (6)
5 min irradiation
10 min irradiation
BCN (9)
5 min irradiation
10 min irradiation
DBCO (8)
5 min irradiation
10 min irradiation
Azide (7)
5 min irradiation
10 min irradiation
R1
R2
R3
GRN-B-HLin :: Green-B Fluorescence (GRN-B-HLin)
RED-V-HLin :: Red-V Fluorescence (RED-V-HLin)

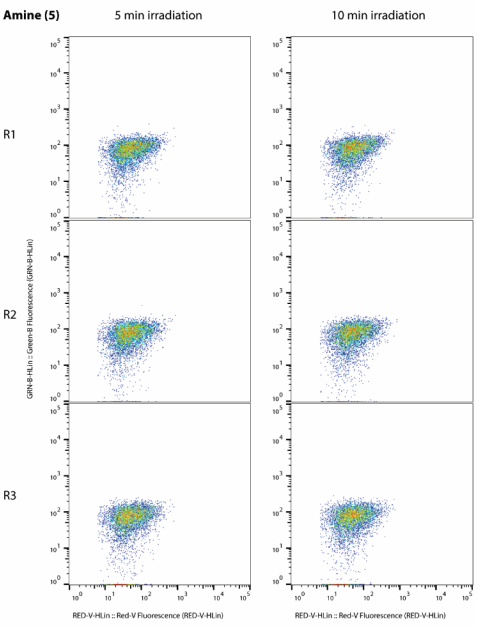

Figure S5. Stability assessment of bioorthogonal groups in 250 mM GSH and 25 mM light-activated radical initiator in MeOH/H2O (1:3). Samples were exposed for 5 or 10 minutes to UV-irradiation (280-320 nm, 145 µW/cm2), followed by incubation to a total time of 30 minutes. N=3 for all experiments (R1-3) shown.

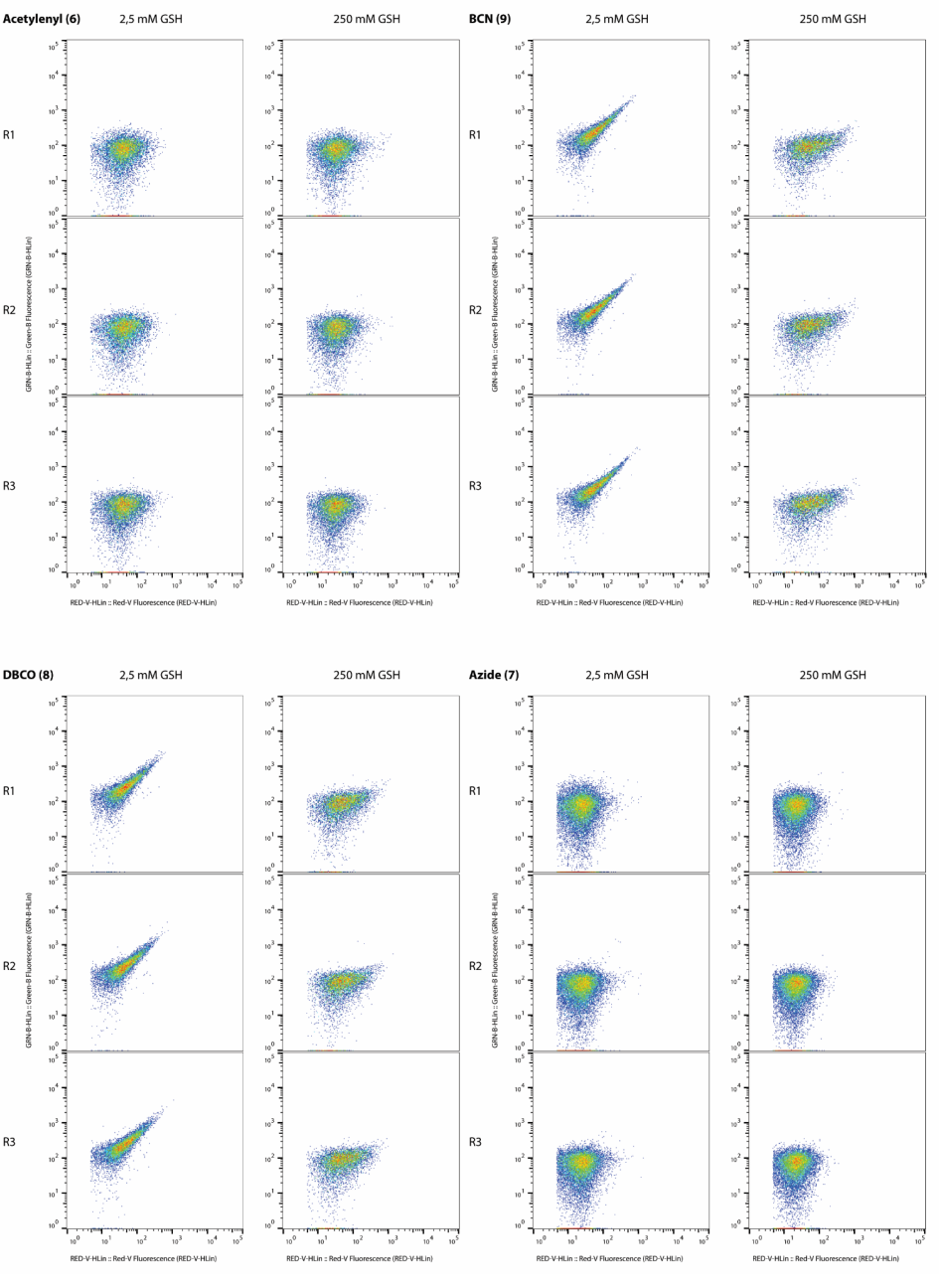
Acetylenyl (6)
2,5 mM GSH
250 mM GSH
BCN (9)
2,5 mM GSH
250 mM GSH
DBCO (8)
2,5 mM GSH
250 mM GSH
Azide (7)
2,5 mM GSH
250 mM GSH
R1
R2
R3
GRN-B-HLin :: Green-B Fluorescence (GRN-B-HLin)
RED-V-HLin :: Red-V Fluorescence (RED-V-HLin)

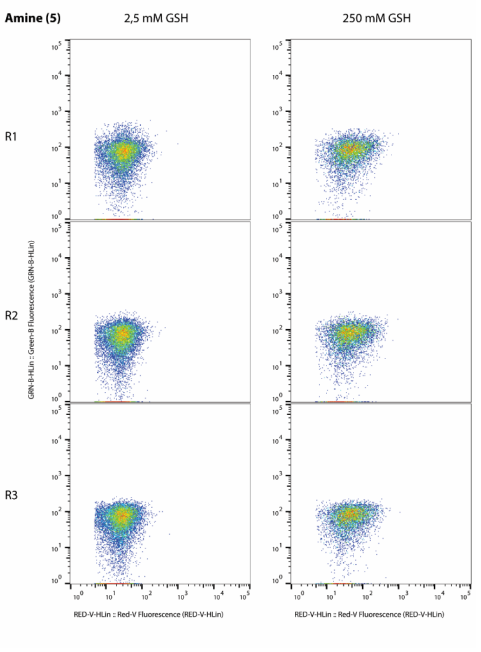

Figure S6. Stability assessment of bioorthogonal groups in 2.5 or 250 mM GSH. N=3 for all experiments (R1-3) shown.

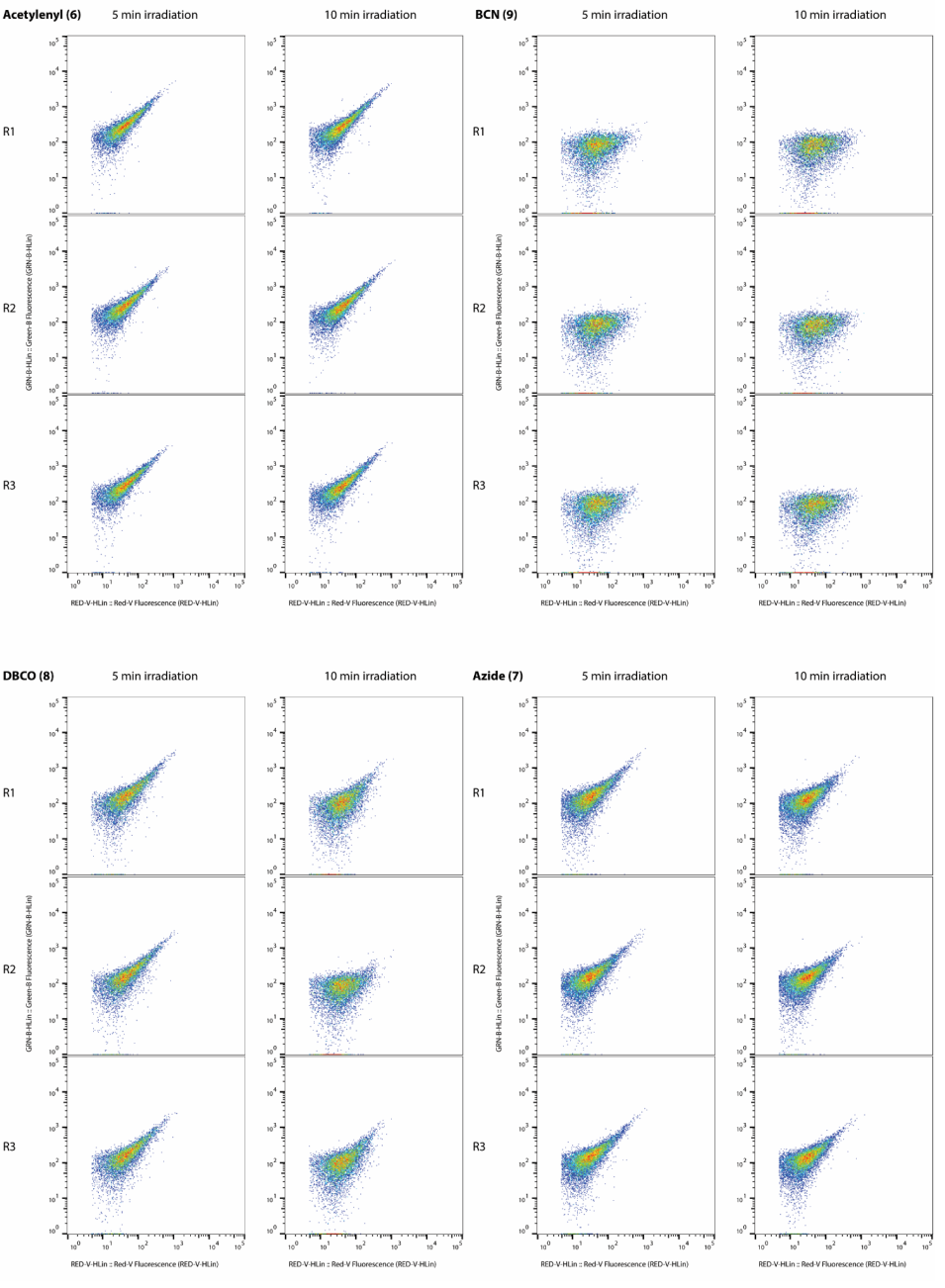
Acetylenyl (6)
5 min irradiation
10 min irradiation
BCN (9)
5 min irradiation
10 min irradiation
DBCO (8)
5 min irradiation
10 min irradiation
Azide (7)
5 min irradiation
10 min irradiation
R1
R2
R3
GRN-B-HLin :: Green-B Fluorescence (GRN-B-HLin)
RED-V-HLin :: Red-V Fluorescence (RED-V-HLin)

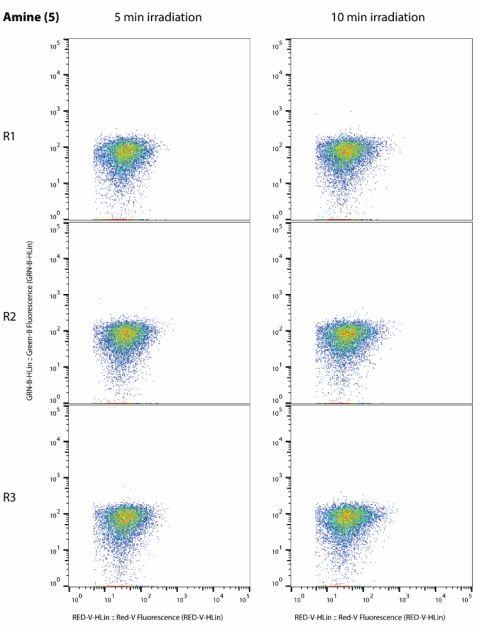

Figure S7. Stability assessment of bioorthogonal groups incubated in 25 mM light-activated radical initiator in MeOH/H2O (1:3). Samples were exposed to UV-irradiation (280-320 nm, 145 µW/cm2) for 5 or 10 minutes, followed by incubation totalling 30 minutes including irradiation time N=3 for all experiments shown (R1-3).

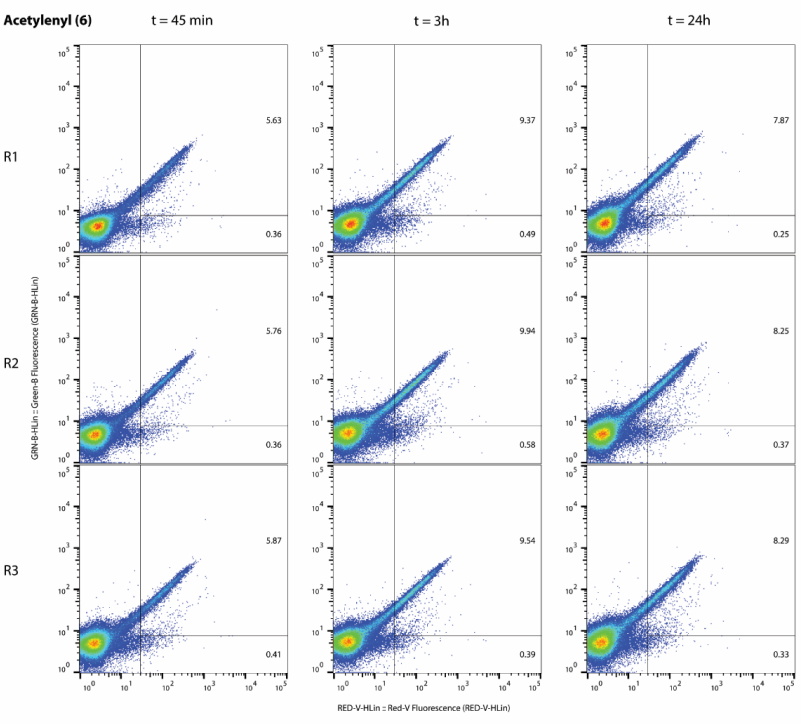
Acetylenyl (6)
t = 45 min
t = 3h
t = 24h
R1
R2
R3
5.63
0.36
9.37
0.49
7.87
0.25
5.76
0.36
9.94
0.58
8.25
0.37
5.87
0.41
9.54
0.39
8.29
0.33
GRN-B-HLin :: Green-B Fluorescence (GRN-B-HLin)
RED-V-HLin :: Red-V Fluorescence (RED-V-HLin)

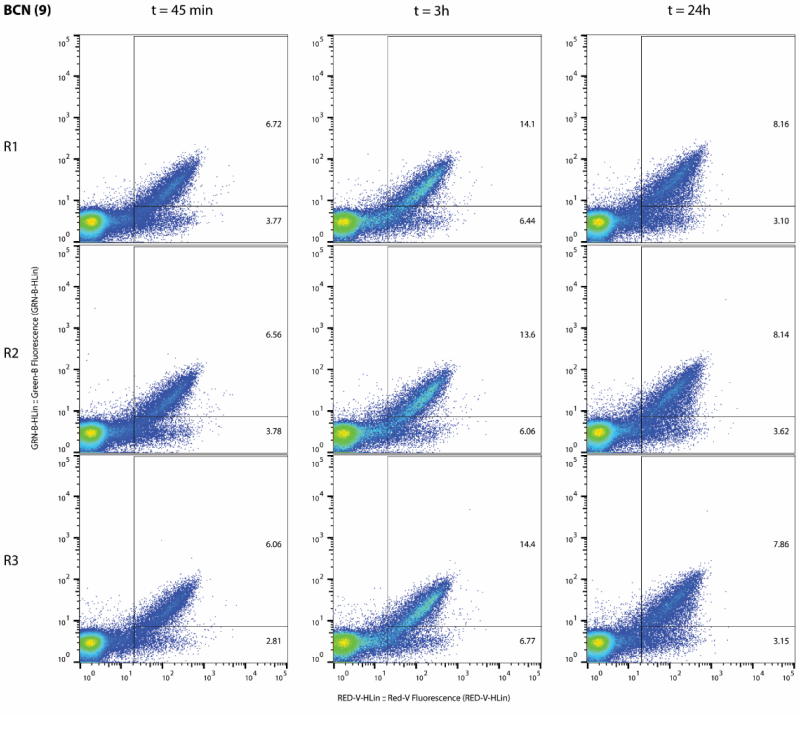
BCN (9)
t = 45 min
t = 3h
t = 24h
R1
R2
R3
6.72
3.77
14.1
6.44
8.16
3.10
6.56
3.78
13.6
6.06
8.14
3.62
6.06
2.81
14.4
6.77
7.86
3.15
GRN-B-HLin :: Green-B Fluorescence (GRN-B-HLin)
RED-V-HLin :: Red-V Fluorescence (RED-V-HLin)

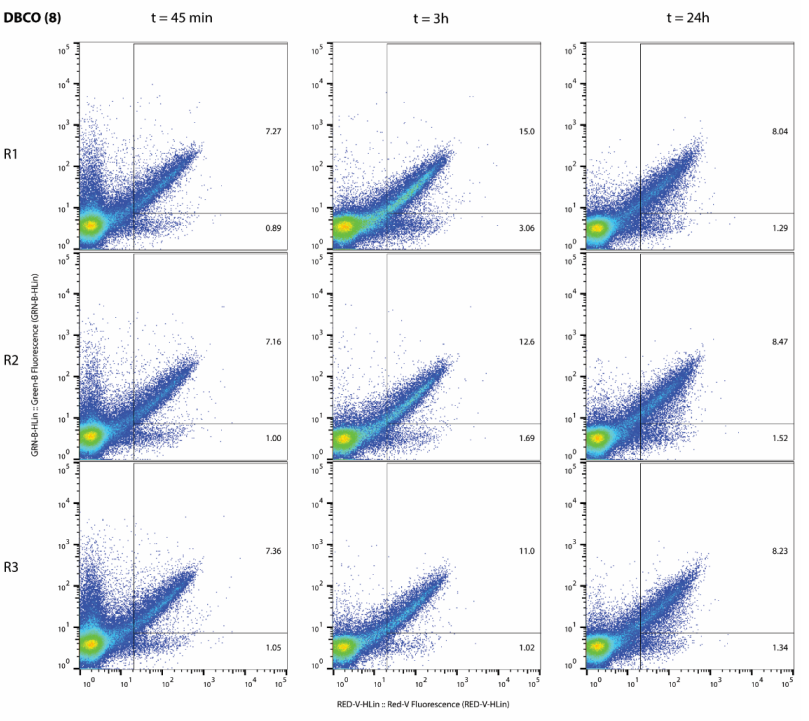
DBCO (8)
t = 45 min
t = 3h
t = 24h
R1
R2
R3
7.27
0.89
15.0
3.06
8.04
1.29
7.16
1.00
12.6
1.69
8.47
1.52
7.36
1.05
11.0
1.02
8.23
1.34
GRN-B-HLin :: Green-B Fluorescence (GRN-B-HLin)
RED-V-HLin :: Red-V Fluorescence (RED-V-HLin)

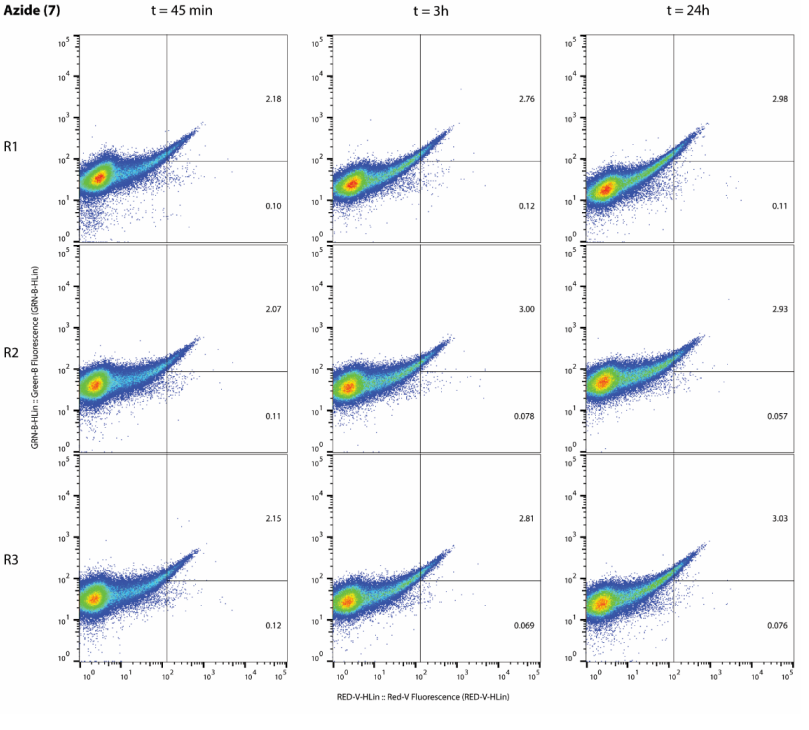
Azide (7)
t = 45 min
t = 3h
t = 24h
R1
R2
R3
2.18
0.10
2.76
0.12
2.98
0.11
2.07
0.11
3.00
0.078
2.93
0.057
2.15
0.12
2.81
0.069
3.03
0.076
GRN-B-HLin :: Green-B Fluorescence (GRN-B-HLin)
RED-V-HLin :: Red-V Fluorescence (RED-V-HLin)

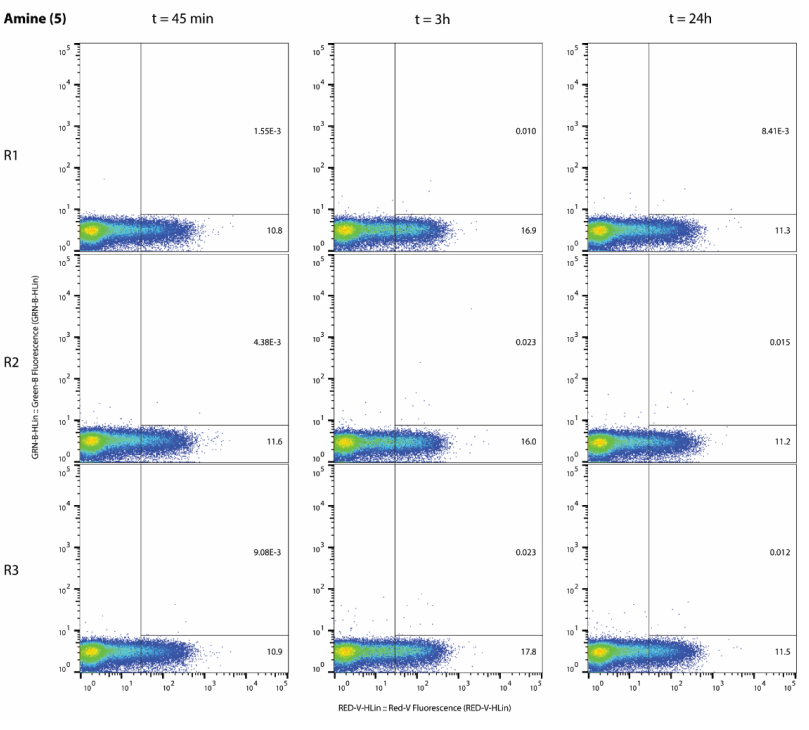

Figure S8. Stability assessment of bioorthogonal groups in DC2.4 phagocytic cells. Cells were allowed to take up the bioorthogonal FluoSpheres for 45 minutes (t = 45 min) followed by a 3 or 24h chase. Two quantification gates were set to exclude cells and debris that had not taken up beads. N=3 for all experiments shown (R1-3).

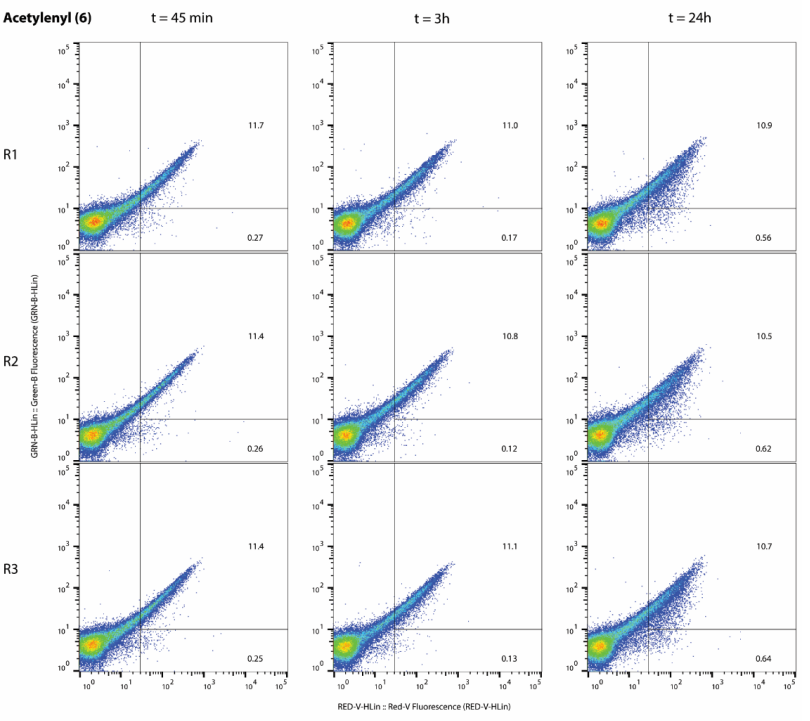
Acetylenyl (6)
t = 45 min
t = 3h
t = 24h
R1
R2
R3
11.7
0.27
11.0
0.17
10.9
0.56
11.4
0.26
10.8
0.12
10.5
0.62
11.4
0.25
11.1
0.13
10.7
0.64
GRN-B-HLin :: Green-B Fluorescence (GRN-B-HLin)
RED-V-HLin :: Red-V Fluorescence (RED-V-HLin)

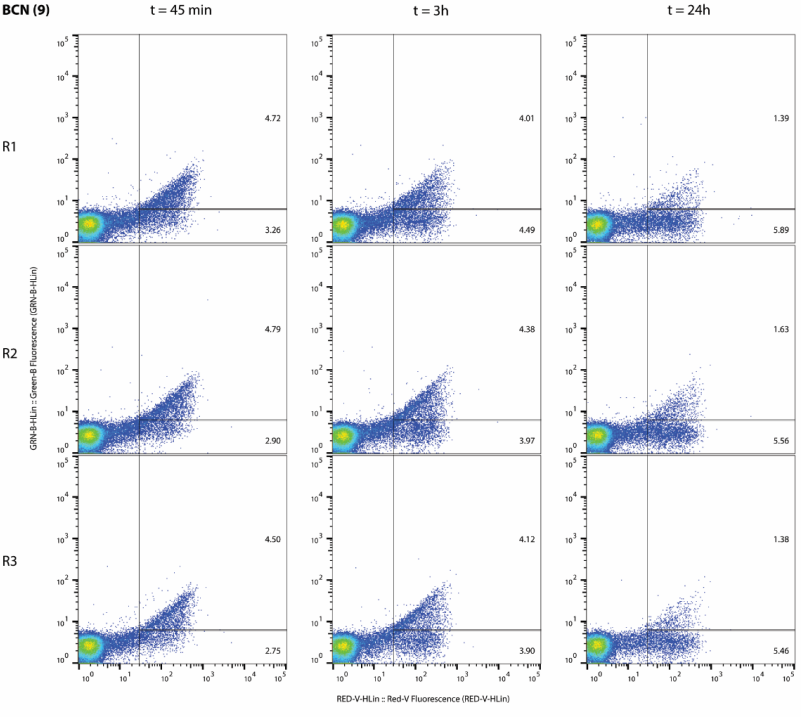
BCN (9)
t = 45 min
t = 3h
t = 24h
R1
R2
R3
4.72
3.26
4.01
4.49
1.39
5.89
4.79
2.90
4.38
3.97
1.63
5.56
4.50
2.75
4.12
3.90
1.38
5.46
GRN-B-HLin :: Green-B Fluorescence (GRN-B-HLin)
RED-V-HLin :: Red-V Fluorescence (RED-V-HLin)

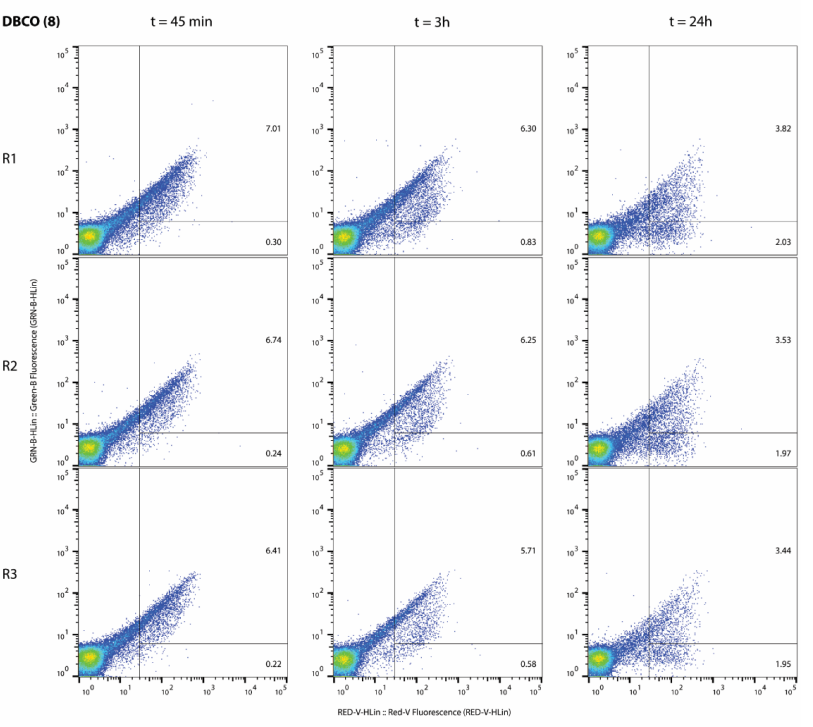
DBCO (8)
t = 45 min
t = 3h
t = 24h
R1
R2
R3
7.01
0.30
6.30
0.83
3.82
2.03
6.74
0.24
6.25
0.61
3.53
1.97
6.41
0.22
5.71
0.58
3.44
1.95
GRN-B-HLin :: Green-B Fluorescence (GRN-B-HLin)
RED-V-HLin :: Red-V Fluorescence (RED-V-HLin)

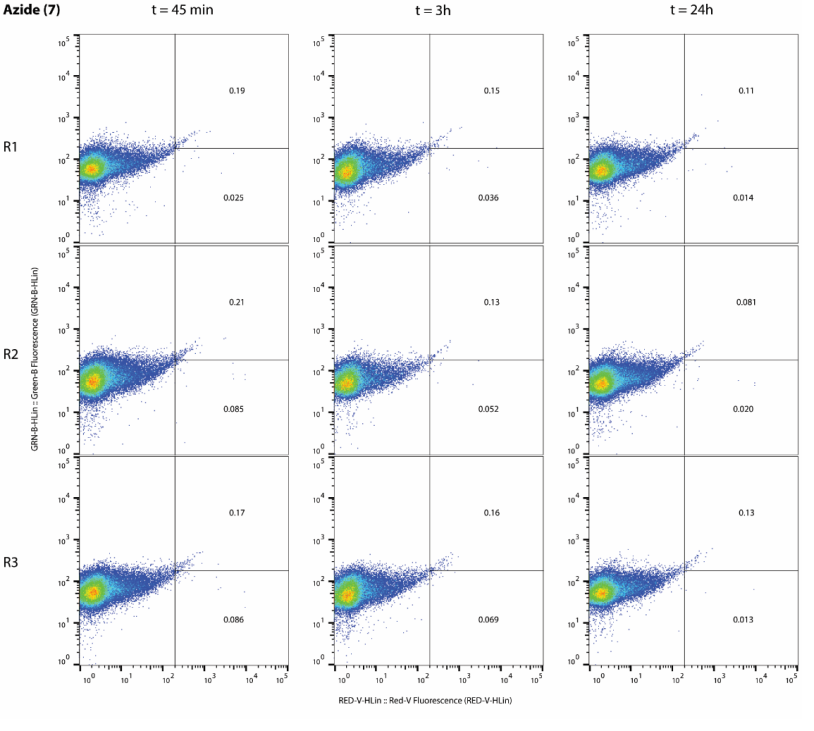
Azide (7)
t = 45 min
t = 3h
t = 24h
R1
R2
R3
0.19
0.025
0.15
0.036
0.11
0.014
0.21
0.085
0.13
0.052
0.081
0.020
0.17
0.086
0.16
0.069
0.13
0.013
GRN-B-HLin :: Green-B Fluorescence (GRN-B-HLin)
RED-V-HLin :: Red-V Fluorescence (RED-V-HLin)

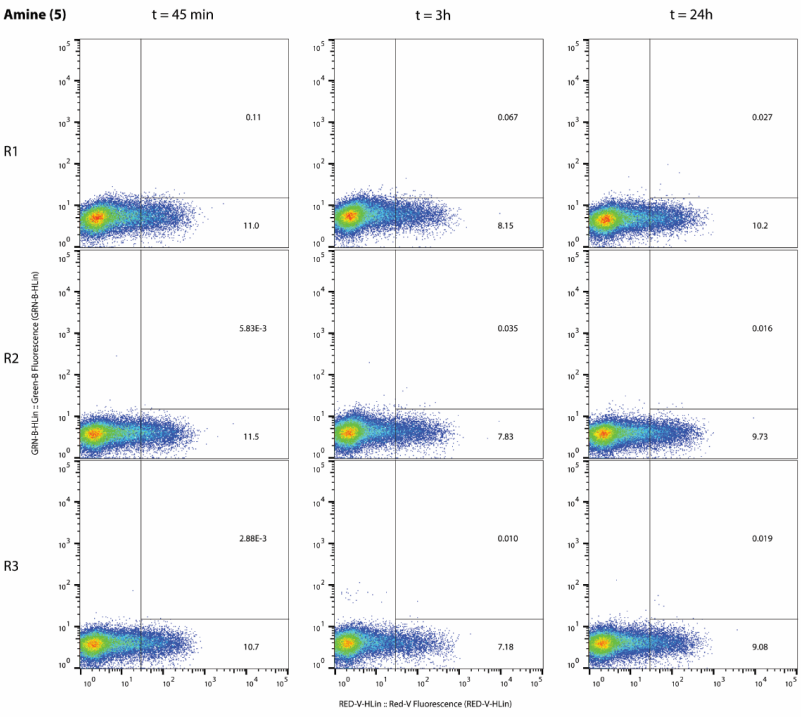

Figure S9. Stability assessment of bioorthogonal groups in RAW 264.7 phagocytic cells. Cells were first allowed to take up the bioorthogonal FluoSpheres for 45 minutes (t = 45 min). Cells were then washed and chased 3 or 24 hours. Two quantification gates were set to exclude cells and debris that had not taken up beads. N=3 shown for all experiments (R1-3).

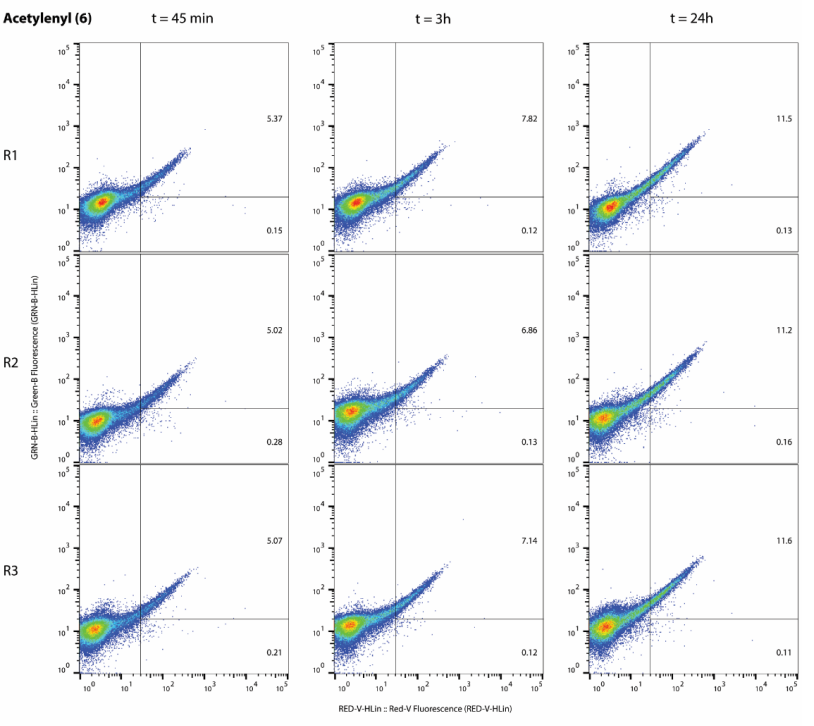
Acetylenyl (6)
t = 45 min
t = 3h
t = 24h
R1
R2
R3
5.37
0.15
7.82
0.12
11.5
0.13
5.02
0.28
6.86
0.13
11.2
0.16
5.07
0.21
7.14
0.12
11.6
0.11
GRN-B-HLin :: Green-B Fluorescence (GRN-B-HLin)
RED-V-HLin :: Red-V Fluorescence (RED-V-HLin)

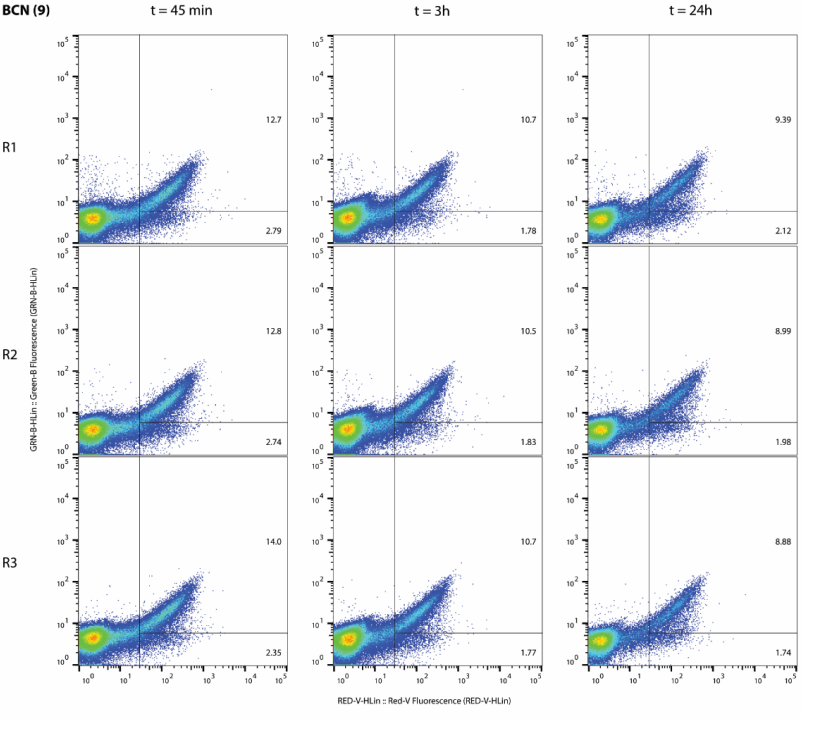
BCN (9)
t = 45 min
t = 3h
t = 24h
R1
R2
R3
12.7
2.79
10.7
1.78
9.39
2.12
12.8
2.74
10.5
1.83
8.99
1.98
14.0
2.35
10.7
1.77
8.88
1.74
GRN-B-HLin :: Green-B Fluorescence (GRN-B-HLin)
RED-V-HLin :: Red-V Fluorescence (RED-V-HLin)

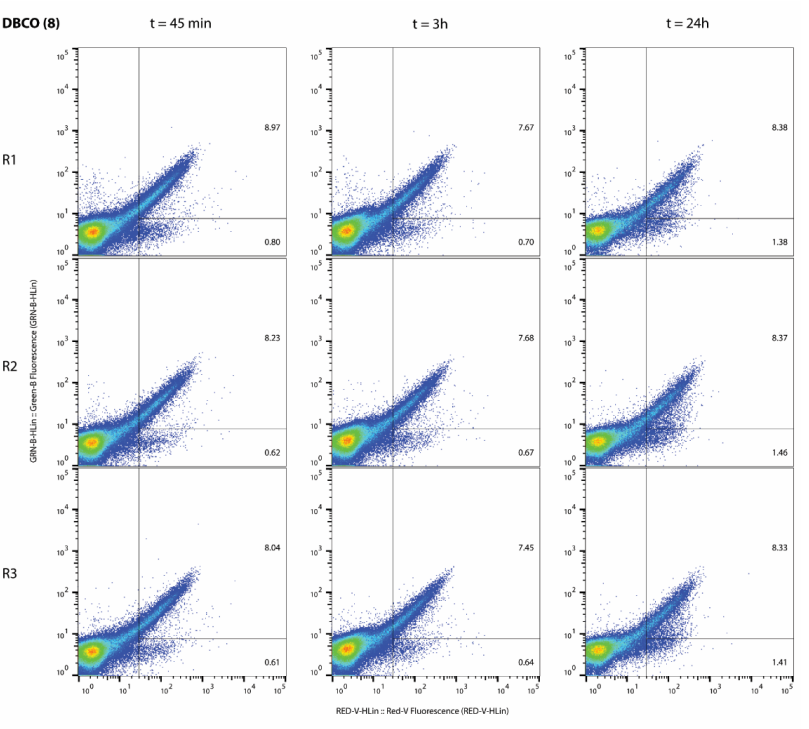
DBCO (8)
t = 45 min
t = 3h
t = 24h
R1
R2
R3
8.97
0.80
7.67
0.70
8.38
1.38
8.23
0.62
7.68
0.67
8.37
1.46
8.04
0.61
7.45
0.64
8.33
1.41
GRN-B-HLin :: Green-B Fluorescence (GRN-B-HLin)
RED-V-HLin :: Red-V Fluorescence (RED-V-HLin)

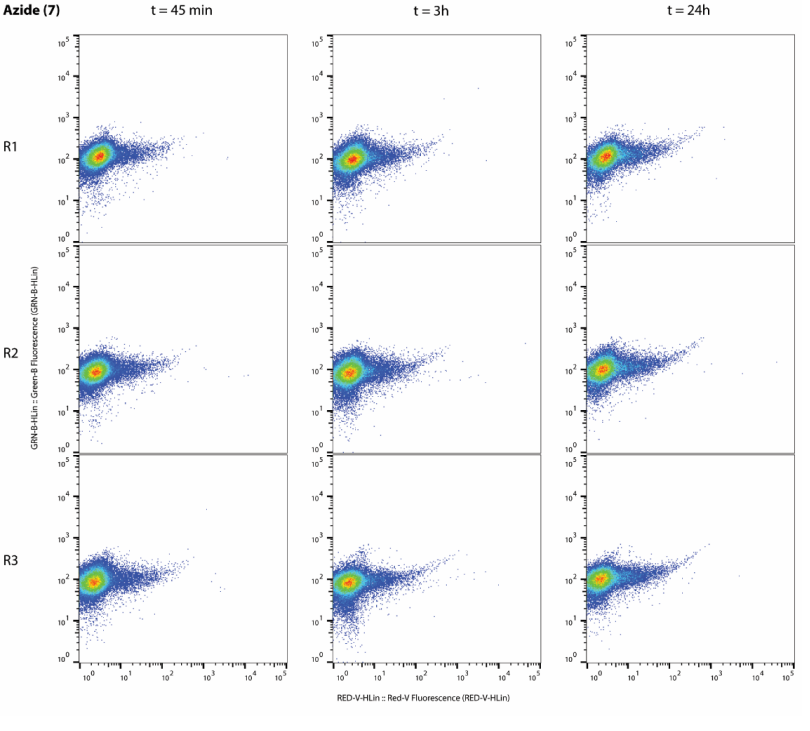
Azide (7)
t = 45 min
t = 3h
t = 24h
R1
R2
R3
GRN-B-HLin :: Green-B Fluorescence (GRN-B-HLin)
RED-V-HLin :: Red-V Fluorescence (RED-V-HLin)

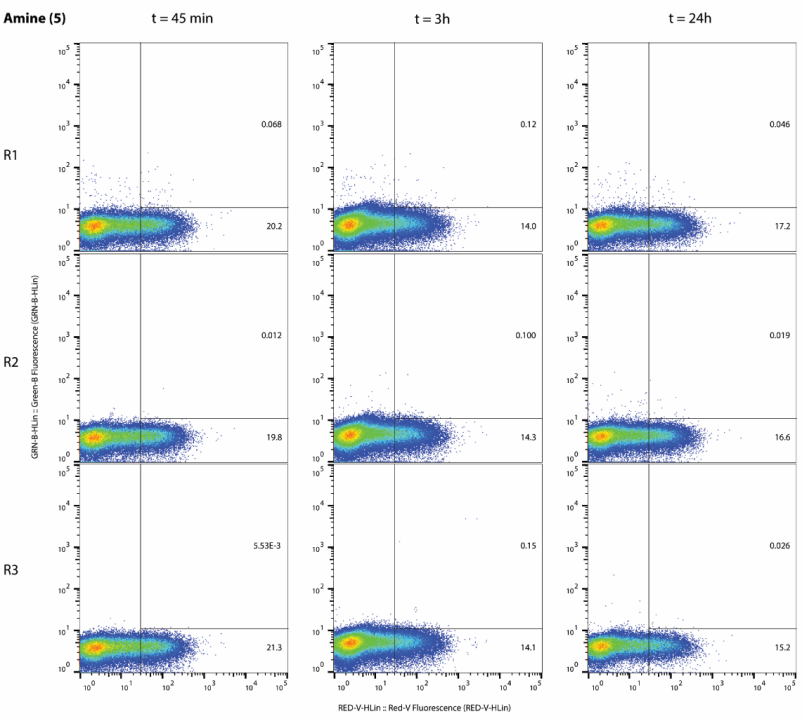

Figure S10. Stability assessment of bioorthogonal groups in DC2.4 phagocytic cells stimulated with zymosan and PMA. Cells were pre-stimulated with zymosan and PMA 24 hours before adding the bioorthogonal FluoSpheres as in Figure S8. N=3 shown for all experiments (R1-3).

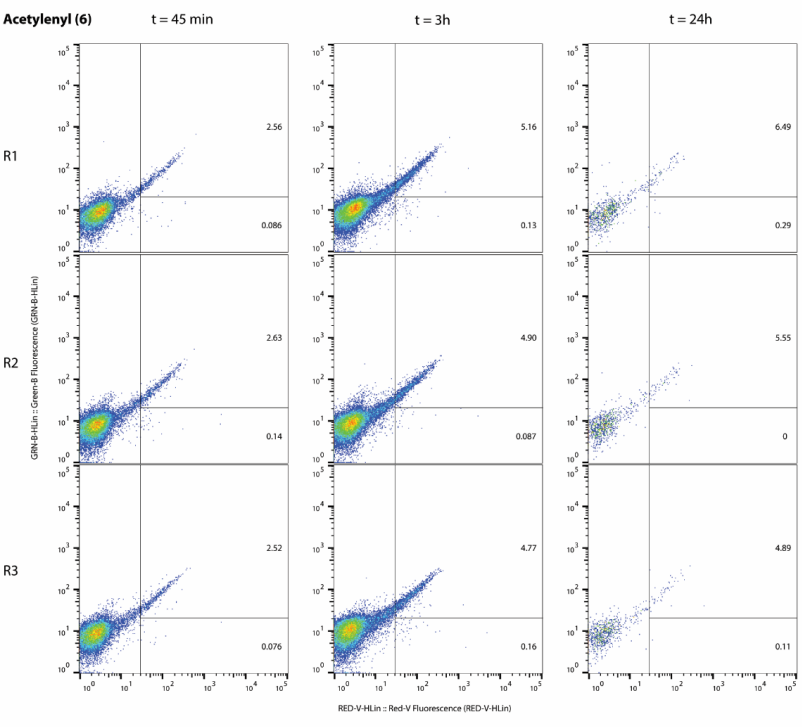
Acetylenyl (6)
t = 45 min
t = 3h
t = 24h
R1
R2
R3
2.56
0.086
5.16
0.13
6.49
0.29
2.63
0.14
4.90
0.087
5.55
0
2.52
0.076
4.77
0.16
4.89
0.11
GRN-B-HLin :: Green-B Fluorescence (GRN-B-HLin)
RED-V-HLin :: Red-V Fluorescence (RED-V-HLin)

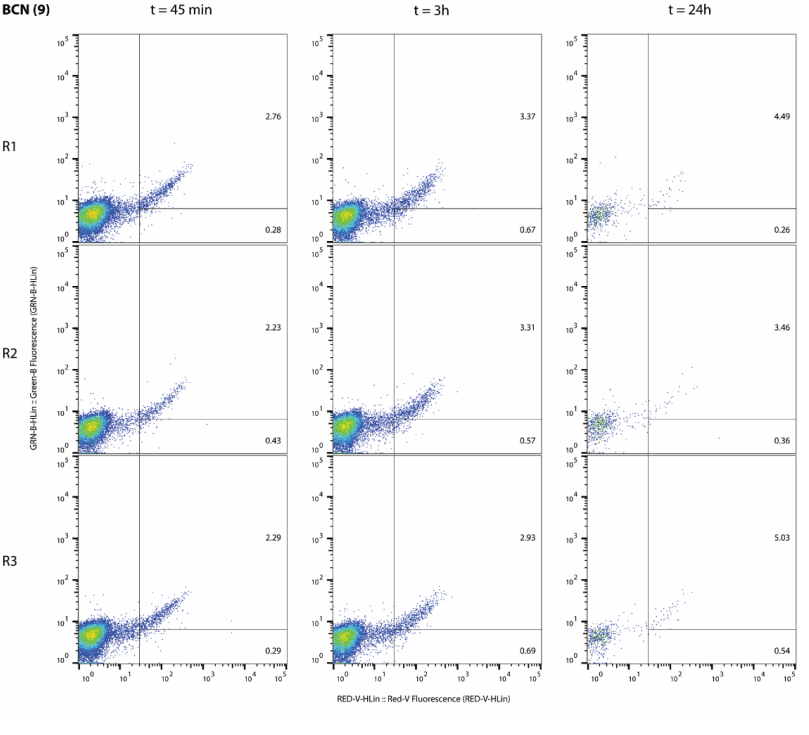
BCN (9)
t = 45 min
t = 3h
t = 24h
R1
R2
R3
2.76
0.28
3.37
0.67
4.49
0.26
2.23
0.43
3.31
0.57
3.46
0.36
2.29
0.29
2.93
0.69
5.03
0.54
GRN-B-HLin :: Green-B Fluorescence (GRN-B-HLin)
RED-V-HLin :: Red-V Fluorescence (RED-V-HLin)

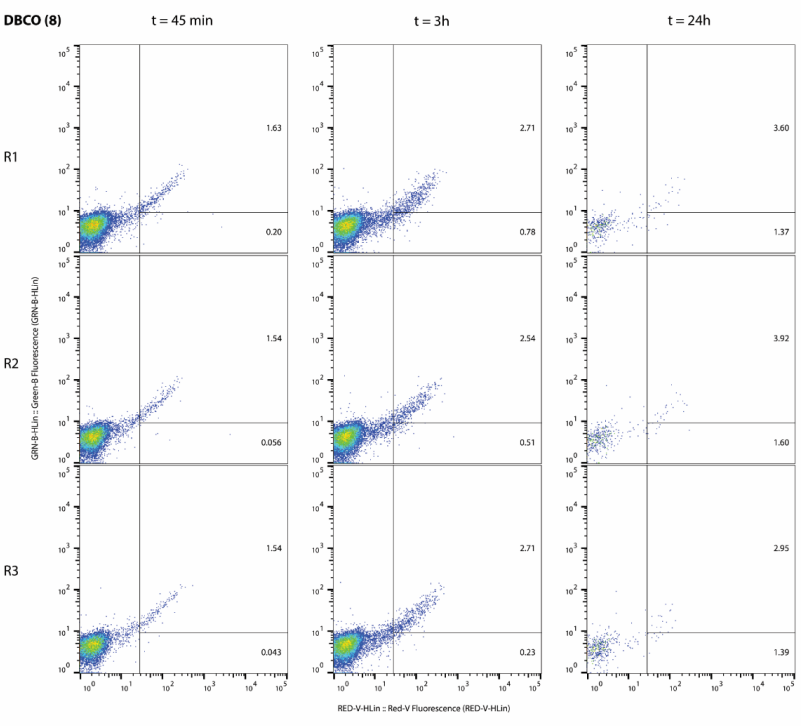
DBCO (8)
t = 45 min
t = 3h
t = 24h
R1
R2
R3
1.63
0.20
2.71
0.78
3.60
1.37
1.54
0.056
2.54
0.51
3.92
1.60
1.54
0.043
2.71
0.23
2.95
1.39
GRN-B-HLin :: Green-B Fluorescence (GRN-B-HLin)
RED-V-HLin :: Red-V Fluorescence (RED-V-HLin)

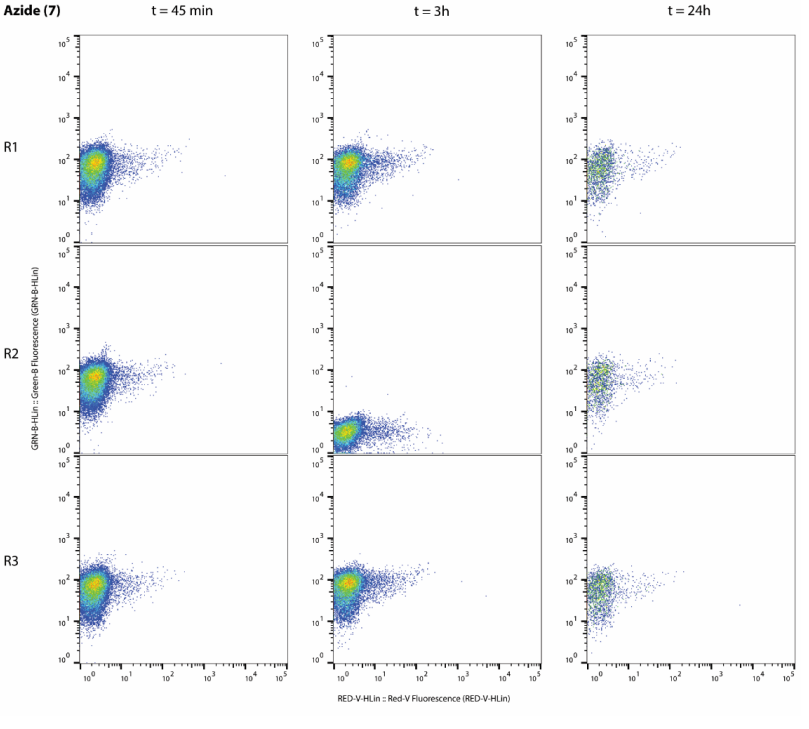
Azide (7)
t = 45 min
t = 3h
t = 24h
R1
R2
R3
GRN-B-HLin :: Green-B Fluorescence (GRN-B-HLin)
RED-V-HLin :: Red-V Fluorescence (RED-V-HLin)

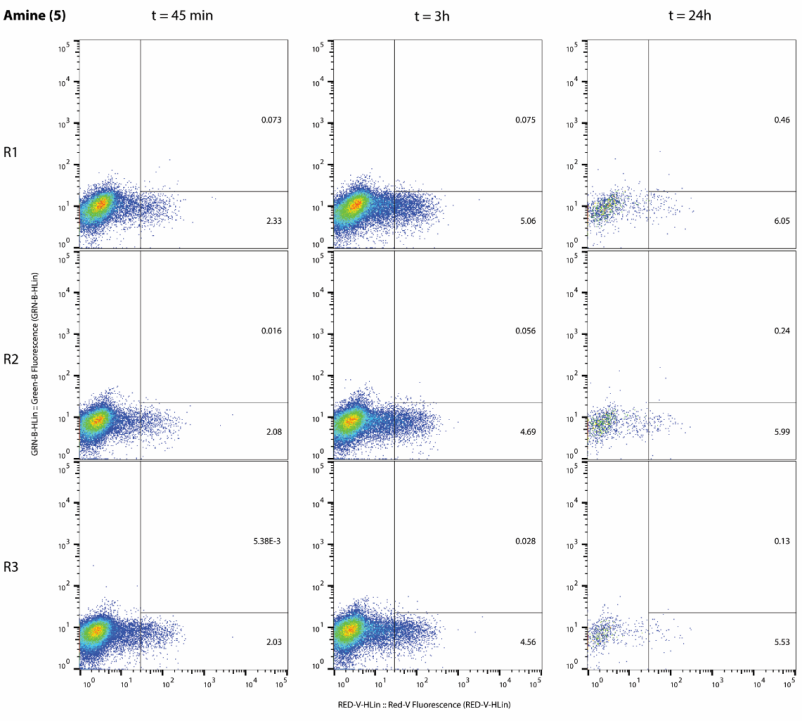

Figure S11. Stability assessment of bioorthogonal groups in RAW264.7 phagocytic cells stimulated with zymosan and PMA. Cells were pre-stimulated with zymosan and PMA 24 hours before adding the bioorthogonal FluoSpheres as in Figure S9. N=3 shown for all experiments (R1-3).

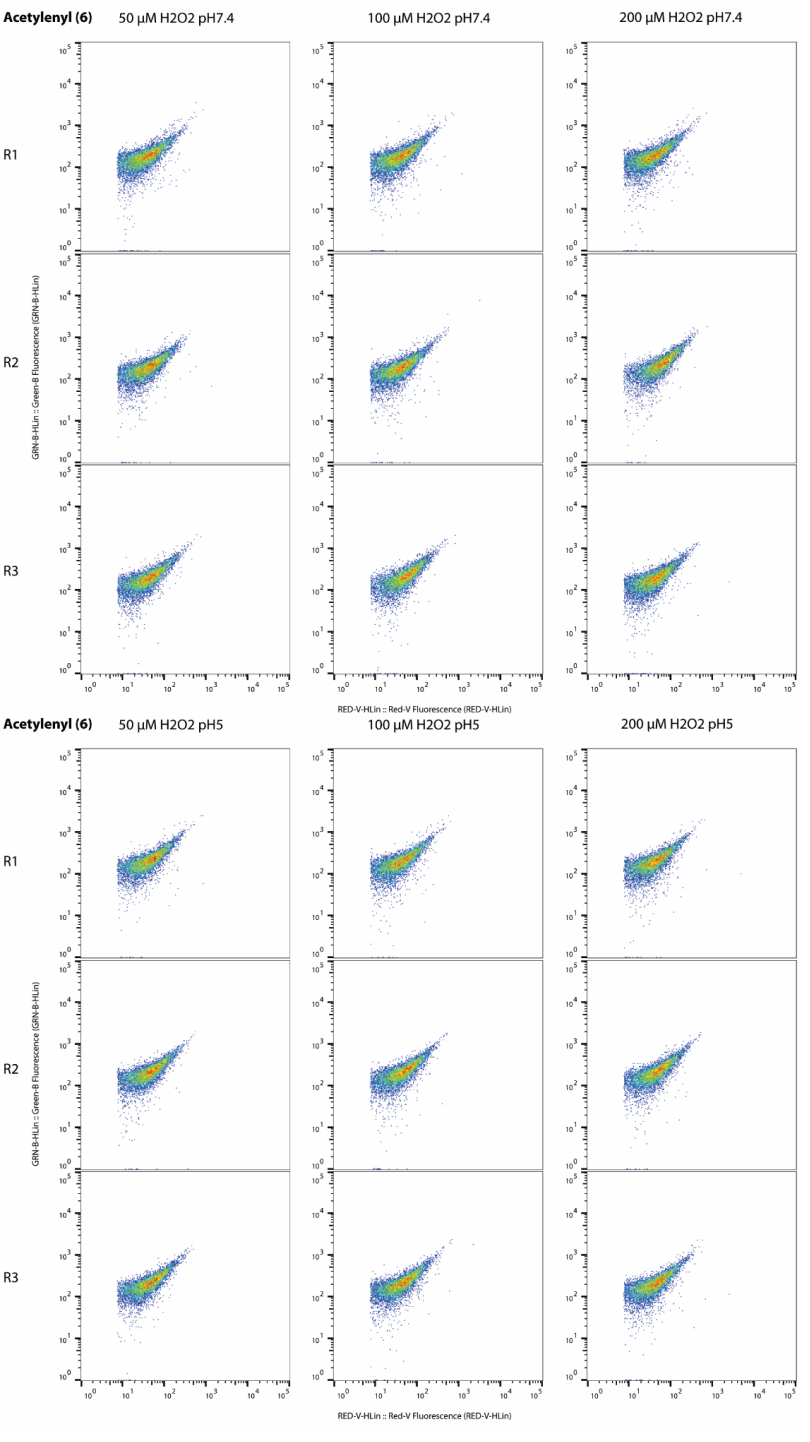
Acetylenyl (6)
50 µM H2O2 pH7.4
100 µM H2O2 pH7.4
200 µM H2O2 pH7.4
R1
R2
R3
GRN-B-HLin :: Green-B Fluorescence (GRN-B-HLin)
RED-V-HLin :: Red-V Fluorescence (RED-V-HLin)
Acetylenyl (6)
50 µM H2O2 pH5
100 µM H2O2 pH5
200 µM H2O2 pH5
R1
R2
R3
GRN-B-HLin :: Green-B Fluorescence (GRN-B-HLin)
RED-V-HLin :: Red-V Fluorescence (RED-V-HLin)

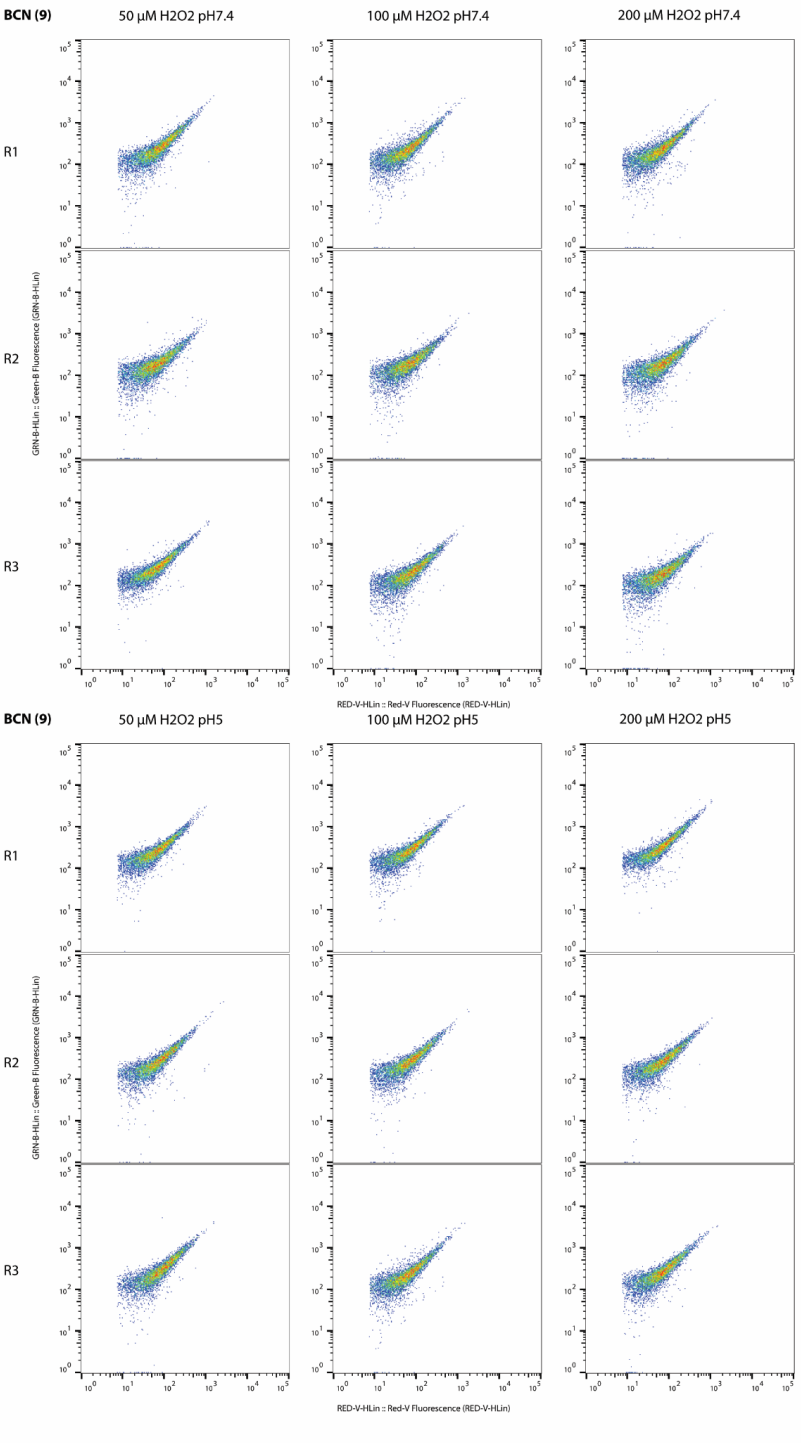
BCN (9)
50 µM H2O2 pH7.4
100 µM H2O2 pH7.4
200 µM H2O2 pH7.4
R1
R2
R3
GRN-B-HLin :: Green-B Fluorescence (GRN-B-HLin)
RED-V-HLin :: Red-V Fluorescence (RED-V-HLin)
BCN (9)
50 µM H2O2 pH5
100 µM H2O2 pH5
200 µM H2O2 pH5
R1
R2
R3
GRN-B-HLin :: Green-B Fluorescence (GRN-B-HLin)
RED-V-HLin :: Red-V Fluorescence (RED-V-HLin)

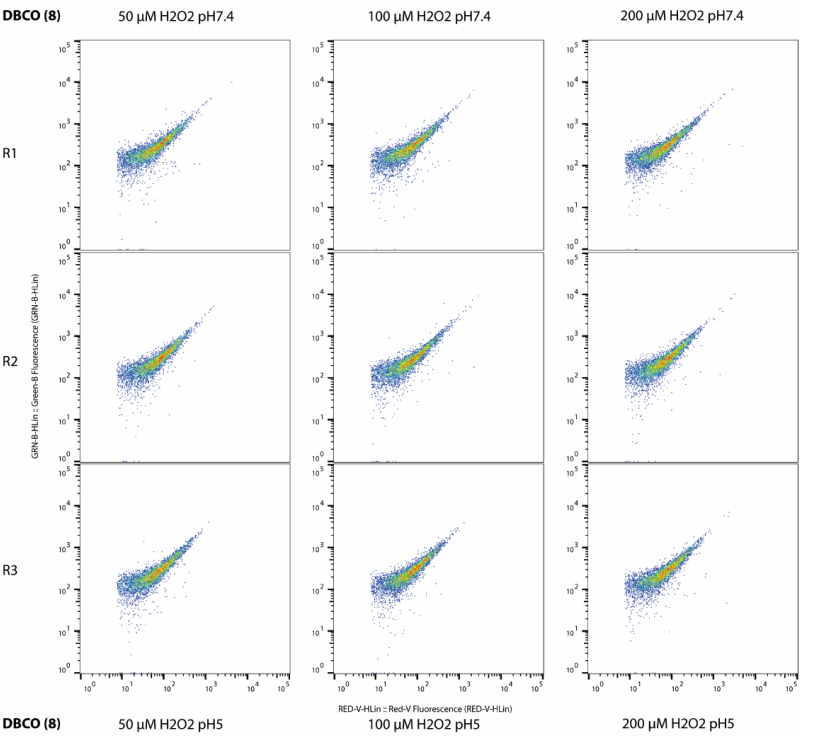
DBCO (8)
50 µM H2O2 pH7.4
100 µM H2O2 pH7.4
200 µM H2O2 pH7.4
R1
R2
R3
GRN-B-HLin :: Green-B Fluorescence (GRN-B-HLin)
RED-V-HLin :: Red-V Fluorescence (RED-V-HLin)

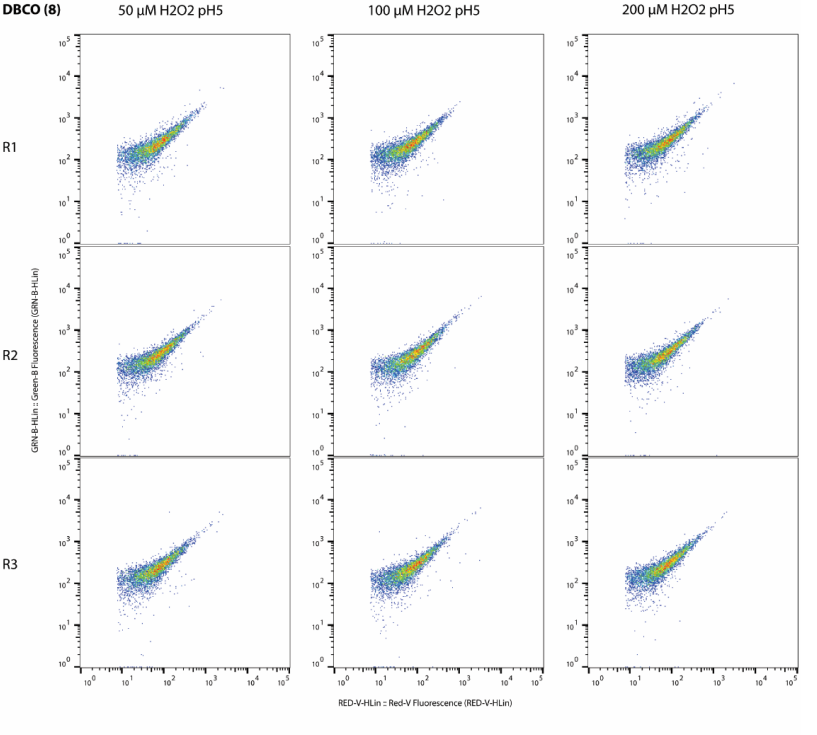
DBCO (8)
50 µM H2O2 pH5
100 µM H2O2 pH5
200 µM H2O2 pH5
R1
R2
R3
GRN-B-HLin :: Green-B Fluorescence (GRN-B-HLin)
RED-V-HLin :: Red-V Fluorescence (RED-V-HLin)

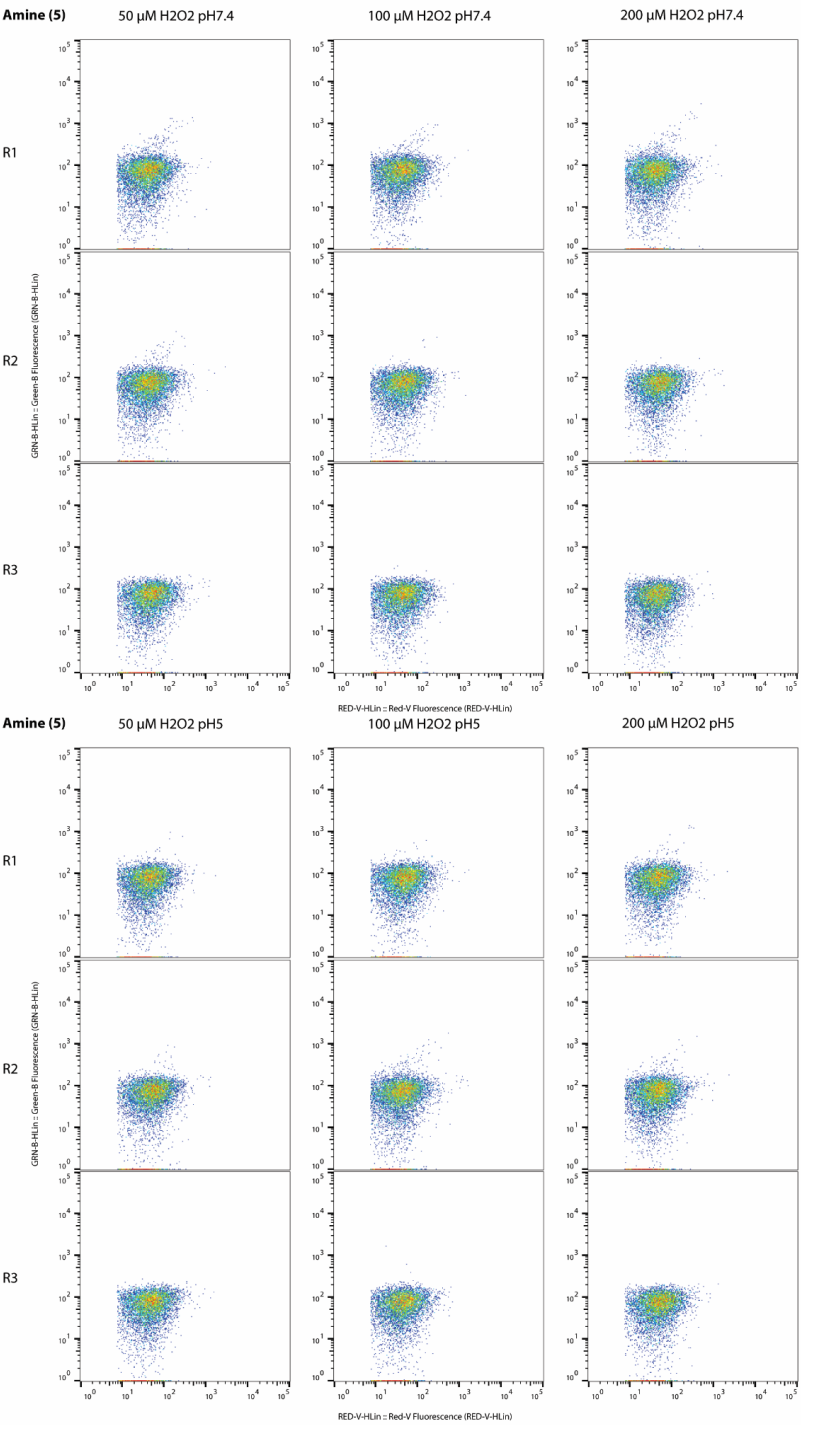
Amine (5)
50 µM H2O2 pH7.4
100 µM H2O2 pH7.4
200 µM H2O2 pH7.4
R1
R2
R3
GRN-B-HLin :: Green-B Fluorescence (GRN-B-HLin)
RED-V-HLin :: Red-V Fluorescence (RED-V-HLin)
Amine (5)
50 µM H2O2 pH5
100 µM H2O2 pH5
200 µM H2O2 pH5
R1
R2
R3
GRN-B-HLin :: Green-B Fluorescence (GRN-B-HLin)
RED-V-HLin :: Red-V Fluorescence (RED-V-HLin)

Figure S12. Stability assessment of bioorthogonal groups incubated with hydrogen peroxide concentrations of 50, 100 or 200 μM at pH 7.4 or pH 5.0. Samples were incubated in the dark at RT for 30 minutes. N =3 shown for all experiments (R1-3).

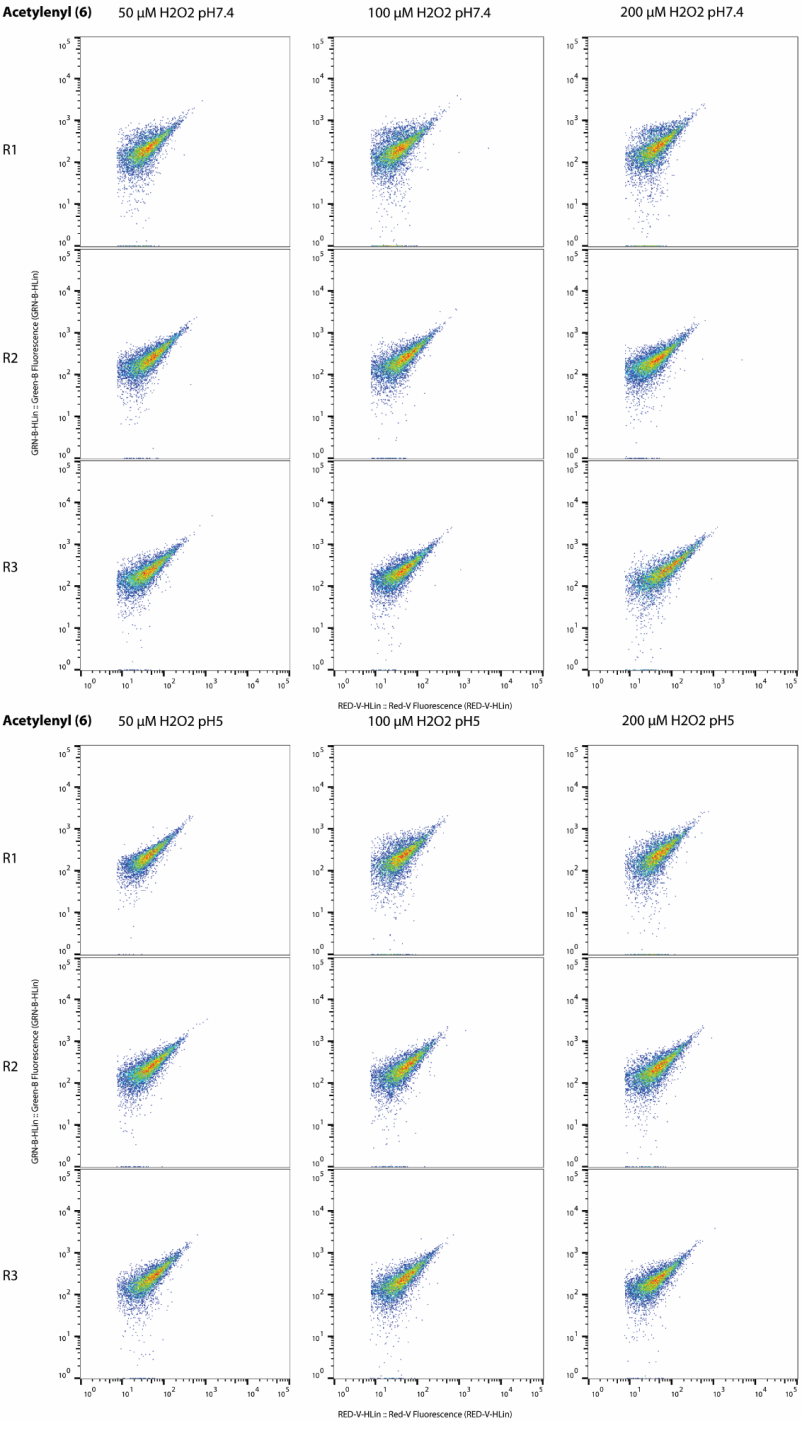
Acetylenyl (6)
50 µM H2O2 pH7.4
100 µM H2O2 pH7.4
200 µM H2O2 pH7.4
R1
R2
R3
GRN-B-HLin :: Green-B Fluorescence (GRN-B-HLin)
RED-V-HLin :: Red-V Fluorescence (RED-V-HLin)
Acetylenyl (6)
50 µM H2O2 pH5
100 µM H2O2 pH5
200 µM H2O2 pH5
R1
R2
R3
GRN-B-HLin :: Green-B Fluorescence (GRN-B-HLin)
RED-V-HLin :: Red-V Fluorescence (RED-V-HLin)

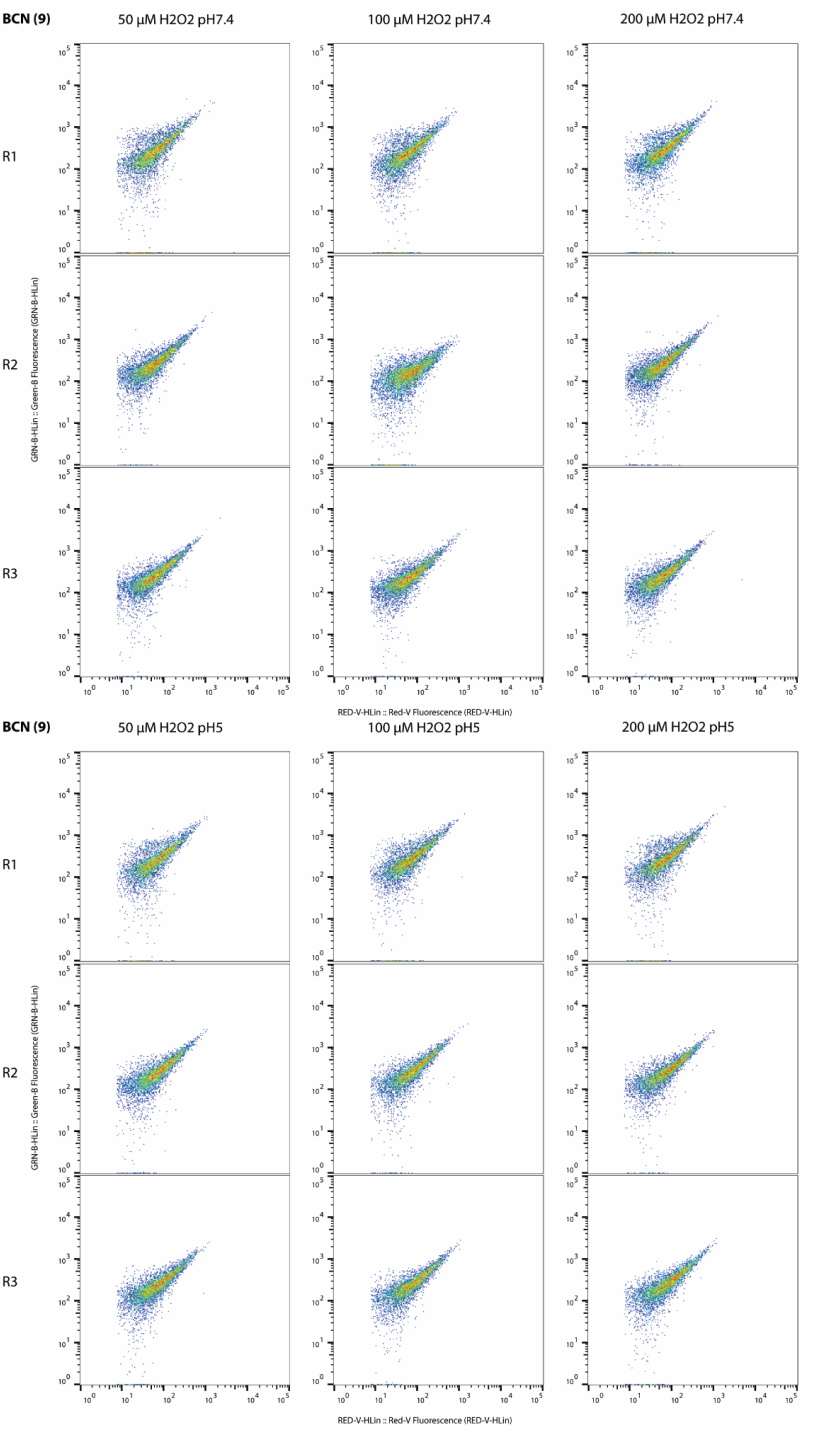
BCN (9)
50 µM H2O2 pH7.4
100 µM H2O2 pH7.4
200 µM H2O2 pH7.4
R1
R2
R3
GRN-B-HLin :: Green-B Fluorescence (GRN-B-HLin)
RED-V-HLin :: Red-V Fluorescence (RED-V-HLin)
BCN (9)
50 µM H2O2 pH5
100 µM H2O2 pH5
200 µM H2O2 pH5
R1
R2
R3
GRN-B-HLin :: Green-B Fluorescence (GRN-B-HLin)
RED-V-HLin :: Red-V Fluorescence (RED-V-HLin)

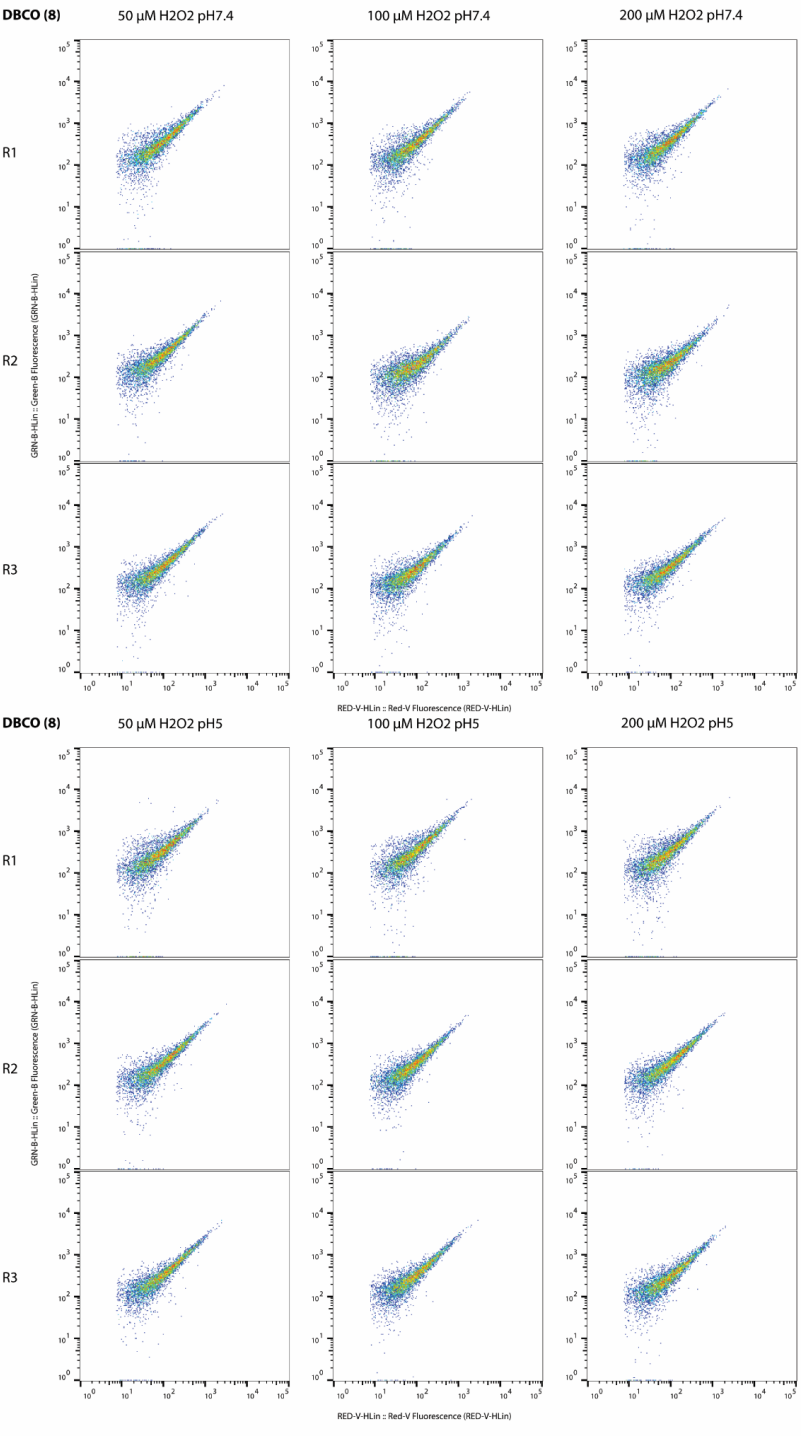
DBCO (8)
50 µM H2O2 pH7.4
100 µM H2O2 pH7.4
200 µM H2O2 pH7.4
R1
R2
R3
GRN-B-HLin :: Green-B Fluorescence (GRN-B-HLin)
RED-V-HLin :: Red-V Fluorescence (RED-V-HLin)
DBCO (8)
50 µM H2O2 pH5
100 µM H2O2 pH5
200 µM H2O2 pH5
R1
R2
R3
GRN-B-HLin :: Green-B Fluorescence (GRN-B-HLin)
RED-V-HLin :: Red-V Fluorescence (RED-V-HLin)

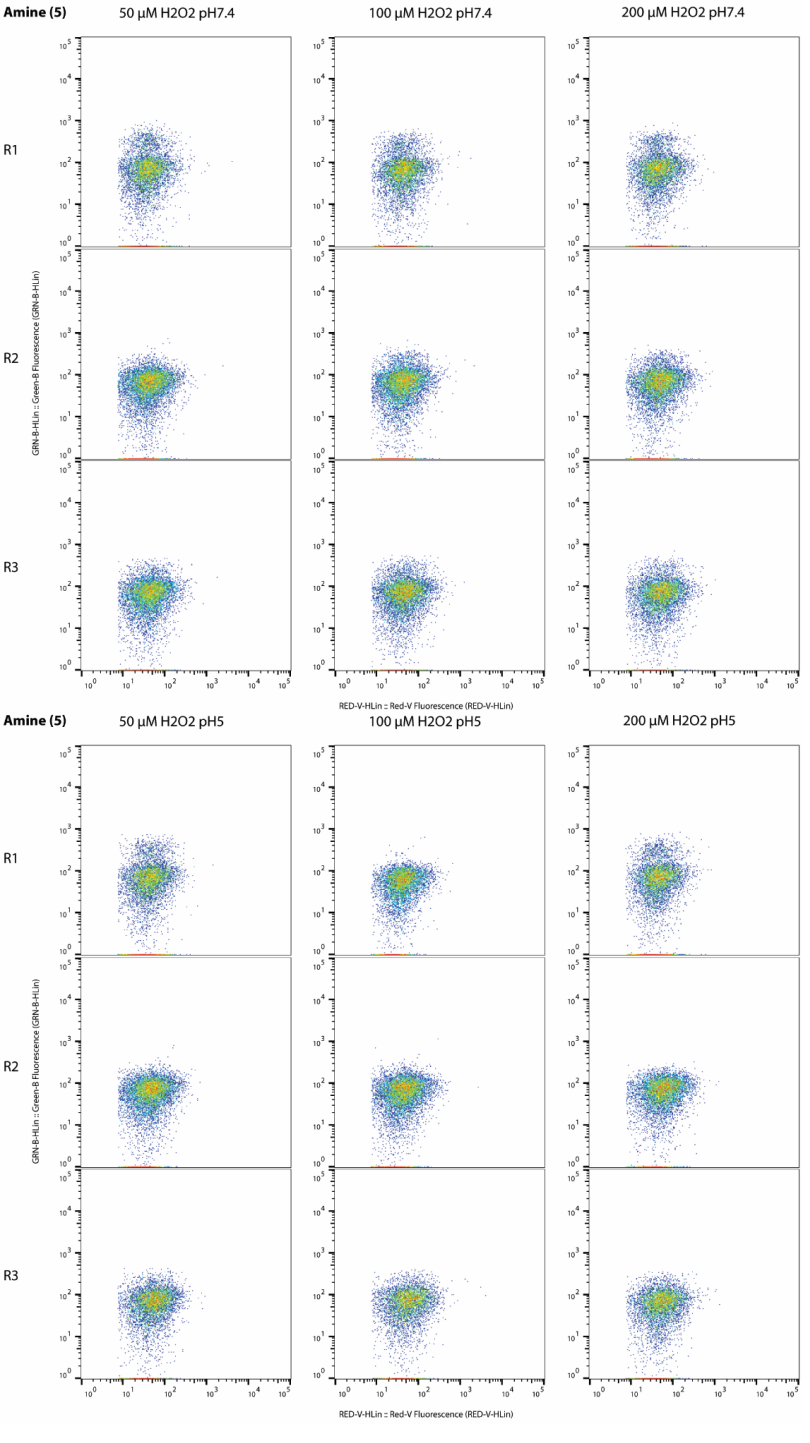
Amine (5)
50 µM H2O2 pH7.4
100 µM H2O2 pH7.4
200 µM H2O2 pH7.4
R1
R2
R3
GRN-B-HLin :: Green-B Fluorescence (GRN-B-HLin)
RED-V-HLin :: Red-V Fluorescence (RED-V-HLin)
Amine (5)
50 µM H2O2 pH5
100 µM H2O2 pH5
200 µM H2O2 pH5
R1
R2
R3
GRN-B-HLin :: Green-B Fluorescence (GRN-B-HLin)
RED-V-HLin :: Red-V Fluorescence (RED-V-HLin)

Figure S13. Stability assessment of bioorthogonal groups incubated with hydrogen peroxide concentrations of 50, 100 or 200 µM at pH 7.4 or pH 5.0. Samples were exposed to UV-irradiation (280-320 nm, 145 µW/cm2) for 5 minutes, followed by incubation for 30 minutes in total. Due to reduction of both bead- and bioorthogonal fluorescence signal, azide **7** was excluded from analysis in this experiment. N=3 shown for all experiments (R1-3).

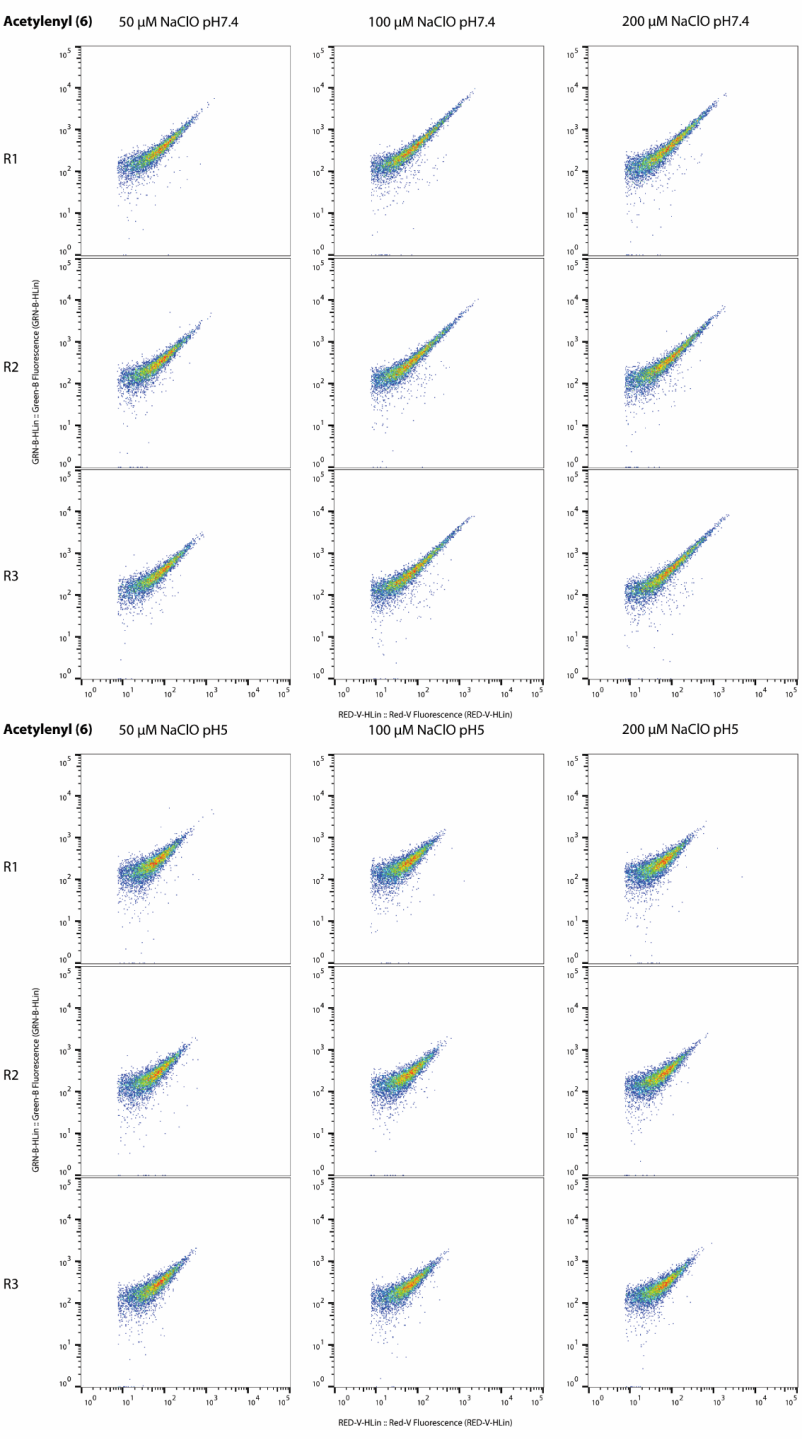
Acetylenyl (6)
50 µM NaClO pH7.4
100 µM NaClO pH7.4
200 µM NaClO pH7.4
R1
R2
R3
GRN-B-HLin :: Green-B Fluorescence (GRN-B-HLin)
RED-V-HLin :: Red-V Fluorescence (RED-V-HLin)
Acetylenyl (6)
50 µM NaClO pH5
100 µM NaClO pH5
200 µM NaClO pH5
R1
R2
R3
GRN-B-HLin :: Green-B Fluorescence (GRN-B-HLin)
RED-V-HLin :: Red-V Fluorescence (RED-V-HLin)

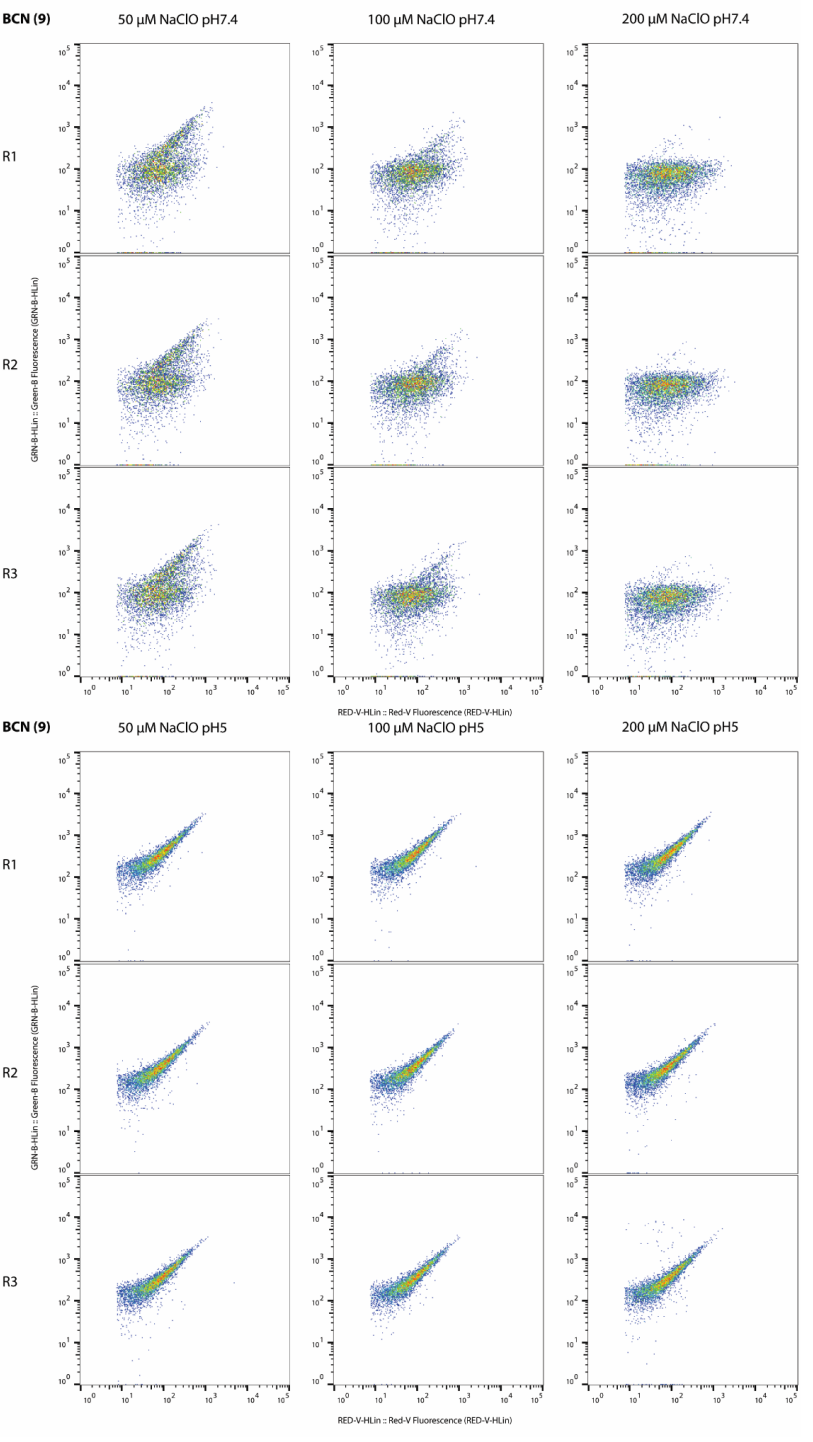
BCN (9)
50 µM NaClO pH7.4
100 µM NaClO pH7.4
200 µM NaClO pH7.4
R1
R2
R3
GRN-B-HLin :: Green-B Fluorescence (GRN-B-HLin)
RED-V-HLin :: Red-V Fluorescence (RED-V-HLin)
BCN (9)
50 µM NaClO pH5
100 µM NaClO pH5
200 µM NaClO pH5
R1
R2
R3
GRN-B-HLin :: Green-B Fluorescence (GRN-B-HLin)
RED-V-HLin :: Red-V Fluorescence (RED-V-HLin)

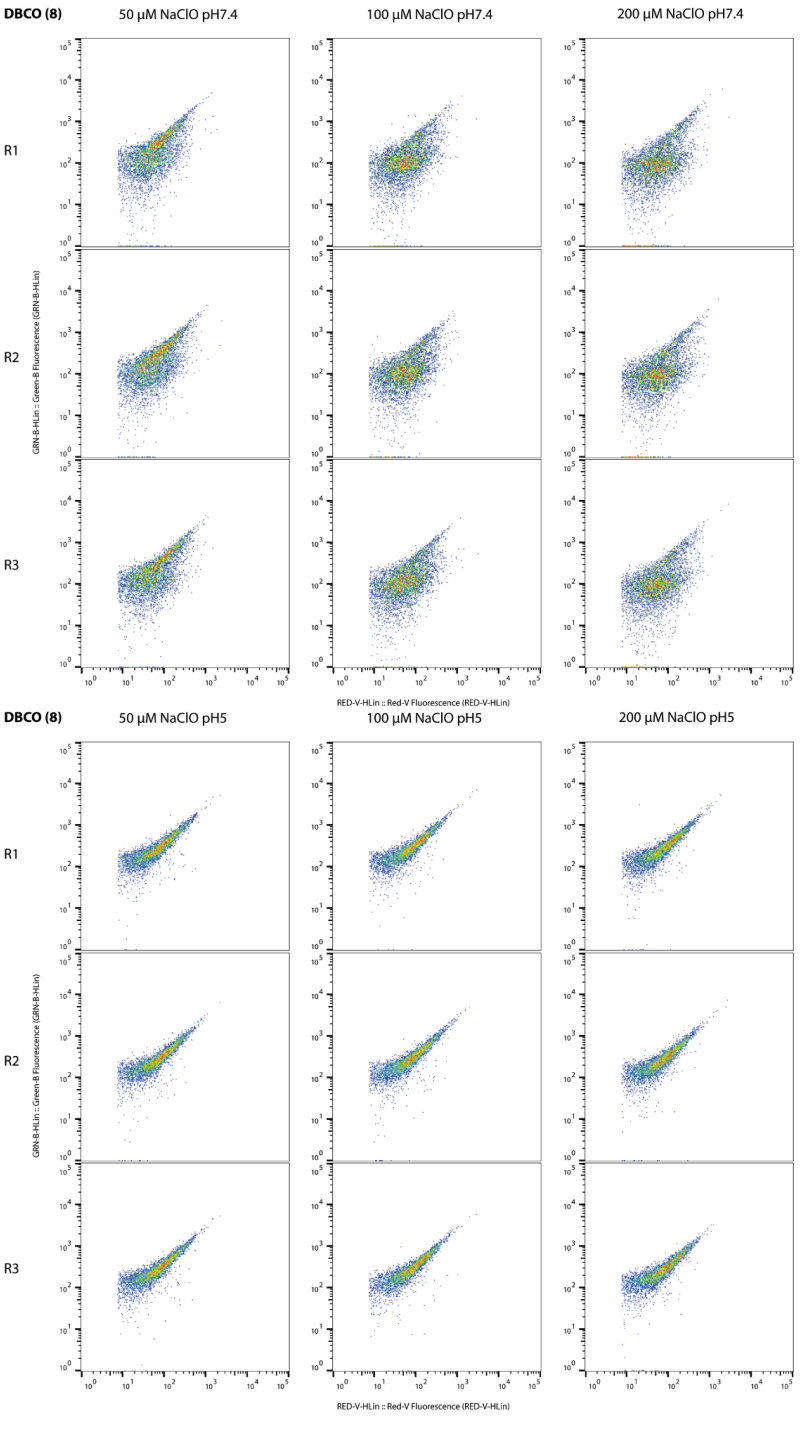
DBCO (8)
50 µM NaClO pH7.4
100 µM NaClO pH7.4
200 µM NaClO pH7.4
R1
R2
R3
GRN-B-HLin :: Green-B Fluorescence (GRN-B-HLin)
RED-V-HLin :: Red-V Fluorescence (RED-V-HLin)
DBCO (8)
50 µM NaClO pH5
100 µM NaClO pH5
200 µM NaClO pH5
R1
R2
R3
GRN-B-HLin :: Green-B Fluorescence (GRN-B-HLin)
RED-V-HLin :: Red-V Fluorescence (RED-V-HLin)

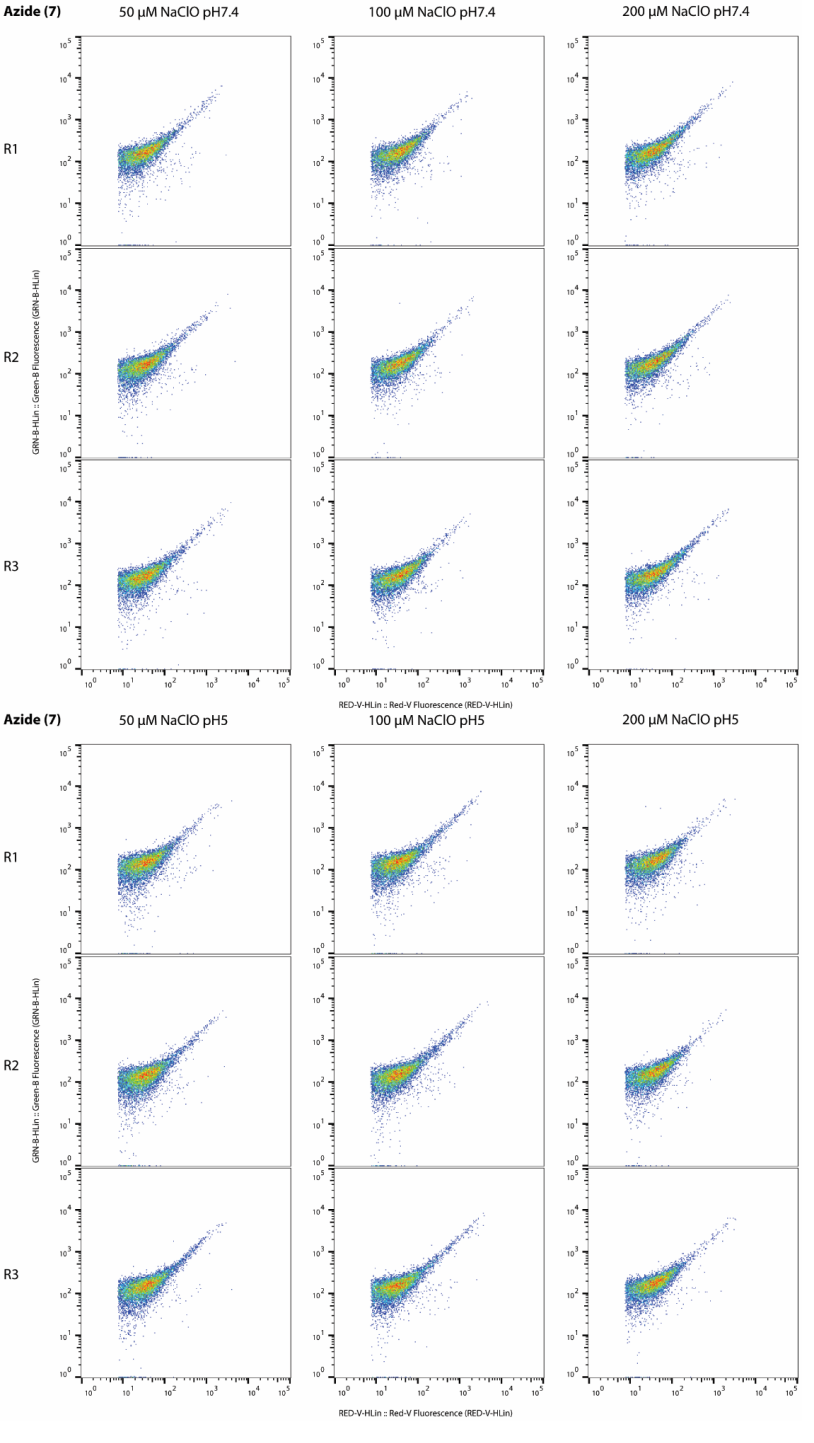
Azide (7)
50 µM NaClO pH7.4
100 µM NaClO pH7.4
200 µM NaClO pH7.4
R1
R2
R3
GRN-B-HLin :: Green-B Fluorescence (GRN-B-HLin)
RED-V-HLin :: Red-V Fluorescence (RED-V-HLin)
Azide (7)
50 µM NaClO pH5
100 µM NaClO pH5
200 µM NaClO pH5
R1
R2
R3
GRN-B-HLin :: Green-B Fluorescence (GRN-B-HLin)
RED-V-HLin :: Red-V Fluorescence (RED-V-HLin)

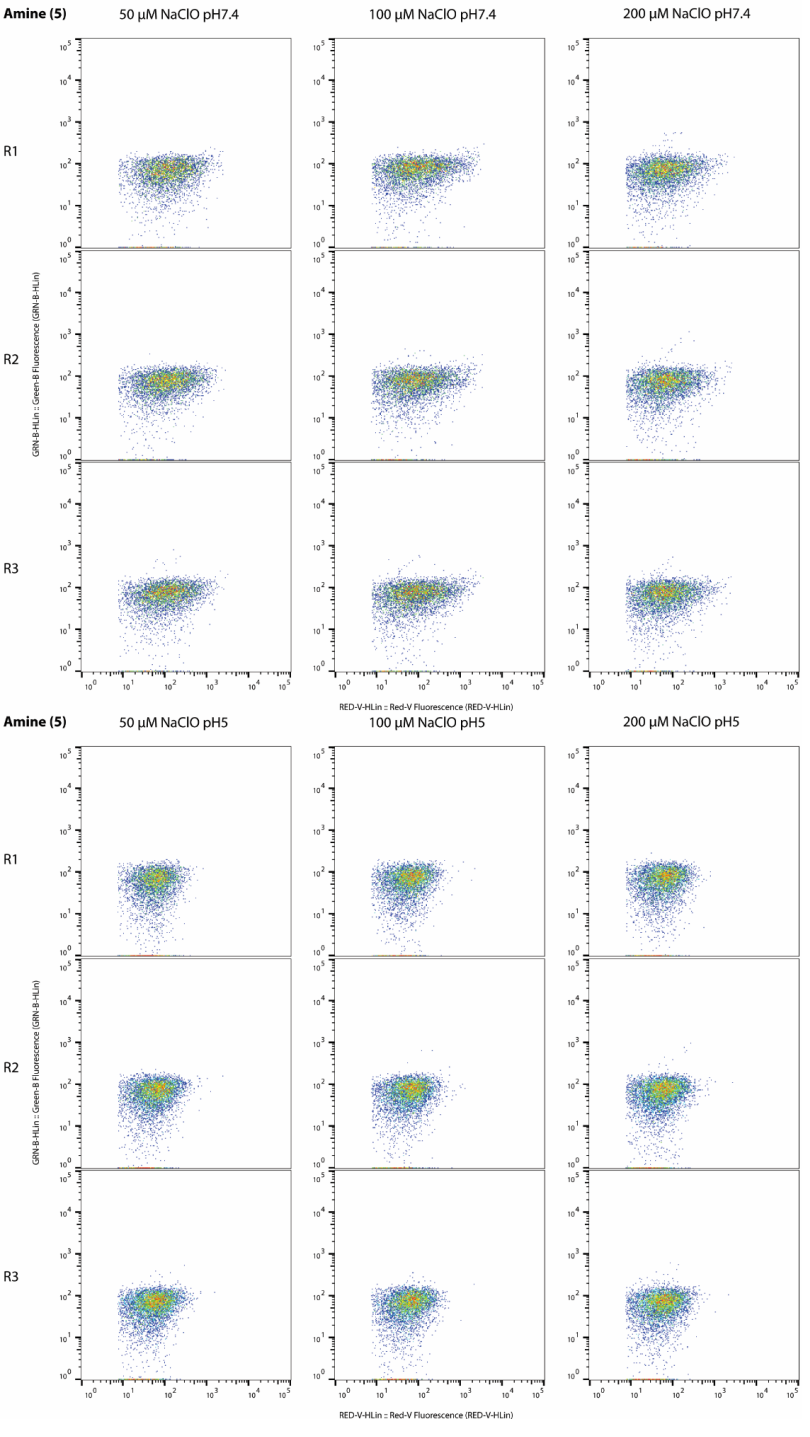
Amine (5)
50 µM NaClO pH7.4
100 µM NaClO pH7.4
200 µM NaClO pH7.4
R1
R2
R3
GRN-B-HLin :: Green-B Fluorescence (GRN-B-HLin)
RED-V-HLin :: Red-V Fluorescence (RED-V-HLin)
Amine (5)
50 µM NaClO pH5
100 µM NaClO pH5
200 µM NaClO pH5
R1
R2
R3
GRN-B-HLin :: Green-B Fluorescence (GRN-B-HLin)
RED-V-HLin :: Red-V Fluorescence (RED-V-HLin)

Figure S14. Stability assessment of bioorthogonal groups incubated with sodium hypochlorite concentrations of 50, 100 or 200 μM at pH 7.4 or 5.0. Samples were incubated at RT for 30 minutes. N=3 for all experiments shown (R1-3).

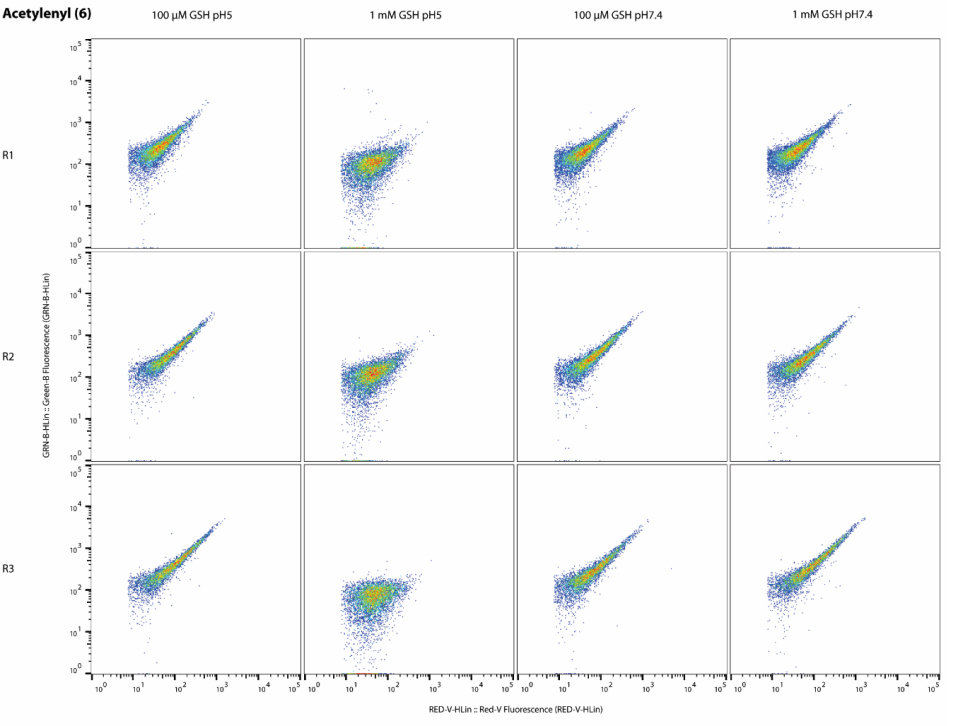
Acetylenyl (6)
100 µM GSH pH5
1 mM GSH pH5
100 µM GSH pH7.4
1 mM GSH pH7.4
R1
R2
R3
GRN-B-HLin :: Green-B Fluorescence (GRN-B-HLin)
RED-V-HLin :: Red-V Fluorescence (RED-V-HLin)

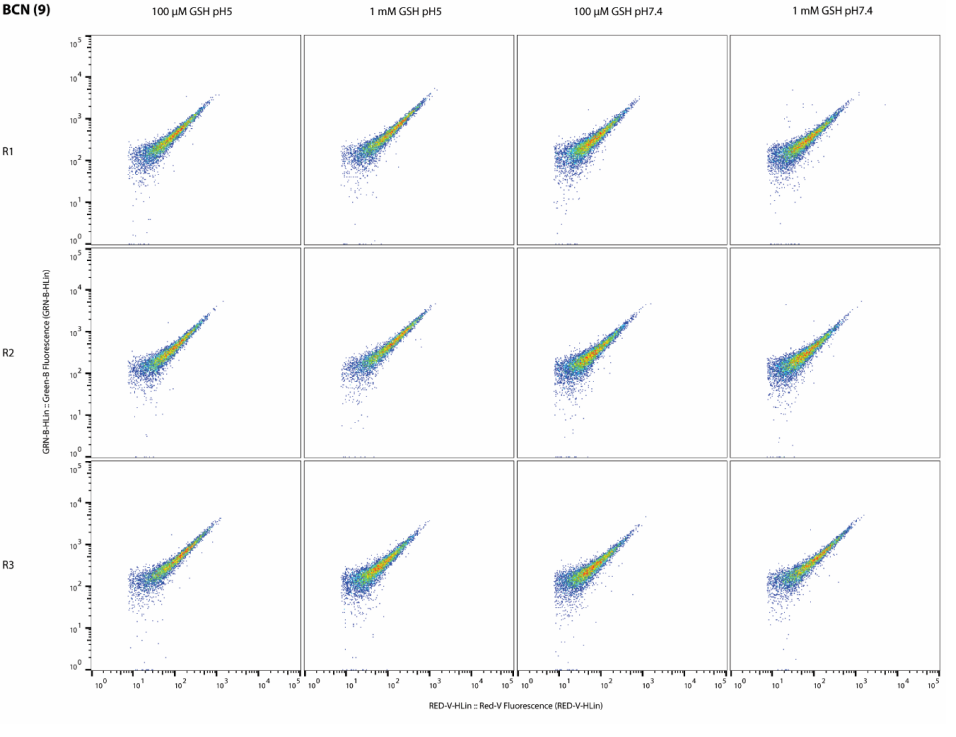
BCN (9)
100 µM GSH pH5
1 mM GSH pH5
100 µM GSH pH7.4
1 mM GSH pH7.4
R1
R2
R3
GRN-B-HLin :: Green-B Fluorescence (GRN-B-HLin)
RED-V-HLin :: Red-V Fluorescence (RED-V-HLin)

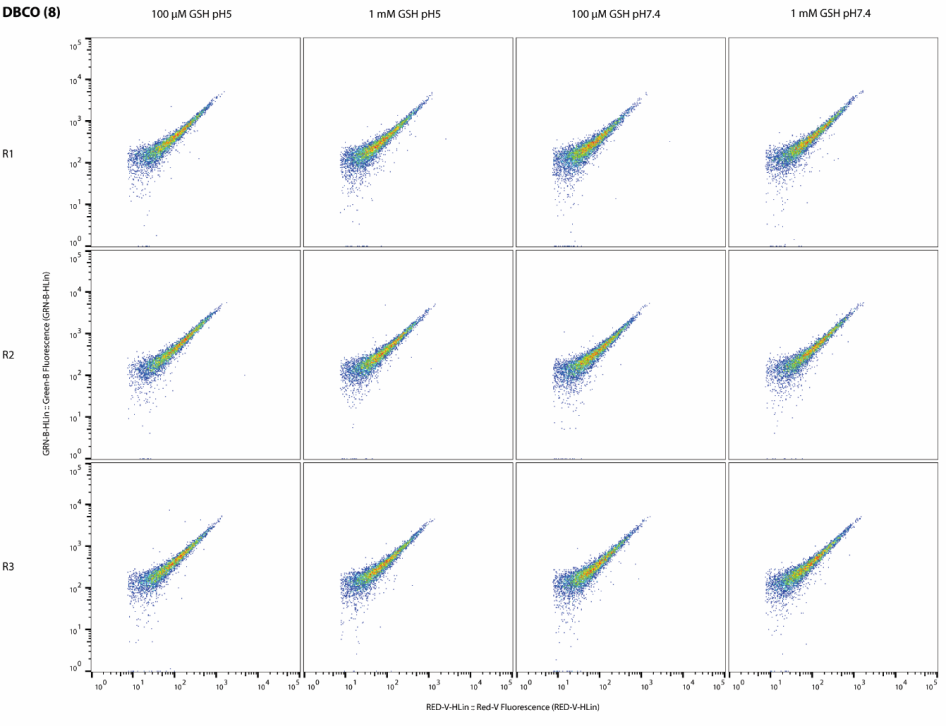
DBCO (8)
100 µM GSH pH5
1 mM GSH pH5
100 µM GSH pH7.4
1 mM GSH pH7.4
R1
R2
R3
GRN-B-HLin :: Green-B Fluorescence (GRN-B-HLin)
RED-V-HLin :: Red-V Fluorescence (RED-V-HLin)

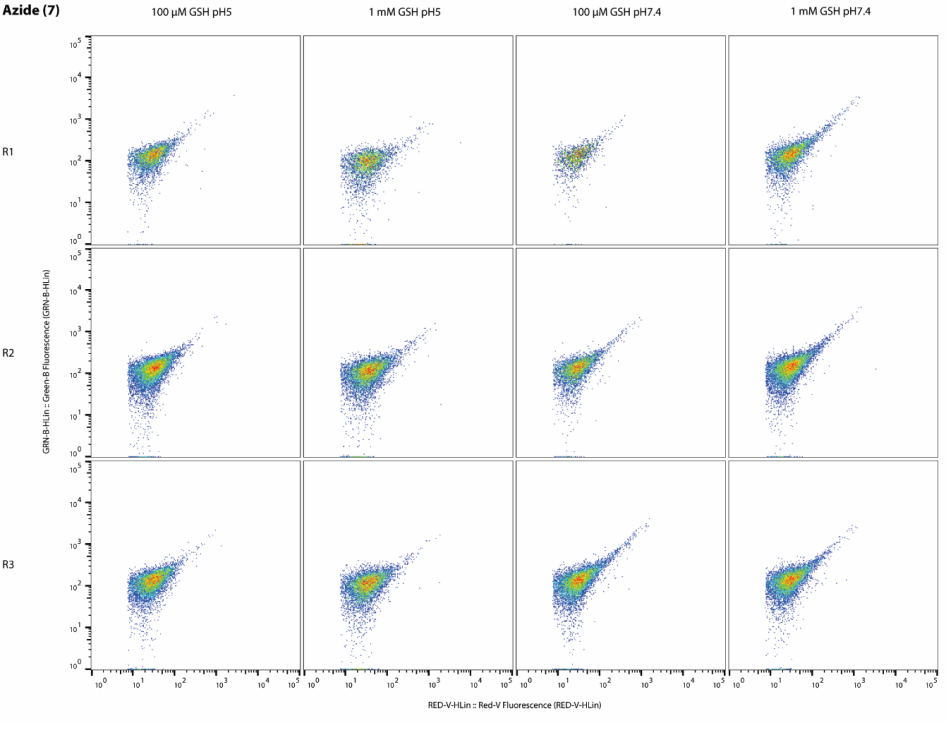
Azide (7)
100 µM GSH pH5
1 mM GSH pH5
100 µM GSH pH7.4
1 mM GSH pH7.4
R1
R2
R3
GRN-B-HLin :: Green-B Fluorescence (GRN-B-HLin)
RED-V-HLin :: Red-V Fluorescence (RED-V-HLin)

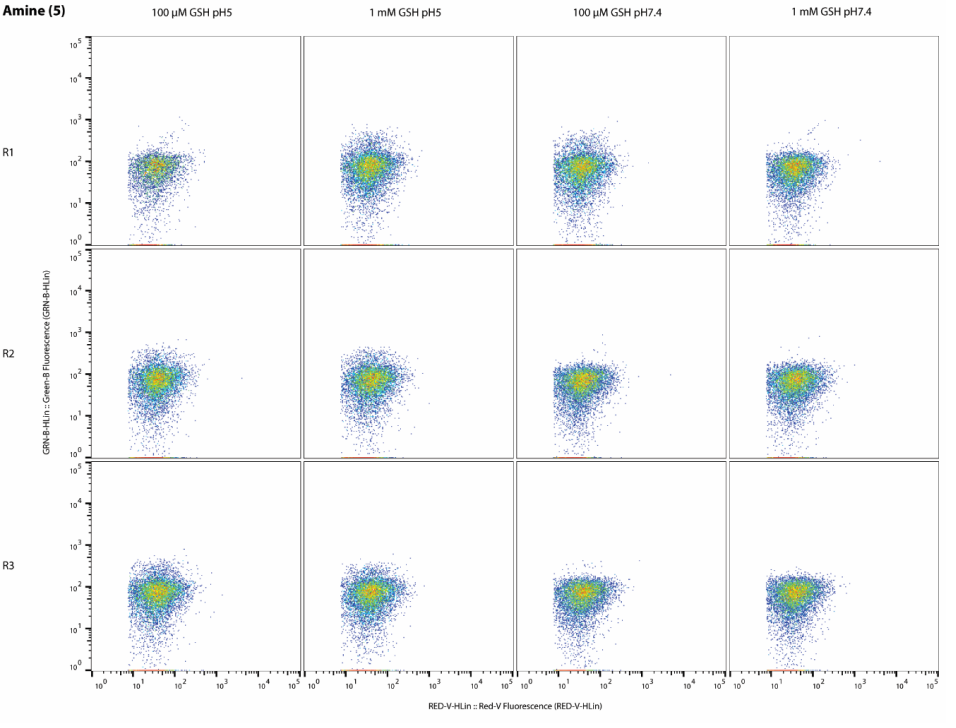

Figure S15. Stability assessment of bioorthogonal groups incubated with concentrations of 100 µM or 1 mM GSH and 10% light-activated radical initiator at pH 7.4 or pH 5.0. Samples were exposed to UV-irradiation (280-320 nm, 145 µW/cm2) for 5 minutes, followed by incubation totaling 30 minutes. N=3 shown for all experiments (R1-3).

3.6 References

(1) Sletten, E. M.; Bertozzi, C. R. Bioorthogonal Chemistry: Fishing for Selectivity in a Sea of Functionality. *Angew. Chemie - Int. Ed.* **2009**, *48* (38), 6974–6998.
(2) McKay, C. S.; Finn, M. G. Click Chemistry in Complex Mixtures: Bioorthogonal Bioconjugation. *Chem. Biol.* **2014**, *21* (9), 1075–1101.
(3) Saxon, E.; Bertozzi, C. R. Cell Surface Engineering by a Modified Staudinger Reaction. *Science* **2000**, *287* (5460), 2007–2010.
(4) Yarema, K. J.; Mahal, L. K.; Bruehl, R. E.; Rodriguez, E. C.; Bertozzi, C. R. Metabolic Delivery of Ketone Groups to Sialic Acid Residues. Application to Cell Surface Glycoform Engineering. *J. Biol. Chem.* **1998**, *273* (47), 31168–31179.
(5) Laughlin, S. T.; Baskin, J. M.; Amacher, S. L.; Bertozzi, C. R. In Vivo Imaging of Membrane-Associated Glycans in Developing Zebrafish. *Science (80-.).* **2008**, *320* (5876), 664–667.
(6) Hang, H. C.; Wilson, J. P.; Charron, G. Bioorthogonal Chemical Reporters for Analyzing Protein Lipidation and Lipid Trafficking. *Acc. Chem. Res.* **2011**, *44* (9), 699–708.
(7) Jao, C. Y.; Salic, A. Exploring RNA Transcription and Turnover in Vivo by Using Click Chemistry. *Proc. Natl. Acad. Sci. U. S. A.* **2008**, *105* (41), 15779–15784.
(8) Salic, A.; Mitchison, T. J. A Chemical Method for Fast and Sensitive Detection of DNA Synthesis in Vivo. *Proc. Natl. Acad. Sci.* **2008**, *105* (7), 2415–2420.
(9) Van Hest, J. C. M.; Kiick, K. L.; Tirrell, D. A. Efficient Incorporation of Unsaturated Methionine Analogues into Proteins in Vivo. *J. Am. Chem. Soc.* **2000**, *122* (7), 1282–1288.
(10) Dieterich, D. C.; Link, A. J.; Graumann, J.; Tirrell, D. A.; Schuman, E. M. Selective Identification of Newly Synthesized Proteins in Mammalian Cells Using Bioorthogonal Noncanonical Amino Acid Tagging (BONCAT). *Proc. Natl. Acad. Sci.* **2006**, *103* (25), 9482–9487.
(11) Siegrist, M. S.; Whiteside, S.; Jewett, J. C.; Aditham, A.; Cava, F.; Bertozzi, C. R. D-Amino Acid Chemical Reporters Reveal Peptidoglycan Dynamics of an Intracellular Pathogen. *ACS Chem. Biol.* **2013**, *8* (3), 500–505.
(12) Siegrist, S. M.; Aditham, A. K.; Espaillat, A.; Cameron, T. A.; Whiteside, S. A.; Cava, F.; Portnoy, D. A.; Bertozzi, C. R. Host Actin Polymerization Tunes the Cell Division Cycle of an Intracellular Pathogen. *Cell Rep.* **2015**, *11* (4), 499–507.
(13) van Elsland, D. M.; Bos, E.; de Boer, W.; Overkleeft, H. S.; Koster, A. J.; van Kasteren, S. I. Detection of Bioorthogonal Groups by Correlative Light and Electron Microscopy Allows Imaging of Degraded Bacteria in Phagocytes. *Chem. Sci.* **2016**, *7* (1), 752–758.
(14) van Elsland, D. M.; van Kasteren, S. I. Imaging Bioorthogonal Groups in Their Ultrastructural Context with Electron Microscopy. *Angew. Chemie - Int. Ed.* **2016**, *55* (33), 9472–9473.
(15) Pawlak, J. B.; Hos, B. J.; Van De Graaff, M. J.; Megantari, O. A.; Meeuwenoord, N.; Overkleeft, H. S.; Filippov, D. V; Ossendorp, F.; Van Kasteren, S. I. The Optimization of Bioorthogonal Epitope Ligation within MHC-I Complexes. *ACS Chem. Biol.* **2016**, *11*, 3172–3178.
(16) Pawlak, J. B.; Gential, G. P. P.; Ruckwardt, T. J.; Bremmers, J. S.; Meeuwenoord, N. J.; Ossendorp, F. A.; Overkleeft, H. S.; Filippov, D. V.; Van Kasteren, S. I. Bioorthogonal Deprotection on the Dendritic Cell Surface for Chemical Control of Antigen Cross-Presentation. *Angew. Chemie - Int. Ed.* **2015**, *54* (19), 5628–5631.
(17) Flannagan, R. S.; Cosío, G.; Grinstein, S. Antimicrobial Mechanisms of Phagocytes and Bacterial Evasion Strategies. *Nat. Rev. Microbiol.* **2009**, *7* (5), 355–366.
(18) Fang, F. C. Antimicrobial Actions of Reactive Oxygen Species. *MBio* **2011**, *2* (5), 1–6.
(19) Winterbourn, C. C.; Hampton, M. B.; Livesey, J. H.; Kettle, A. J. Modeling the Reactions

of Superoxide and Myeloperoxidase in the Neutrophil Phagosome: Implications for Microbial Killing. *J. Biol. Chem.* **2006**, *281* (52), 39860–39869.

(20) Xiong, Q.; Tezuka, Y.; Kaneko, T.; Li, H.; Tran, L. Q.; Hase, K.; Namba, T.; Kadota, S. Inhibition of Nitric Oxide by Phenylethanoids in Activated Macrophages. *Eur. J. Pharmacol.* **2000**, *400* (1), 137–144.

(21) Slauch, J. M. How Does the Oxidative Burst of Macrophages Kill Bacteria? Still an Open Question. *Mol. Microbiol.* **2011**, *80* (3), 580–583.

(22) Furtmüller, P. G.; Obinger, C.; Hsuanyu, Y.; Dunford, H. B. Mechanism of Reaction of Myeloperoxidase with Hydrogen Peroxide and Chloride Ion. *Eur. J. Biochem.* **2000**, *267* (19), 5858–5864.

(23) Klebanoff, S. J.; Kettle, A. J.; Rosen, H.; Winterbourn, C. C.; Nauseef, W. M. Myeloperoxidase: A Front-Line Defender against Phagocytosed Microorganisms. *J. Leukoc. Biol.* **2013**, *93* (2), 185–198.

(24) Ohkuma, S.; Poole, B. Fluorescence Probe Measurement of the Intralysosomal PH in Living Cells and the Perturbation of PH by Various Agents. *Proc. Natl. Acad. Sci.* **1978**, *75* (7), 3327–3331.

(25) Arunachalam, B.; Phan, U. T.; Geuze, H. J.; Cresswell, P. Enzymatic Reduction of Disulfide Bonds in Lysosomes: Characterization of a Gamma-Interferon-Inducible Lysosomal Thiol Reductase (GILT). *Proc. Natl. Acad. Sci. U. S. A.* **2000**, *97* (2), 745–750.

(26) Stoka, V.; Turk, V.; Turk, B. Lysosomal Cathepsins and Their Regulation in Aging and Neurodegeneration. *Ageing Res. Rev.* **2016**, *32*, 22–37.

(27) Turk, V.; Stoka, V.; Vasiljeva, O.; Renko, M.; Sun, T.; Turk, B.; Turk, D. Cysteine Cathepsins: From Structure, Function and Regulation to New Frontiers. *Biochim. Biophys. Acta - Proteins Proteomics* **2012**, *1824* (1), 68–88.

(28) Balce, D. R.; Yates, R. M. Redox-Sensitive Probes for the Measurement of Redox Chemistries within Phagosomes of Macrophages and Dendritic Cells. *Redox Biol.* **2013**, *1* (1), 467–474.

(29) Zhang, X. X.; Wang, Z.; Yue, X.; Ma, Y.; Kiesewetter, D. O.; Chen, X. PH-Sensitive Fluorescent Dyes: Are They Really Ph-Sensitive in Cells? *Mol. Pharm.* **2013**, *10* (5), 1910–1917.

(30) Shieh, P.; Siegrist, M. S.; Cullen, A. J.; Bertozzi, C. R. Imaging Bacterial Peptidoglycan with Near-Infrared Fluorogenic Azide Probes. *Proc. Natl. Acad. Sci.* **2014**, *111* (15), 5456–5461.

(31) Liechti, G. W.; Kuru, E.; Hall, E.; Kalinda, A.; Brun, Y. V.; Vannieuwenhze, M.; Maurelli, A. T. A New Metabolic Cell-Wall Labelling Method Reveals Peptidoglycan in Chlamydia Trachomatis. *Nature* **2014**, *506* (7489), 507–510.

(32) Lo Conte, M.; Staderini, S.; Marra, A.; Sanchez-Navarro, M.; Davis, B. G.; Dondoni, A. Multi-Molecule Reaction of Serum Albumin Can Occur through Thiol-Yne Coupling. *Chem. Commun.* **2011**, *47* (39), 11086.

(33) Ekkebus, R.; Van Kasteren, S. I.; Kulathu, Y.; Scholten, A.; Berlin, I.; Geurink, P. P.; De Jong, A.; Goerdayal, S.; Neefjes, J.; Heck, A. J. R.; Komander, D.; Ovaa, H. On Terminal Alkynes That Can React with Active-Site Cysteine Nucleophiles in Proteases. *J. Am. Chem. Soc.* **2013**, *135* (8), 2867–2870.

(34) Sommer, S.; Weikart, N. D.; Linne, U.; Mootz, H. D. Covalent Inhibition of SUMO and Ubiquitin-Specific Cysteine Proteases by an in Situ Thiol-Alkyne Addition. *Bioorganic Med. Chem.* **2013**, *21* (9), 2511–2517.

(35) Tian, H.; Sakmar, T. P.; Huber, T. A Simple Method for Enhancing the Bioorthogonality of Cyclooctyne Reagent. *Chem. Commun.* **2016**, *52* (31), 5451–5454.

(36) Jiang, X.; Yu, Y.; Chen, J.; Zhao, M.; Chen, H.; Song, X.; Matzuk, A. J.; Carroll, S. L.; Tan, X.; Sizovs, A.; Cheng, N.; Wang, M. C.; Wang, J. Quantitative Imaging of Glutathione in Live Cells Using a Reversible Reaction-Based Ratiometric Fluorescent Probe. *ACS Chem.*

Biol. **2015**, *10* (3), 864–874.

(37) Murrey, H. E.; Judkins, J. C.; Am Ende, C. W.; Ballard, T. E.; Fang, Y.; Riccardi, K.; Di, L.; Guilmette, E. R.; Schwartz, J. W.; Fox, J. M.; Johnson, D. S. Systematic Evaluation of Bioorthogonal Reactions in Live Cells with Clickable HaloTag Ligands: Implications for Intracellular Imaging. *J. Am. Chem. Soc.* **2015**, *137* (35), 11461–11475.

(38) Beatty, K. E.; Fisk, J. D.; Smart, B. P.; Lu, Y. Y.; Szychowski, J.; Hangauer, M. J.; Baskin, J. M.; Bertozzi, C. R.; Tirrell, D. A. Live-Cell Imaging of Cellular Proteins by a Strain-Promoted Azide-Alkyne Cycloaddition. *ChemBioChem* **2010**, *11* (15), 2092–2095.

(39) Hume, D. A. Macrophages as APC and the Dendritic Cell Myth. *J. Immunol.* **2008**, *181* (9), 5829–5835.

(40) Vono, M.; Lin, A.; Norrby-Teglund, A.; Koup, R. A.; Liang, F.; Loré, K. Neutrophils Acquire the Capacity for Antigen Presentation to Memory CD41 T Cells in Vitro and Ex Vivo. *Blood* **2017**, *129* (14), 1991–2001.

(41) Oh, N.; Park, J. H. Endocytosis and Exocytosis of Nanoparticles in Mammalian Cells. *Int. J. Nanomedicine* **2014**, *9* (SUPPL.1), 51–63.

(42) Helft, J.; Böttcher, J.; Chakravarty, P.; Zelenay, S.; Huotari, J.; Schraml, B. U.; Goubau, D.; Reis e Sousa, C. GM-CSF Mouse Bone Marrow Cultures Comprise a Heterogeneous Population of CD11c+MHCII+ Macrophages and Dendritic Cells. *Immunity* **2015**, *42* (6), 1197–1211.

(43) Steinkamp, J.; Wilson, J.; Saunders, G.; Stewart, C. Phagocytosis: Flow Cytometric Quantitation with Fluorescent Microspheres. *Science (80-.).* **1982**, *215* (4528), 64–66.

(44) Borrmann, A.; Milles, S.; Plass, T.; Dommerholt, J.; Verkade, J. M. M.; Wießler, M.; Schultz, C.; van Hest, J. C. M.; van Delft, F. L.; Lemke, E. A. Genetic Encoding of a Bicyclo[6.1.0]Nonyne-Charged Amino Acid Enables Fast Cellular Protein Imaging by Metal-Free Ligation. *ChemBioChem* **2012**, *13* (14), 2094–2099.

(45) Meldal, M.; Tomøe, C. W. Cu-Catalyzed Azide - Alkyne Cycloaddition. *Chem. Rev.* **2008**, *108* (8), 2952–3015.

(46) Agard, N. J.; Prescher, J. A.; Bertozzi, C. R. A Strain-Promoted [3 + 2] Azide-Alkyne Cycloaddition for Covalent Modification of Biomolecules in Living Systems. *J. Am. Chem. Soc.* **2004**, *126* (46), 15046–15047.

(47) Dommerholt, J.; Rutjes, F. P. J. T.; van Delft, F. L. Strain-Promoted 1,3-Dipolar Cycloaddition of Cycloalkynes and Organic Azides. *Top. Curr. Chem.* **2016**, *374* (2), 1–20.

(48) Lang, K.; Davis, L.; Wallace, S.; Mahesh, M.; Cox, D. J.; Blackman, M. L.; Fox, J. M.; Chin, J. W. Genetic Encoding of Bicyclononynes and Trans-Cyclooctenes for Site-Specific Protein Labeling in Vitro and in Live Mammalian Cells via Rapid Fluorogenic Diels-Alder Reactions. *J. Am. Chem. Soc.* **2012**, *134* (25), 10317–10320.

(49) van den Bosch, S. M.; Rossin, R.; Renart Verkerk, P.; ten Hoeve, W.; Janssen, H. M.; Lub, J.; Robillard, M. S. Evaluation of Strained Alkynes for Cu-Free Click Reaction in Live Mice. *Nucl. Med. Biol.* **2013**, *40* (3), 415–423.

(50) Bernardin, A.; Cazet, A.; Guyon, L.; Delannoy, P.; Vinet, F.; Bonnaffé, D.; Texier, I. Copper-Free Click Chemistry for Highly Luminescent Quantum Dot Conjugates: Application to in Vivo Metabolic Imaging. *Bioconjug. Chem.* **2010**, *21* (4), 583–588.

(51) Ngo, J. T.; Adams, S. R.; Deerinck, T. J.; Boassa, D.; Rodriguez-Rivera, F.; Palida, S. F.; Bertozzi, C. R.; Ellisman, M. H.; Tsien, R. Y. Click-EM for Imaging Metabolically Tagged Nonprotein Biomolecules. *Nat. Chem. Biol.* **2016**, *12* (6), 459–465.

(52) Patterson, D. M.; Prescher, J. A. Orthogonal Bioorthogonal Chemistries. *Curr. Opin. Chem. Biol.* **2015**, *28*, 141–149.

(53) Hong, V.; Steinmetz, N. F.; Manchester, M.; Finn, M. G. Labeling Live Cells by Copper-Catalyzed Alkyne - Azide Click Chemistry. *Bioconjugate chem.* **2010**, *21* (10), 1912–1916.

(54) Udenfriend, S.; Stein, S.; Böhlen, P.; Dairman, W.; Leimgruber, W.; Weigele, M. Fluorescamine: A Reagent for Assay of Amino Acids, Peptides, Proteins, and Primary Amines in the Picomole Range. *Science (80-.).* **1972**, *178* (4063), 871–872.
(55) van Geel, R.; Pruijn, G. J. M.; van Delft, F. L.; Boelens, W. C. Preventing Thiol-Yne Addition Improves the Specificity of Strain-Promoted Azide–Alkyne Cycloaddition. *Bioconjug. Chem.* **2012**, *23* (3), 392–398.
(56) Lockhart, J.; Blitz, M.; Heard, D.; Seakins, P.; Shannon, R. Kinetic Study of the OH + Glyoxal Reaction: Experimental Evidence and Quantification of Direct OH Recycling. *J. Phys. Chem. A* **2013**, *117* (43), 11027–11037.
(57) Senosiain, J. P.; Klippenstein, S. J.; Miller, J. A. The Reaction of Acetylene with Hydroxyl Radicals. *J. Phys. Chem. A* **2005**, *109* (27), 6045–6055.
(58) Shen, Z.; Reznikoff, G.; Dranoff, G.; Rock, K. L. Cloned Dendritic Cells Can Present Exogenous Antigens on Both MHC Class I and Class II Molecules. *J. Immunol.* **1997**, *158* (6), 2723–2730.
(59) Ralph, P.; Nakoinz, I. Antibody-Dependent Killing of Erythrocyte and Tumor Targets by Macrophage-Related Cell Lines: Enhancement by PPD and LPS. *J. Immunol.* **1977**, *119* (3), 950–954.
(60) Raschke, W.; Baird, S.; Ralph, P.; Nakoinz, I. Functional Macrophage Cell Lines Transformed by Abelson Leukaemia Virus. *Cell* **1978**, *15* (September), 261–267.
(61) Ferenbach, D.; Hughes, J. Macrophages and Dendritic Cells: What Is the Difference? *Kidney Int.* **2008**, *74* (1), 5–7.
(62) Rybicka, J. M.; Balce, D. R.; Chaudhuri, S.; Allan, E. R. O.; Yates, R. M. Phagosomal Proteolysis in Dendritic Cells Is Modulated by NADPH Oxidase in a PH-Independent Manner. *EMBO J.* **2012**, *31* (4), 932–944.
(63) Savina, A.; Peres, A.; Cebrian, I.; Carmo, N.; Moita, C.; Hacohen, N.; Moita, L. F.; Amigorena, S. The Small GTPase Rac2 Controls Phagosomal Alkalinization and Antigen Crosspresentation Selectively in CD8+ Dendritic Cells. *Immunity* **2009**, *30* (4), 544–555.
(64) Savina, A.; Jancic, C.; Hugues, S.; Guermonprez, P.; Vargas, P.; Moura, I. C.; Lennon-Duménil, A. M.; Seabra, M. C.; Raposo, G.; Amigorena, S. NOX2 Controls Phagosomal PH to Regulate Antigen Processing during Crosspresentation by Dendritic Cells. *Cell* **2006**, *126* (1), 205–218.
(65) Kapellos, T. S.; Taylor, L.; Lee, H.; Cowley, S. A.; James, W. S.; Iqbal, A. J.; Greaves, D. R. A Novel Real Time Imaging Platform to Quantify Macrophage Phagocytosis. *Biochem. Pharmacol.* **2016**, *116*, 107–119.
(66) Rybicka, J. M.; Balce, D. R.; Khan, M. F.; Krohn, R. M.; Yates, R. M. NADPH Oxidase Activity Controls Phagosomal Proteolysis in Macrophages through Modulation of the Lumenal Redox Environment of Phagosomes. *Proc. Natl. Acad. Sci. U. S. A.* **2010**, *107* (23), 10496–10501.
(67) Adachi, Y.; Kindzelskii, A. L.; Petty, A. R.; Huang, J.-B.; Maeda, N.; Yotsumoto, S.; Aratani, Y.; Ohno, N.; Petty, H. R. IFN-γ Primes RAW264 Macrophages and Human Monocytes for Enhanced Oxidant Production in Response to CpG DNA via Metabolic Signaling: Roles of TLR9 and Myeloperoxidase Trafficking. *J. Immunol.* **2006**, *176* (8), 5033–5040.
(68) Vanderven, B. C.; Yates, R. M.; Russell, D. G. Intraphagosomal Measurement of the Magnitude and Duration of the Oxidative Burst. *Traffic* **2009**, *10* (4), 372–378.
(69) van Kasteren, S. I.; Overkleeft, H. S. Endo-Lysosomal Proteases in Antigen Presentation. *Curr. Opin. Chem. Biol.* **2014**, *23*, 8–15.
(70) Van Kasteren, S. I.; Berlin, I.; Colbert, J. D.; Keane, D.; Ovaa, H.; Watts, C. A Multifunctional Protease Inhibitor to Regulate Endolysosomal Function. *ACS Chem. Biol.* **2011**, *6* (11), 1198–1204.
(71) Mantegazza, A. R.; Savina, A.; Vermeulen, M.; Pérez, L.; Geffner, J.; Hermine, O.;

Rosenzweig, S. D.; Faure, F.; Amigorena, S. NADPH Oxidase Controls Phagosomal PH and Antigen Cross-Presentation in Human Dendritic Cells. *Blood* **2008**, *112* (12), 4712–4722.

(72) Song, J. S.; Kim, Y. J.; Han, K. U.; Yoon, B. D.; Kim, J. W. Zymosan and PMA Activate the Immune Responses of Mutz3-Derived Dendritic Cells Synergistically. *Immunol. Lett.* **2015**, *167* (1), 41–46.

(73) Kelly, E. K.; Wang, L.; Ivashkiv, L. B. Calcium-Activated Pathways and Oxidative Burst Mediate Zymosan-Induced Signaling and IL-10 Production in Human Macrophages. *J. Immunol.* **2010**, *184* (10), 5545–5552.

(74) Winterbourn, C. C.; Kettle, A. J. Redox Reactions and Microbial Killing in the Neutrophil Phagosome. *Antioxidants Redox Signal.* **2013**, *18* (6), 642–660.

(75) Klebanoff, S. J. Myeloperoxidase: Friend and Foe. *J. Leukoc. Biol.* **2005**, *77* (5), 598–625.

(76) Scholz, W.; Platzer, B.; Schumich, A.; Höcher, B.; Fritsch, G.; Knapp, W.; Strobl, H. Initial Human Myeloid/Dendritic Cell Progenitors Identified by Absence of Myeloperoxidase Protein Expression. *Exp. Hematol.* **2004**, *32* (3), 270–276.

(77) Pickl, W. F.; Majdic, O.; Kohl, P.; Stöckl, J.; Riedl, E.; Scheinecker, C.; Bello-Fernandez, C.; Knapp, W. Molecular and Functional Characteristics of Dendritic Cells Generated from Highly Purified CD14+ Peripheral Blood Monocytes. *J. Immunol.* **1996**, *157* (9), 3850–3859.

(78) Nunes, P.; Demaurex, N.; Dinauer, M. C. Regulation of the NADPH Oxidase and Associated Ion Fluxes During Phagocytosis. *Traffic* **2013**, *14* (11), 1118–1131.

(79) Segal, A. W.; Geisow, M.; Garcia, R.; Harper, A.; Miller, R. The Respiratory Burst of Phagocytic Cells Is Associated with a Rise in Vacuolar PH. *Nature* **1981**, *290* (5805), 406–409.

(80) Yuan, K.; Liu, Y.; Chen, H. N.; Zhang, L.; Lan, J.; Gao, W.; Dou, Q.; Nice, E. C.; Huang, C. Thiol-Based Redox Proteomics in Cancer Research. *Proteomics* **2015**, *15* (2–3), 287–299.

(81) Zeida, A.; Guardia, C. M.; Lichtig, P.; Perissinotti, L. L.; Defelipe, L. A.; Turjanski, A.; Radi, R.; Trujillo, M.; Estrin, D. A. Thiol Redox Biochemistry: Insights from Computer Simulations. *Biophys. Rev.* **2014**, *6* (1), 27–46.

(82) Poole, T. H.; Reisz, J. A.; Zhao, W.; Poole, L. B.; Furdui, C. M.; King, S. B. Strained Cycloalkynes as New Protein Sulfenic Acid Traps. *J. Am. Chem. Soc.* **2014**, *136* (17), 6167–6170.

(83) Lang, K.; Chin, J. W. Bioorthogonal Reactions for Labeling Proteins. *ACS Chem. Biol.* **2014**, *9* (1), 16–20.

(84) Blackman, M. L.; Royzen, M.; Fox, J. M. Tetrazine Ligation: Fast Bioconjugation Based on Inverse-Electron-Demand Diels-Alder Reactivity. *J. Am. Chem. Soc.* **2008**, *130* (41), 13518–13519.

(85) Oliveira, B. L.; Guo, Z.; Bernardes, G. J. L. Inverse Electron Demand Diels–Alder Reactions in Chemical Biology. *Chem. Soc. Rev.* **2017**, *46* (16), 4895–4950.

(86) Song, W.; Wang, Y.; Qu, J.; Lin, Q. Selective Functionalization of a Genetically Encoded Alkene-Containing Protein via “Photoclick Chemistry” in Bacterial Cells. *J. Am. Chem. Soc.* **2008**, *130* (30), 9654–9655.

(87) Andersen, K. A.; Aronoff, M. R.; McGrath, N. A.; Raines, R. T. Diazo Groups Endure Metabolism and Enable Chemoselectivity in Cellulo. *J. Am. Chem. Soc.* **2015**, *137* (7), 2412–2415.